HAL
open science

A discontinuous Galerkin spectral element method for a nonconservative compressible multicomponent flow model

Rémi Abgrall, Pratik Rai, Florent Renac

To cite this version:

Rémi Abgrall, Pratik Rai, Florent Renac. A discontinuous Galerkin spectral element method for a nonconservative compressible multicomponent flow model. Journal of Computational Physics, 2023, 472, pp.111693. 10.1016/j.jcp.2022.111693 . hal-03878132

HAL Id: hal-03878132

https://hal.science/hal-03878132v1

Submitted on 29 Nov 2022

HAL is a multi-disciplinary open access archive for the deposit and dissemination of scientific research documents, whether they are published or not. The documents may come from teaching and research institutions in France or abroad, or from public or private research centers.

L'archive ouverte pluridisciplinaire **HAL**, est destinée au dépôt et à la diffusion de documents scientifiques de niveau recherche, publiés ou non, émanant des établissements d'enseignement et de recherche français ou étrangers, des laboratoires publics ou privés.

A discontinuous Galerkin spectral element method for a nonconservative compressible multicomponent flow model

Rémi Abgrall[a], Pratik Rai,[b,*], Florent Renac[c,*]

[a]*Institute of Mathematics, University of Zürich, Switzerland*

[b]*DTIS, ONERA, Université de Toulouse, France*

[c]*DAAA, ONERA, Université Paris Saclay F-92322 Châtillon, France*

Abstract

In this work, we propose an accurate, robust (the solution remains in the set of states), and stable discretization of a nonconservative model for the simulation of compressible multicomponent flows with shocks and material interfaces. We consider the gamma-based model by Shyue [J. Comput. Phys., 142 (1998), 208–242] where each component follows a stiffened gas equation of state (EOS). We here extend the framework proposed in Renac [J. Comput. Phys., 382 (2019), 1–26] and Coquel et al. [J. Comput. Phys. 431 (2021), 110135] for the discretization of hyperbolic systems, with both fluxes and nonconservative products, to unstructured meshes with curved elements in multiple space dimensions. The framework relies on a high-order discontinuous Galerkin spectral element method (DGSEM) using collocation of quadrature and interpolation points as proposed by Gassner [SIAM J. Sci. Comput., 35 (2013)] in the case of hyperbolic conservation laws. We modify the integrals over discretization elements where we replace the physical fluxes and nonconservative products by two-point numerical fluctuations. The contributions of this work are threefold. First, we analyze the semi-discrete DGSEM discretization of general hyperbolic systems with conservative and nonconservative terms and derive the conditions to obtain a scheme that is high-order accurate, free-stream preserving, and entropy stable when excluding material interfaces. Second, we design a three-point scheme with a HLLC solver for the gamma-based model that does not require a root-finding algorithm for the approximation of the nonconservative products. The scheme is proved to be robust and entropy stable for convex entropies, to preserve uniform profiles of pressure and velocity across material interfaces (material interface preservation), and to satisfy a discrete minimum principle on the specific entropy and maximum principles on the parameters of the EOS. Third, the HLLC solver is applied at interfaces in the DGSEM scheme, while we consider two kinds of fluctuations in the integrals over discretization elements: the former is entropy conservative (EC), while the latter preserves material interfaces (CP). Time integration is performed using high-order strong-stability preserving Runge-Kutta schemes. The fully discrete scheme is shown to preserve material interfaces with CP fluctuations. Under a given condition on the time step, both EC and CP fluctuations ensure that the cell-averaged solution remains in the set of states; satisfy a minimum principle on any convex entropy and maximum principles on the EOS parameters. These results allow to use existing limiters in order to restore positivity, and discrete maximum principles of degrees-of-freedom within elements. Numerical experiments in one and two space dimensions on flows with discontinuous solutions support the conclusions of our analysis and highlight stability, robustness and accuracy of the DGSEM scheme with either CP, or EC fluctuations, while the scheme with CP fluctuations is shown to offer better resolution capabilities.

Keywords. Compressible multicomponent flows, Nonconservative hyperbolic systems, Discontinuous Galerkin method, Summation-by-parts, Material interface capturing, Entropy stability, High-order accuracy

AMS subject classifications. 65M12, 65M70, 76T10

1. Introduction

The discussion in this paper focuses on the approximation in multiple space dimensions of a compressible multicomponent flow model in nonconservative form. We consider a gamma-based model [53] for a mixture with a stiffened gas equation of state (EOS) approximating components including both gas and compressible liquids (hereafter referred to as the SG-gamma model). The model is written in quasi-conservative form [1] to preserve velocity and pressure profiles across material interfaces separating

*Corresponding author's email addresses: pratik.rai@polytechnique.edu (Pratik Rai), florent.renac@onera.fr (Florent Renac)

different components. The model approximates mixture quantities and presents the main advantage of being independent of the number of components. We are here interested in high-order, robust (i.e., preserving the solution in the set of admissible states), and entropy stable simulations of flows with shocks, material interfaces, and complex interactions triggering small scale flow phenomena. Numerical approximation of multicomponent and multiphase flows based on interface capturing methods has been the subject of numerous works (see, e.g. [36, 51] and references therein).

We discretize the SG-gamma model using the discontinuous Galerkin spectral element method (DGSEM) with Gauss-Lobatto quadrature rules [39]. The DGSEM uses diagonal norm summation-by-parts (SBP) operators [24] and, in the case of hyperbolic conservation laws, falls into the general framework of conservative elementwise flux differencing schemes [21]. In this framework, using entropy conservative (EC) numerical fluxes from Tadmor [55], semi-discrete EC finite-difference and spectral collocation schemes have been derived in [21, 24]. The framework has been extended to nonconservative hyperbolic systems on Cartesian meshes in [47, 14] by using EC numerical fluctuations from [9]. In both frameworks, a semi-discrete entropy inequality may be obtained by replacing physical fluxes and nonconservative products with EC numerical fluxes or fluctuations within discretization elements, while using entropy stable ones at interfaces between elements. The design of the latter relies either on adding upwind-type dissipation [33] to EC numerical fluxes and fluctuations [7, 22, 17, 25, 47, 14], or on designing approximate Riemann solvers [18, 49, 46]. Note that the SBP operators take into account the numerical quadrature when approximating integrals compared to other schemes that require their exact evaluation to achieve entropy stability [34, 30, 31].

Here, we extend the framework proposed in [47] to multidimensional unstructured meshes with curved elements by using tensor multiplication of quadrature rules and function basis [39] that satisfy geometric conservation laws (the so-called metric identities [38]) at the discrete level. This framework has been recently applied to the approximation with a well-balanced DGSEM of balance laws with geometric source terms on multidimensional high-order meshes in [63]. We here rather focus on specific properties of discretizations of nonconservative multicomponent flows: preservation of material interfaces, discrete conservation of physical fluxes, maximum principles on purely transported quantities such as the EOS parameters, and entropy stability. The latter property presents some difficulties due to the form of the entropy associated to SG-gamma model. First, as a model for the mixture, the properties of the individual components, such as mass and void fractions, are not known in general which prevents the evaluation of the entropy variables necessary for the derivation of EC fluctuations from the Castro et al. condition [9]. Then, the entropy is not convex as is often the case in phase transition models [29] which will restrict the entropy stability across shocks not interacting with material fronts. We here circumvent these difficulties by considering a specific entropy that allows the evaluation of the entropy variables. This entropy satisfies a Gibbs relation and thus defines a complete EOS [42] and is concave with respect to two thermodynamic intensive properties of the mixture, so entropy stability can be ensured when excluding material interfaces. Let us stress that material interfaces do not require the scheme to be entropy stable, but rather a consistent approximation of the energy equations to ensure pressure equilibrium [1]. We thus also design material interface preserving (CP) fluctuations to preserve at the discrete level pressure and velocity fields across such interfaces.

We then design a HLLC solver [58, 60] for the SG-gamma model that does not require a root-finding algorithm to evaluate the nonconservative product in contrast to other schemes [19, 11, 56]. We analyze the properties of a three-point scheme using the HLLC solver and prove that the scheme is robust and entropy stable for convex entropies defining a complete EOS, preserves uniform profiles of pressure and velocity across material interfaces, and satisfies a discrete minimum principle on the specific entropy and maximum principles on the parameters of the EOS. We then apply the HLLC solver at mesh interfaces in the DGSEM scheme and analyze the properties of the fully discrete scheme with an explicit first-order Euler time integration. We derive conditions on the time step so that the cell-averaged solution is a convex combination of degrees-of-freedom (DOFs) and updates of three-point schemes, as a result the scheme inherits the properties of the three-point scheme. In particular, the DGSEM scheme satisfies a minimum principle on the entropy irrespective of the fluctuations (EC or CP) that are used in the discretization elements. As a consequence, the DGSEM with CP fluctuations within elements and the HLLC solver at interfaces is able to handle shocks and to preserve material interfaces. Time integration is performed using high-order strong-stability preserving Runge-Kutta schemes that are convex combinations of explicit Euler schemes, while linear scaling limiters [65, 66] are applied at the end of each stage to impose positivity and maximum principles at all DOFs within discretization elements.

This paper is organized as follows. The SG-gamma model and the entropy pair are described in section 2. We then introduce the semi-discrete DGSEM scheme on multidimensional and high-order unstructured meshes in section 3. In section 4, we derive CP and EC numerical fluxes for the SG-gamma model, and in section 5, we propose the HLLC approximate Riemann solver and analyze its properties. We recall the main properties of the fully-discrete DGSEM scheme in section 6. A posteriori limiters are described in section 7. The results are assessed by numerical experiments in one and two space dimensions in section 8 and concluding remarks about this work are given in section 9.

2. The SG-gamma model

2.1. Governing equations and thermodynamic model

In this work, we consider the gamma-based compressible multicomponent flow model where each component is assumed to be a stiffened gas [53] and refer to it as the SG-gamma model. The main interest in this model is that the number of unknowns is independent of the number of components. We are here interested in high-order approximations of the associated Cauchy problem in d space dimensions for flows with n_s components:

$$\partial_t \mathbf{u} + \nabla_{\mathbf{x}} \cdot \mathbf{f}(\mathbf{u}) + \mathbf{c}(\mathbf{u})\nabla_{\mathbf{x}}\mathbf{u} = 0, \qquad \mathbf{x} \in \mathbb{R}^d, t > 0, \tag{1a}$$

$$\mathbf{u}(\mathbf{x}, 0) = \mathbf{u}_0(\mathbf{x}), \quad \mathbf{x} \in \mathbb{R}^d, \tag{1b}$$

where $\mathbf{x} = (x_1, \dots, x_d)$ are the spatial coordinates, $\mathbf{f}(\mathbf{u}) = \left(\mathbf{f}_1(\mathbf{u}), \dots, \mathbf{f}_d(\mathbf{u})\right)$, $\mathbf{c}(\mathbf{u})\nabla_{\mathbf{x}}\mathbf{u} = \sum_{i=1}^{d} \mathbf{c}_i(\mathbf{u})\partial_{x_i}\mathbf{u}$, and

$$\mathbf{u} = \begin{pmatrix} \rho \\ \rho\mathbf{v} \\ \rho E \\ \Gamma \\ \Pi \end{pmatrix}, \quad \mathbf{f}(\mathbf{u}) = \begin{pmatrix} \rho\mathbf{v}^\top \\ \rho\mathbf{v}\mathbf{v}^\top + \mathrm{p}\mathbf{I} \\ (\rho E + \mathrm{p})\mathbf{v}^\top \\ 0 \\ 0 \end{pmatrix}, \quad \mathbf{c}(\mathbf{u})\nabla_{\mathbf{x}}\mathbf{u} = \begin{pmatrix} 0 \\ 0 \\ 0 \\ \mathbf{v}\cdot\nabla_{\mathbf{x}}\Gamma \\ \mathbf{v}\cdot\nabla_{\mathbf{x}}\Pi \end{pmatrix}, \tag{2}$$

represent the vector of state variables, the physical fluxes and the nonconservative products[1], respectively. The mixture density, momentum, total energy, and internal energy are defined as

$$\rho = \sum_{i=1}^{n_s} \alpha_i\rho_i, \quad \rho\mathbf{v} = \sum_{i=1}^{n_s} \alpha_i\rho_i\mathbf{v}_i, \quad \rho E = \rho e + \frac{1}{2}\rho\mathbf{v}\cdot\mathbf{v}, \quad \rho e = \sum_{i=1}^{n_s} \alpha_i\rho_i e_i,$$

where ρ_i, $\mathbf{v}_i$, and e_i represent the density, the velocity vector and the specific internal energy of the ith component. The model assumes immiscible phases and thus imposes a saturation condition on the void fractions α_i:

$$\sum_{i=1}^{n_s} \alpha_i = 1. \tag{3}$$

The partial pressures are related to partial densities and specific internal energies through the stiffened gas EOS:

$$\mathrm{p}_i(\rho_i, e_i) = (\gamma_i - 1)\rho_i e_i - \gamma_i \mathrm{p}_{\infty_i}, \quad e_i = \mathrm{C}_{\mathrm{v}i} T_i + \frac{\mathrm{p}_{\infty_i}}{\rho_i}, \quad i = 1, \dots, n_s, \tag{4}$$

where $\gamma_i = \mathrm{C}_{\mathrm{p}i}/\mathrm{C}_{\mathrm{v}i} > 1$ is the ratio of specific heats, T_i is the temperature of the species, and $\mathrm{p}_{\infty_i} \geqslant 0$ is a pressure-like constant. Observe that when $\mathrm{p}_{\infty_i} = 0$ in (4) we recover the polytropic EOS. Assuming thermal equilibrium of the species, $T_i(\rho_i, e_i) = T(\rho, e)$, $1 \leqslant i \leqslant n_s$, the EOS for the mixture is indeed conveniently defined by [53]

$$\frac{\mathrm{p} + \gamma\mathrm{p}_\infty}{(\gamma - 1)} = \mathrm{p}\Gamma + \Pi = \rho e, \quad \rho e = \rho \mathrm{C}_{\mathrm{v}} T + \sum_{i=1}^{n_s} \alpha_i \mathrm{p}_{\infty_i}, \tag{5}$$

where $\mathrm{C}_{\mathrm{v}} = \sum_{i=1}^{n_s} Y_i \mathrm{C}_{\mathrm{v}i}$ denotes the specific heat at constant volume of the mixture, the $Y_i = \frac{\alpha_i\rho_i}{\rho}$ are the mass fractions of the species, and the EOS parameters Γ and Π are defined by

$$\Gamma = \frac{1}{\gamma - 1} = \sum_{i=1}^{n_s} \frac{\alpha_i}{\gamma_i - 1}, \quad \Pi = \frac{\gamma\mathrm{p}_\infty}{\gamma - 1} = \sum_{i=1}^{n_s} \frac{\alpha_i\gamma_i\mathrm{p}_{\infty_i}}{\gamma_i - 1}. \tag{6}$$

[1]The components of the third-order tensor in (1a) read $\mathbf{c}(\mathbf{u})_{ijk} = \mathbf{c}_k(\mathbf{u})_{ij}$ with the $\mathbf{c}_k(\mathbf{u})$ in $\mathbb{R}^{n_{eq}\times n_{eq}}$, so the ith component of $\mathbf{c}(\mathbf{u})\nabla\mathbf{u}$ reads $\sum_{j=1}^{n_{eq}}\sum_{k=1}^{d} \mathbf{c}(\mathbf{u})_{ijk}\partial_{x_k}\mathbf{u}_j$. Likewise, for $\mathbf{n} = (n_1, \dots, n_d)^\top$, we have $\mathbf{c}(\mathbf{u})\mathbf{n} = \sum_{i=1}^{d} n_i\mathbf{c}_i(\mathbf{u})$.

Hyperbolicity of the SG-gamma model requires that the solutions to (1) belong to the set of states

$$\Omega_{\mathrm{GM}} = \Big\{\mathbf{u} \in \mathbb{R}^{n_{eq}} \,:\, \rho > 0,\ \mathbf{v} \in \mathbb{R}^d,\ \rho e > \mathrm{p}_\infty,\ \Gamma > 0,\ \Pi \geqslant 0\Big\}, \tag{7}$$

with $n_{eq} = d + 4$. The matrix-valued function $\sum_{i=1}^d n_i\Big(\mathbf{f}_i'(\mathbf{u}) + \mathbf{c}_i(\mathbf{u})\Big)$ in $\mathbb{R}^{n_{eq}\times n_{eq}}$ admits real eigenvalues

$$\lambda_1(\mathbf{u}) = \mathbf{v}\cdot\mathbf{n} - c, \quad \lambda_2(\mathbf{u}) = \cdots = \lambda_{n_{eq}-1}(\mathbf{u}) = \mathbf{v}\cdot\mathbf{n}, \quad \lambda_{n_{eq}}(\mathbf{u}) = \mathbf{v}\cdot\mathbf{n} + c, \tag{8}$$

for all unit vector $\mathbf{n} = (n_1, \ldots, n_d)$, where $c = \sqrt{\gamma(\gamma-1)(\rho e - \mathrm{p}_\infty)/\rho}$ is the speed of sound of the mixture. Here, $\{\lambda_i\}_{2\leqslant i\leqslant n_{eq}-1}$ are associated to linearly degenerate (LD) fields, while λ_1 and $\lambda_{n_{eq}}$ are associated to genuinely nonlinear (GNL) fields. Observe that (1a) is not strictly hyperbolic as the eigenvalues associated to the LD fields are not distinct.

2.2. *Entropy pair*

Solutions to (1) may develop discontinuities and (1a) has to be understood in the sense of distributions where we look for weak solutions. Weak solutions are not necessarily unique and (1) must be supplemented with further admissibility conditions to select the physical solution. We here focus on entropy inequalities

$$\partial_t\eta(\mathbf{u}) + \nabla_{\mathbf{x}}\cdot\mathbf{q}(\mathbf{u}) \leqslant 0, \qquad \mathbf{x}\in\mathbb{R}^d, t > 0, \tag{9}$$

for some convex entropy – entropy flux pair $(\eta(\mathbf{u}), \mathbf{q}(\mathbf{u}))$. One common way to derive such pair consists in considering partial entropies of the species $s_i(\rho_i, \theta) = -\mathrm{C}_{\mathrm{v}i}\,(\ln\theta + (\gamma_i - 1)\ln\rho_i)$, where $\theta = 1/T$ is the inverse of the temperature, that satisfies a Gibbs relation

$$T\,\mathrm{d}s_i = \mathrm{d}e_i - \frac{\mathrm{p}_i}{\rho_i^2}\mathrm{d}\rho_i, \tag{10}$$

so the mixture entropy reads

$$\sum_{i=1}^{n_s} Y_i s_i = -\mathrm{C}_{\mathrm{v}}\ln\theta - \sum_{i=1}^{n_s} Y_i(\gamma_i - 1)\mathrm{C}_{\mathrm{v}i}\ln\rho_i.$$

Unfortunately, we cannot use this entropy to derive EC fluxes in section 4 because they would require to evaluate the Y_i which is not possible from $\mathbf{u}$ in (2). Hence, here we consider an alternative pair

$$\eta(\mathbf{u}) = -\rho s, \quad \mathbf{q}(\mathbf{u}) = -\rho s\mathbf{v}, \tag{11}$$

where, upon introducing $\tau = \frac{1}{\rho}$ the covolume of the mixture, the specific entropy reads

$$s(\tau, e, \mathrm{C}_{\mathrm{v}}, \Gamma, \Pi) = \mathrm{C}_{\mathrm{v}}\ln\left(\frac{\mathrm{p}+\mathrm{p}_\infty}{\rho^\gamma}\right) \overset{(6)}{=} \mathrm{C}_{\mathrm{v}}\left(\ln\left(e - \frac{\Pi}{\Gamma+1}\tau\right) + \frac{1}{\Gamma}\ln\tau - \ln\Gamma\right). \tag{12}$$

The rationale for considering this entropy is as follows. First, we will see in section 4.2 that the EC fluctuations can be explicitly computed without knowledge of the individual mass fractions. Then, for smooth solutions of (1a), we have

$$\partial_t\mathrm{C}_{\mathrm{v}} + \mathbf{v}\cdot\nabla_{\mathbf{x}}\mathrm{C}_{\mathrm{v}} = 0, \quad \partial_t\tau + \mathbf{v}\cdot\nabla_{\mathbf{x}}\tau = \tau\nabla_{\mathbf{x}}\cdot\mathbf{v}, \quad \partial_t e + \mathbf{v}\cdot\nabla_{\mathbf{x}}e = -\tau\mathrm{p}\nabla_{\mathbf{x}}\cdot\mathbf{v},$$

hence

$$\partial_t s + \mathbf{v}\cdot\nabla_{\mathbf{x}}s = \partial_\tau s\Big(\partial_t\tau + \mathbf{v}\cdot\nabla_{\mathbf{x}}\tau\Big) + \partial_e s\Big(\partial_t e + \mathbf{v}\cdot\nabla_{\mathbf{x}}e\Big) = \tau\nabla_{\mathbf{x}}\cdot\mathbf{v}(\partial_\tau s - \mathrm{p}\partial_e s) = \mathrm{C}_{\mathrm{v}}\nabla_{\mathbf{x}}\cdot\mathbf{v}\left(\frac{1}{\Gamma} - \frac{\mathrm{p}_\infty}{\rho e - \mathrm{p}_\infty} - \frac{\mathrm{p}}{\rho e - \mathrm{p}_\infty}\right) \overset{(5)}{=} 0,$$

so the mixture entropy is conserved, i.e., (9) is an equality. Moreover, $(\tau, e) \mapsto s(\tau, e, \mathrm{C_v}, \Gamma, \Pi)$ is obviously strictly concave in Ω_{GM} and from the first equality in the above relation, we conclude that the inequality in (9) makes sense even if $\eta(\mathbf{u})$ is not strictly convex which is often the case in phase transition models [29]. Finally, differentiating (12) while fixing $\mathrm{C_v}$, Γ and Π, gives

$$\mathrm{d}s = \mathrm{C_v}\left(\frac{\mathrm{dp}}{\mathrm{p}+\mathrm{p}_\infty} - \gamma\frac{\mathrm{d}\rho}{\rho}\right) \overset{(5)}{=} \mathrm{C_v}\left(\frac{(\gamma-1)\mathrm{d}(\rho e)}{\mathrm{p}+\mathrm{p}_\infty} - \gamma\frac{\mathrm{d}\rho}{\rho}\right) = \frac{\rho \mathrm{C_v}}{\rho e - \mathrm{p}_\infty}\left(\mathrm{d}e - \frac{\mathrm{p}}{\rho^2}\mathrm{d}\rho\right), \tag{13}$$

so the entropy satisfies a Gibbs relation similar to (10) but with a different temperature $\tilde{T} = \frac{1}{\rho \mathrm{C_v}}(\rho e - \mathrm{p}_\infty)$ instead of T in (5). The entropy hence defines a complete EOS with both pressure and temperature [42]. This latter observation will be important in section 5 to prove entropy stability of the HLLC solver through the existence of local minimum entropy principles (see proof of Lemma 5.1).

We end this section by deriving the entropy variables associated to the entropy $\eta(\mathbf{u})$ in (11) when considering pure phases. For pure phases, we have $\mathrm{d}\gamma = \mathrm{d}\Pi = 0$ so we obtain

$$\begin{aligned}
\mathrm{d}\eta = -\rho \mathrm{d}s - s\mathrm{d}\rho \overset{(12)}{=} -\rho \mathrm{C_v}\frac{\mathrm{d}(\mathrm{p}+\mathrm{p}_\infty)}{\mathrm{p}+\mathrm{p}_\infty} + \gamma \mathrm{C_v}\mathrm{d}\rho - s\mathrm{d}\rho &\overset{(5)}{=} -\rho \mathrm{C_v}(\gamma-1)\frac{\mathrm{d}\rho e}{\mathrm{p}+\mathrm{p}_\infty} + \gamma \mathrm{C_v}\mathrm{d}\rho - s\mathrm{d}\rho \\
&= -\rho\frac{(\gamma-1)\mathrm{C_v}}{\mathrm{p}+\mathrm{p}_\infty}\left(\mathrm{d}\rho E - \mathbf{v}\cdot\mathrm{d}\rho\mathbf{v} + \frac{\mathbf{v}\cdot\mathbf{v}}{2}\mathrm{d}\rho\right) + \gamma \mathrm{C_v}\mathrm{d}\rho - s\mathrm{d}\rho \\
&\overset{(15)}{=} -\zeta \mathrm{d}\rho E + \zeta\mathbf{v}\cdot\mathrm{d}\rho\mathbf{v} + \left(\gamma \mathrm{C_v} - s - \zeta\frac{\mathbf{v}\cdot\mathbf{v}}{2}\right)\mathrm{d}\rho,
\end{aligned}$$

and we thus obtain the following expression of the entropy variables

$$\boldsymbol{\vartheta}(\mathbf{u}) = \frac{\partial}{\partial \mathbf{u}}\eta(\mathbf{u}) = \begin{pmatrix} \gamma \mathrm{C_v} - s - \zeta\frac{\mathbf{v}\cdot\mathbf{v}}{2} \\ \zeta\mathbf{v} \\ -\zeta \\ 0 \\ 0 \end{pmatrix} \quad \forall \mathbf{u} \in \Omega_{\mathrm{GM}}, \tag{14}$$

where

$$\zeta = \frac{(\gamma-1)\mathrm{C_v}\rho}{\mathrm{p}+\mathrm{p}_\infty}. \tag{15}$$

3. The discontinuous Galerkin spectral element method (DGSEM)

In this section, we recall the DGSEM framework [14, 39, 47] which is used to discretize the Cauchy problem (1). Here, the space domain $\Omega = \mathbb{R}^d$ is discretized using a mesh Ω_h consisting of nonoverlapping and nonempty cells κ (quadrangles for $d = 2$ and hexahedra for $d = 3$) forming a partition of Ω. By $\mathcal{E}_h$ we denote the set of interfaces in Ω_h. For the sake of clarity, we introduce the DGSEM in two space dimensions $d = 2$, as the extension to $d = 3$ is straightforward while its derivation for $d = 1$ can be found in [14, 48].

3.1. Numerical approximation and function space

Let us consider the reference element $\mathrm{I}^2 = [-1, 1]^2$ with coordinates $\boldsymbol{\xi} = (\xi, \eta)$ and the reference edge $\mathrm{I} = [-1, 1]$, the functions $\mathbf{x}_\kappa(\boldsymbol{\xi})$ and $\mathbf{x}_e(\xi)$ map reference to physical element and edge, respectively. The approximate solution of (1) is sought in the function space of piecewise polynomials

$$\mathcal{V}_h^p = \left\{\phi \in L^2(\Omega_h) : \phi_\kappa \circ \mathbf{x}_\kappa(\boldsymbol{\xi}) \in Q^p(\mathrm{I}^2), \forall \kappa \in \Omega_h\right\},$$

where $Q^p(\mathrm{I}^2)$ denotes the space of polynomials over the reference element I^2 formed by the tensor product of polynomials of degree at most p in each direction. The approximate solution reads

$$\mathbf{u}_h(\mathbf{x}, t) := \sum_{i,j=0}^{p} \phi_\kappa^{ij}(\mathbf{x})\mathbf{U}_\kappa^{ij}(t) \quad \forall \mathbf{x} \in \kappa, \quad \kappa \in \Omega_h, \quad t \geqslant 0, \tag{16}$$

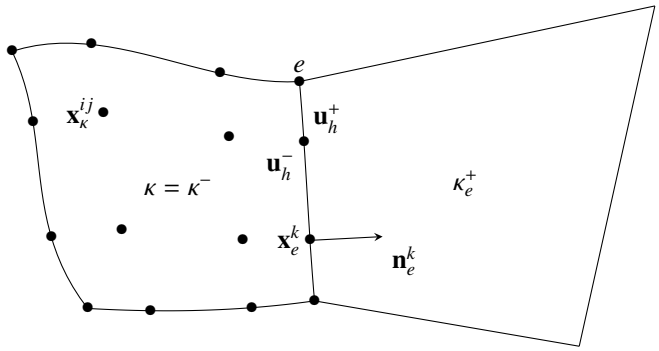

Figure 1: Notations for the mesh in two space dimensions: cell $\kappa \in \Omega_h$ with quadrature points $\mathbf{x}_\kappa^{ij}$ (bullets •), edge $e \in \partial\kappa$ with quadrature point $\mathbf{x}_e^k$, associated unit outward normal $\mathbf{n}_e^k$, and traces of the approximate solution $\mathbf{u}_h^\pm$ on e; adjacent cell κ_e^+ sharing edge e.

where $\{\phi_\kappa^{ij}\}_{0\leqslant i,j\leqslant p}$ constitutes a basis of $\mathcal{V}_h^p$ restricted onto κ, with dimension $(p+1)^2$, and $\{\mathbf{U}_\kappa^{ij}\}_{0\leqslant i,j\leqslant p}$ are the DOFs. Let $\ell_{0\leqslant k\leqslant p}$ denote the Lagrange interpolation polynomials associated to the Gauss-Lobatto nodes over I: $-1 = \xi_0 < \xi_1 < \cdots < \xi_p = 1$. We define the basis functions as the tensor products of these polynomials:

$$\phi_\kappa^{ij}(\mathbf{x}) = \phi^{ij}(\mathbf{x}_\kappa(\boldsymbol{\xi})) = \ell_i(\xi)\ell_j(\eta), \quad 0 \leqslant i, j \leqslant p, \tag{17}$$

which satisfy the following cardinality relation

$$\phi_\kappa^{ij}(\mathbf{x}_\kappa^{i'j'}) = \phi_\kappa^{ij}(\mathbf{x}_\kappa(\boldsymbol{\xi}_{i'j'})) = \ell_i(\xi_{i'})\ell_j(\eta_{j'}) = \delta_{ii'}\delta_{jj'}, \quad 0 \leqslant i, i', j, j' \leqslant p, \tag{18}$$

where $\delta_{ii'}$ is the Kronecker delta. The DOFs are therefore point values of the solution: $\mathbf{U}_\kappa^{ij}(t) = \mathbf{u}_h(\mathbf{x}_\kappa^{ij}, t)$. Likewise, the elements κ are interpolated on the same grid of quadrature points as the numerical solution, i.e., $\mathbf{x}_\kappa(\boldsymbol{\xi}) = \sum_{0\leqslant i,j\leqslant p} \ell_i(\xi)\ell_j(\eta)\mathbf{x}_\kappa^{ij}$ and $\mathbf{x}_e(\xi) = \sum_{k=0}^p \ell_i(\xi)\mathbf{x}_e^k$ (see Figure 1).

The integrals over elements and interfaces are approximated by using Gauss-Lobatto quadrature rules where the quadrature and interpolation points are collocated:

$$\int_\kappa f(\mathbf{x})\mathrm{d}V \approx \sum_{i,j=0}^p \omega_i\omega_j J_\kappa^{ij} f(\mathbf{x}_\kappa^{ij}), \qquad \int_e f(\mathbf{x})dS \approx \sum_{k=0}^p \omega_k J_e^k f(\mathbf{x}_e^k), \tag{19}$$

where $\omega_i, \omega_j > 0$ are the quadrature weights and $J_\kappa^{ij} = J_\kappa(\mathbf{x}_\kappa^{ij}) = |\nabla_{\boldsymbol{\xi}}\mathbf{x}_\kappa(\boldsymbol{\xi}_{ij})|$, and $J_e^k = J_e(\mathbf{x}_e^k) = |\nabla_\xi \mathbf{x}_e(\xi_k)|$. The cell-averaged solution thus reads

$$\langle\mathbf{u}\rangle_\kappa(t) := \sum_{i,j=0}^p \omega_i\omega_j \frac{J_\kappa^{ij}}{|\kappa|}\mathbf{U}_\kappa^{ij}(t) \approx \frac{1}{|\kappa|}\int_\kappa \mathbf{u}_h(\mathbf{x}, t)\mathrm{d}V, \tag{20}$$

where $|\kappa| = \sum_{i,j=0}^p \omega_i\omega_j J_\kappa^{ij}$ is the volume of the cell κ.

We also introduce the discrete difference matrix with entries

$$D_{ik} = \ell_k'(\xi_i), \quad 0 \leqslant i, k \leqslant p, \tag{21}$$

where the property $\sum_{l=0}^p \ell_l \equiv 1$ implies

$$\sum_{l=0}^p D_{kl} = 0 \quad \forall 0 \leqslant k \leqslant p. \tag{22}$$

The discrete difference matrix is known to satisfy the SBP property [39]:

$$\omega_k D_{kl} + \omega_l D_{lk} = \delta_{kp}\delta_{lp} - \delta_{k0}\delta_{l0} \quad \forall 0 \leqslant k, l \leqslant p. \tag{23}$$

Finally, the discretization is assumed to satisfy the following metric identities [38]

$$\sum_{k=0}^{p} D_{ik} J_\kappa^{kj} \nabla_{\mathbf{x}} \xi(\mathbf{x}_\kappa^{kj}) + D_{jk} J_\kappa^{ik} \nabla_{\mathbf{x}} \eta(\mathbf{x}_\kappa^{ik}) = 0 \quad \forall 0 \leqslant i, j \leqslant p, \tag{24}$$

and volume and edge metric terms are related by

$$J_\kappa^{pj} \nabla \xi(\mathbf{x}_\kappa^{pj}) = J_e(\mathbf{x}_\kappa^{pj}) \mathbf{n}_e(\mathbf{x}_\kappa^{pj}), \quad J_\kappa^{0j} \nabla \xi(\mathbf{x}_\kappa^{0j}) = -J_e(\mathbf{x}_\kappa^{0j}) \mathbf{n}_e(\mathbf{x}_\kappa^{0j}), \quad J_\kappa^{ip} \nabla \eta(\mathbf{x}_\kappa^{ip}) = J_e(\mathbf{x}_\kappa^{ip}) \mathbf{n}_e(\mathbf{x}_\kappa^{ip}), \quad J_\kappa^{i0} \nabla \eta(\mathbf{x}_\kappa^{i0}) = -J_e(\mathbf{x}_\kappa^{i0}) \mathbf{n}_e(\mathbf{x}_\kappa^{i0}), \tag{25}$$

for $0 \leqslant i, j \leqslant p$, where $\mathbf{n}_e$ denotes the unit normal to e in $\partial\kappa$ pointing outward from κ (see Figure 1).

3.2. Semi-discrete form

Following [23, 14, 47], we multiply (1a) with a test function $v_h \in \mathcal{V}_h^p$ and perform double integration-by-parts to get the semi-discrete weak form of (1a): find $\mathbf{u}_h$ in $(\mathcal{V}_h^p)^{n_{eq}}$ such that

$$\sum_{\kappa \in \Omega_h} \int_\kappa v_h \Big(\partial_t \mathbf{u}_h + \nabla_{\mathbf{x}} \cdot \mathbf{f}(\mathbf{u}_h) + \mathbf{c}(\mathbf{u}_h) \nabla_{\mathbf{x}} \mathbf{u}_h \Big) \mathrm{d}V + \sum_{e \in \mathcal{E}_h} \int_e v_h^- \mathbf{D}^-(\mathbf{u}_h^-, \mathbf{u}_h^+, \mathbf{n}_e) + v_h^+ \mathbf{D}^+(\mathbf{u}_h^-, \mathbf{u}_h^+, \mathbf{n}_e) \mathrm{d}S = 0 \quad \forall v_h \in \mathcal{V}_h^p,$$

where $\mathbf{u}_h^\pm(\mathbf{x}, t) = \lim_{\varepsilon \downarrow 0} \mathbf{u}_h(\mathbf{x} \pm \varepsilon \mathbf{n}_e(\mathbf{x}), t)$ are the traces of $\mathbf{u}_h$ at $\mathbf{x}$ on a given cell interface $e \in \mathcal{E}_h$ (see Figure 1) and $\mathbf{D}^\pm(\cdot, \cdot, \cdot)$ are the numerical fluctuations that are applied at the interfaces and are considered under the form

$$\mathbf{D}^-(\mathbf{u}^-, \mathbf{u}^+, \mathbf{n}) = \mathbf{h}(\mathbf{u}^-, \mathbf{u}^+, \mathbf{n}) - \mathbf{f}(\mathbf{u}^-) \cdot \mathbf{n} + \mathbf{d}^-(\mathbf{u}^-, \mathbf{u}^+, \mathbf{n}), \tag{26a}$$

$$\mathbf{D}^+(\mathbf{u}^-, \mathbf{u}^+, \mathbf{n}) = \mathbf{f}(\mathbf{u}^+) \cdot \mathbf{n} - \mathbf{h}(\mathbf{u}^-, \mathbf{u}^+, \mathbf{n}) + \mathbf{d}^+(\mathbf{u}^-, \mathbf{u}^+, \mathbf{n}), \tag{26b}$$

to allow proper discretizations of each term in (1a), they satisfy the consistency relations

$$\mathbf{h}(\mathbf{u}, \mathbf{u}, \mathbf{n}) = \mathbf{f}(\mathbf{u}) \cdot \mathbf{n}, \quad \mathbf{d}^\pm(\mathbf{u}, \mathbf{u}, \mathbf{n}) = 0 \quad \forall \mathbf{u} \in \Omega_{\text{GM}}, \tag{27}$$

and will be introduced in section 5.

We then substitute v_h for the Lagrange interpolation polynomials (17) and consider the quadrature rules (19). Using the discrete difference matrix (21), the semi-discrete problem reads: find $\mathbf{u}_h$ in $(\mathcal{V}_h^p)^{n_{eq}}$ such that

$$\begin{aligned} \omega_i \omega_j J_\kappa^{ij} \frac{\mathrm{d}}{\mathrm{d}t} \mathbf{U}_\kappa^{ij} + \omega_i \omega_j J_\kappa^{ij} \sum_{k=0}^{p} \Big(D_{ik} \left(\mathbf{f}(\mathbf{U}_\kappa^{kj}) + \mathbf{c}(\mathbf{U}_\kappa^{ij}) \mathbf{U}_\kappa^{kj} \right) \nabla_{\mathbf{x}} \xi(\boldsymbol{\xi}_{ij}) + D_{jk} \left(\mathbf{f}(\mathbf{U}_\kappa^{ik}) + \mathbf{c}(\mathbf{U}_\kappa^{ij}) \mathbf{U}_\kappa^{ik} \right) \nabla_{\mathbf{x}} \eta(\boldsymbol{\xi}_{ij}) \Big) \\ + \sum_{e \in \partial\kappa} \sum_{k=0}^{p} \phi_\kappa^{ij}(\mathbf{x}_e^k) \omega_k J_e^k \mathbf{D}^- \Big(\mathbf{U}_\kappa^{ij}, \mathbf{u}_h^+(\mathbf{x}_e^k, t), \mathbf{n}_e^k \Big) \quad \forall t > 0, \quad \kappa \in \Omega_h, \quad 0 \leqslant i, j \leqslant p, \end{aligned} \tag{28}$$

where by (18) $\phi_\kappa^{ij}(\mathbf{x}_e^k) = 1$ if $\mathbf{x}_\kappa^{ij} = \mathbf{x}_e^k$ and $\phi_\kappa^{ij}(\mathbf{x}_e^k) = 0$ else.

The initial condition (1b) is projected onto the function space:

$$\mathbf{U}_\kappa^{ij}(0) = \mathbf{u}_0(x_\kappa^{ij}) \quad \forall \kappa \in \Omega_h, \quad 0 \leqslant i, j \leqslant p. \tag{29}$$

The integral over elements $\kappa \in \Omega_h$ in (28) should be modified where we replace the physical fluxes and nonconservative products with numerical fluctuations of the form [9, 10, 14, 47]

$$\mathbf{D}_X^-(\mathbf{u}^-, \mathbf{u}^+, \mathbf{n}) = \mathbf{h}_X(\mathbf{u}^-, \mathbf{u}^+, \mathbf{n}) - \mathbf{f}(\mathbf{u}^-) \cdot \mathbf{n} + \mathbf{d}_X^-(\mathbf{u}^-, \mathbf{u}^+, \mathbf{n}), \tag{30a}$$

$$\mathbf{D}_X^+(\mathbf{u}^-, \mathbf{u}^+, \mathbf{n}) = \mathbf{f}(\mathbf{u}^+) \cdot \mathbf{n} - \mathbf{h}_X(\mathbf{u}^-, \mathbf{u}^+, \mathbf{n}) + \mathbf{d}_X^+(\mathbf{u}^-, \mathbf{u}^+, \mathbf{n}), \tag{30b}$$

where the subscript X will refer to either ec or cp to denote either entropy conservative or contact preserving numerical fluctuations, respectively, that will be introduced in section 4. The modified scheme now reads

$$\begin{aligned}\omega_i\omega_j J_\kappa^{ij}\frac{\mathrm{d}}{\mathrm{d}t}\mathbf{U}_\kappa^{ij} + \omega_i\omega_j\sum_{k=0}^{p}\Big(D_{ik}\tilde{\mathbf{D}}_X(\mathbf{U}_\kappa^{ij},\mathbf{U}_\kappa^{kj},\mathbf{n}_{(i,k)j}) + D_{jk}\tilde{\mathbf{D}}_X(\mathbf{U}_\kappa^{ij},\mathbf{U}_\kappa^{ik},\mathbf{n}_{i(j,k)})\Big)\\ + \sum_{e\in\partial\kappa}\sum_{k=0}^{p}\phi_\kappa^{ij}(\mathbf{x}_e^k)\omega_k J_e^k\mathbf{D}^-\Big(\mathbf{U}_\kappa^{ij},\mathbf{u}_h^+(\mathbf{x}_e^k,t),\mathbf{n}_e^k\Big)\quad \forall t>0,\quad \kappa\in\Omega_h,\quad 0\leqslant i,j\leqslant p,\end{aligned}\tag{31}$$

where

$$\tilde{\mathbf{D}}_X(\mathbf{u}^-,\mathbf{u}^+,\mathbf{n}) := \mathbf{D}_X^-(\mathbf{u}^-,\mathbf{u}^+,\mathbf{n}) - \mathbf{D}_X^+(\mathbf{u}^+,\mathbf{u}^-,\mathbf{n}),\tag{32a}$$

$$\overset{(30)}{\underset{(22)}{=}}\mathbf{h}_X(\mathbf{u}^-,\mathbf{u}^+,\mathbf{n}) + \mathbf{h}_X(\mathbf{u}^+,\mathbf{u}^-,\mathbf{n}) + \mathbf{d}_X^-(\mathbf{u}^-,\mathbf{u}^+,\mathbf{n}) - \mathbf{d}_X^+(\mathbf{u}^+,\mathbf{u}^-,\mathbf{n}),\tag{32b}$$

and

$$\mathbf{n}_{(i,k)j} = \frac{1}{2}\Big(J_\kappa^{ij}\nabla_{\mathbf{x}}\xi(\boldsymbol{\xi}_{ij}) + J_\kappa^{kj}\nabla_{\mathbf{x}}\xi(\boldsymbol{\xi}_{kj})\Big),\quad \mathbf{n}_{i(j,k)} = \frac{1}{2}\Big(J_\kappa^{ij}\nabla_{\mathbf{x}}\eta(\boldsymbol{\xi}_{ij}) + J_\kappa^{ik}\nabla_{\mathbf{x}}\eta(\boldsymbol{\xi}_{ik})\Big)\tag{33}$$

must be introduced to keep conservation of the physical fluxes [64] and preserve uniform states.

The numerical flux and fluctuations in (30) satisfy the consistency conditions

$$\mathbf{h}_X(\mathbf{u},\mathbf{u},\mathbf{n}) = \mathbf{f}(\mathbf{u})\cdot\mathbf{n},\quad \mathbf{d}_X^\pm(\mathbf{u},\mathbf{u},\mathbf{n}) = 0\quad \forall\mathbf{u}\in\Omega_{\text{GM}},\tag{34}$$

and entropy conservative (EC) fluctuations $\mathbf{D}_{ec}^\pm(\cdot,\cdot,\cdot)$ satisfy [9]

$$\boldsymbol{\vartheta}(\mathbf{u}^-)^\top\mathbf{D}_{ec}^-(\mathbf{u}^-,\mathbf{u}^+,\mathbf{n}) + \boldsymbol{\vartheta}(\mathbf{u}^+)^\top\mathbf{D}_{ec}^+(\mathbf{u}^-,\mathbf{u}^+,\mathbf{n}) = [\![\mathbf{q}(\mathbf{u})]\!]\cdot\mathbf{n}\quad \forall\mathbf{u}^\pm\in\Omega_{\text{GM}},\tag{35}$$

where $[\![v_h]\!] = v_h^+ - v_h^-$ and $\boldsymbol{\vartheta}(\mathbf{u}) := \nabla_{\mathbf{u}}\eta(\mathbf{u})$ denotes the entropy variables. Additionally, the interface fluctuations (26) in (28) are assumed to be entropy stable:

$$\boldsymbol{\vartheta}(\mathbf{u}^-)^\top\mathbf{D}^-(\mathbf{u}^-,\mathbf{u}^+,\mathbf{n}) + \boldsymbol{\vartheta}(\mathbf{u}^+)^\top\mathbf{D}^+(\mathbf{u}^-,\mathbf{u}^+,\mathbf{n}) \geqslant [\![\mathbf{q}(\mathbf{u})]\!]\cdot\mathbf{n}\quad \forall\mathbf{u}^\pm\in\Omega_{\text{GM}}.\tag{36}$$

The theorem below summarizes the main properties of the semi-discrete scheme (31) for the discretization of general systems of the form (1a).

Theorem 3.1. *Let $\mathbf{D}_X^\pm(\cdot,\cdot,\cdot)$ in (30) be consistent fluctuations with $\mathbf{d}_X^\pm(\cdot,\cdot,\cdot)$ in (32) satisfying*

$$\mathbf{d}_X^\pm(\mathbf{u}^-,\mathbf{u}^+,\mathbf{n}) = C^\pm(\mathbf{u}^-,\mathbf{u}^+,\mathbf{n})[\![\mathbf{u}]\!],\tag{37a}$$

$$C(\mathbf{u}^-,\mathbf{u}^+,\mathbf{n}) := C^+(\mathbf{u}^-,\mathbf{u}^+,\mathbf{n}) + C^-(\mathbf{u}^-,\mathbf{u}^+,\mathbf{n}),\tag{37b}$$

$$C(\mathbf{u}^-,\mathbf{u}^+,\mathbf{n}) + C(\mathbf{u}^+,\mathbf{u}^-,\mathbf{n}) = \Big(\boldsymbol{c}(\mathbf{u}^-) + \mathbf{c}(\mathbf{u}^+)\Big)\mathbf{n},\tag{37c}$$

$$C(\mathbf{u},\mathbf{u},\mathbf{n}) = \mathbf{c}(\mathbf{u})\mathbf{n},\tag{37d}$$

where $\mathbf{n} = (n_1,\ldots,n_d)^\top$, $\mathbf{c}(\mathbf{u})\mathbf{n} = \sum_{i=1}^d n_i\mathbf{c}_i(\mathbf{u})$, and $[\![\mathbf{u}]\!] = \mathbf{u}^+ - \mathbf{u}^-$, and let $\mathbf{D}^-(\cdot,\cdot,\cdot)$ in (28) be consistent (27) fluctuations. Then, the semi-discrete scheme (31) has the following properties:

(i) it is a high-order accurate approximation of smooth enough solutions to (1);

(ii) it preserves uniform states (free-stream preservation);

(iii) the cell-averaged solution (20) satisfies the following cell-averaged semi-discrete scheme

$$\begin{aligned}|\kappa|\frac{\mathrm{d}}{\mathrm{d}t}\langle\mathbf{u}_h\rangle_\kappa(t) + \sum_{i,j,k=0}^{p}\omega_i\omega_j\Big(D_{ik}\mathbf{c}(\mathbf{U}_\kappa^{ij})\mathbf{n}_{(i,k)j}\mathbf{U}_\kappa^{kj} + D_{jk}\mathbf{c}(\mathbf{U}_\kappa^{ij})\mathbf{n}_{i(j,k)}\mathbf{U}_\kappa^{ik}\Big)\\ + \sum_{e\in\partial\kappa}\sum_{k=0}^{p}\omega_k J_e^k\Big(\mathbf{h}\Big(\mathbf{u}_h^-(\mathbf{x}_e^k,t),\mathbf{u}_h^+(\mathbf{x}_e^k,t),\mathbf{n}_e^k\Big) + \mathbf{d}^-\Big(\mathbf{u}_h^-(\mathbf{x}_e^k,t),\mathbf{u}_h^+(\mathbf{x}_e^k,t),\mathbf{n}_e^k\Big)\Big)\quad \forall t>0,\quad \kappa\in\Omega_h,\end{aligned}\tag{38}$$

which ensures a discretely conservative approximation of the physical fluxes in (1a);

(iv) if the fluctuations $\mathbf{D}_X(\cdot,\cdot,\cdot)$ in the volume integral are further assumed to be EC (35) and the fluctuations at interfaces $\mathbf{D}(\cdot,\cdot,\cdot)$ are entropy stable (36) for a convex entropy pair $(\eta(\mathbf{u}),\mathbf{q}(\mathbf{u}))$, then the following semi-discrete entropy inequality holds:

$$|\kappa|\frac{\mathrm{d}}{\mathrm{d}t}\langle\eta(\mathbf{u}_h)\rangle_\kappa + \sum_{e\in\partial\kappa}\sum_{k=0}^{p}\omega_k J_e^k Q\Big(\mathbf{u}_h^-(\mathbf{x}_e^k,t),\mathbf{u}_h^+(\mathbf{x}_e^k,t),\mathbf{n}_e^k\Big) \leqslant 0 \quad \forall t>0, \quad \kappa\in\Omega_h, \tag{39}$$

with the consistent and conservative entropy flux

$$Q(\mathbf{u}^-,\mathbf{u}^+,\mathbf{n}) = \frac{1}{2}\Big(\mathbf{q}(\mathbf{u}^-)+\mathbf{q}(\mathbf{u}^+)\Big)\cdot\mathbf{n} + \frac{1}{2}\boldsymbol{\vartheta}(\mathbf{u}^-)^\top\mathbf{D}^-(\mathbf{u}^-,\mathbf{u}^+,\mathbf{n}) - \frac{1}{2}\boldsymbol{\vartheta}(\mathbf{u}^+)^\top\mathbf{D}^+(\mathbf{u}^-,\mathbf{u}^+,\mathbf{n}). \tag{40}$$

Proof. Preliminary: By the metric identities (24) and (22), the metric terms in (33) satisfy

$$\sum_{k=0}^{p} D_{ik}\mathbf{n}_{(i,k)j} + D_{jk}\mathbf{n}_{i(j,k)} = \frac{1}{2}\sum_{k=0}^{p} D_{ik}\Big(J_\kappa^{ij}\nabla\xi(\mathbf{x}_\kappa^{ij}) + J_\kappa^{kj}\nabla\xi(\mathbf{x}_\kappa^{kj})\Big) + D_{jk}\Big(J_\kappa^{ij}\nabla\eta(\mathbf{x}_\kappa^{ij}) + J_\kappa^{kj}\nabla\eta(\mathbf{x}_\kappa^{ik})\Big) = 0. \tag{41}$$

High-order accuracy: It is sufficient to prove that the volume integral in (31) is a high-order approximation of $\nabla\cdot\mathbf{f}(\mathbf{u})+\mathbf{c}(\mathbf{u})\nabla\mathbf{u}$ at $(\mathbf{x}_\kappa^{ij},t)$ for smooth enough solutions. High-order accuracy of the conservative term $\nabla\cdot\mathbf{f}(\mathbf{u})$ has been proved in [12, 45] and the high-order accuracy of $\mathbf{c}(\mathbf{u})\nabla\mathbf{u}$ in one space dimension has been proved in [47, Th. 3.2]. Since we are using tensor products of one-dimensional operators, the proof of accuracy follows by considering each space dimension independently.

Free-stream preservation: Let us assume that $\mathbf{U}_\kappa^{ij} = \mathbf{U}$ in the space residuals for all $\kappa\in\Omega_h$ and $0\leqslant i,j\leqslant p$, then by consistency: $\mathbf{D}^-(\mathbf{U},\mathbf{U},\mathbf{n}_e^k)=0$ and $\tilde{\mathbf{D}}_X(\mathbf{u}^-,\mathbf{u}^+,\mathbf{n}) = 2\mathbf{f}(\mathbf{U})\cdot\mathbf{n}$. Further using (41), (31) becomes

$$0 = \omega_i\omega_j J_\kappa^{ij}\frac{\mathrm{d}}{\mathrm{d}t}\mathbf{U}_\kappa^{ij} + \omega_i\omega_j\sum_{k=0}^{p} 2\mathbf{f}(\mathbf{U})(D_{ik}\mathbf{n}_{(i,k)j} + D_{jk}\mathbf{n}_{i(j,k)}) = \omega_i\omega_j J_\kappa^{ij}\frac{\mathrm{d}}{\mathrm{d}t}\mathbf{U}_\kappa^{ij}.$$

Cell-averaged semi-discrete scheme: Summing up (31) over $0\leqslant i,j\leqslant p$ gives

$$|\kappa|\frac{\mathrm{d}}{\mathrm{d}t}\langle\mathbf{u}_h\rangle_\kappa(t) + \sum_{j=0}^{p}\omega_j A_j + \sum_{i=0}^{p}\omega_i B_i + \sum_{e\in\partial\kappa}\sum_{k=0}^{p}\omega_k J_e^k\mathbf{D}^-\Big(\mathbf{u}_h^-(\mathbf{x}_e^k,t),\mathbf{u}_h^+(\mathbf{x}_e^k,t),\mathbf{n}_e^k\Big) = 0,$$

where from (32), we have

$$A_j = \sum_{i,k=0}^{p}\omega_i D_{ik}\tilde{\mathbf{D}}_X(\mathbf{U}_\kappa^{ij},\mathbf{U}_\kappa^{kj},\mathbf{n}_{(i,k)j}) = \sum_{i,k=0}^{p}\omega_i D_{ik}\Big(\mathbf{h}_X(\mathbf{U}_\kappa^{ij},\mathbf{U}_\kappa^{kj},\mathbf{n}_{(i,k)j}) + \mathbf{h}_X(\mathbf{U}_\kappa^{kj},\mathbf{U}_\kappa^{ij},\mathbf{n}_{(i,k)j}) + \mathbf{d}^-(\mathbf{U}_\kappa^{ij},\mathbf{U}_\kappa^{kj},\mathbf{n}_{(i,k)j}) - \mathbf{d}^+(\mathbf{U}_\kappa^{kj},\mathbf{U}_\kappa^{ij},\mathbf{n}_{(i,k)j})\Big)$$

$$B_i = \sum_{j,k=0}^{p}\omega_j D_{jk}\tilde{\mathbf{D}}_X(\mathbf{U}_\kappa^{ij},\mathbf{U}_\kappa^{ik},\mathbf{n}_{i(j,k)}) = \sum_{j,k=0}^{p}\omega_j D_{jk}\Big(\mathbf{h}_X(\mathbf{U}_\kappa^{ij},\mathbf{U}_\kappa^{ik},\mathbf{n}_{i(j,k)}) + \mathbf{h}_X(\mathbf{U}_\kappa^{ik},\mathbf{U}_\kappa^{ij},\mathbf{n}_{i(j,k)}) + \mathbf{d}^-(\mathbf{U}_\kappa^{ij},\mathbf{U}_\kappa^{ik},\mathbf{n}_{i(j,k)}) - \mathbf{d}^+(\mathbf{U}_\kappa^{ik},\mathbf{U}_\kappa^{ij},\mathbf{n}_{i(j,k)})\Big)$$

Let us consider the first term. Using (25), we have

$$\begin{aligned}
A_j &\overset{(23)}{\underset{(34)}{=}} J_e(\mathbf{x}_\kappa^{pj})\mathbf{f}(\mathbf{U}_\kappa^{pj})\cdot\mathbf{n}_e(\mathbf{x}_\kappa^{pj}) + J_e(\mathbf{x}_\kappa^{0j})\mathbf{f}(\mathbf{U}_\kappa^{0j})\cdot\mathbf{n}_e(\mathbf{x}_\kappa^{0j}) \\
&+ \sum_{i,k=0}^{p}\omega_i D_{ik}\mathbf{h}_X(\mathbf{U}_\kappa^{ij},\mathbf{U}_\kappa^{kj},\mathbf{n}_{(i,k)j}) - \omega_k D_{ki}\mathbf{h}_X(\mathbf{U}_\kappa^{kj},\mathbf{U}_\kappa^{ij},\mathbf{n}_{(i,k)j}) + \omega_i D_{ik}\mathbf{d}^-(\mathbf{U}_\kappa^{ij},\mathbf{U}_\kappa^{kj},\mathbf{n}_{(i,k)j}) + \omega_k D_{ki}\mathbf{d}^+(\mathbf{U}_\kappa^{kj},\mathbf{U}_\kappa^{ij},\mathbf{n}_{(i,k)j}) \\
&\overset{i\leftrightarrow k}{\underset{(37a,b)}{=}} J_e(\mathbf{x}_\kappa^{pj})\mathbf{f}(\mathbf{U}_\kappa^{pj})\cdot\mathbf{n}_e(\mathbf{x}_\kappa^{pj}) + J_e(\mathbf{x}_\kappa^{0j})\mathbf{f}(\mathbf{U}_\kappa^{0j})\cdot\mathbf{n}_e(\mathbf{x}_\kappa^{0j}) + \sum_{i,k=0}^{p}\omega_i D_{ik}C(\mathbf{U}_\kappa^{ij},\mathbf{U}_\kappa^{kj},\mathbf{n}_{(i,k)j})(\mathbf{U}_\kappa^{kj}-\mathbf{U}_\kappa^{ij}) \\
&\overset{(23)}{\underset{(37d)}{=}} J_e(\mathbf{x}_\kappa^{pj})\Big(\mathbf{f}(\mathbf{U}_\kappa^{pj})\cdot\mathbf{n}_e(\mathbf{x}_\kappa^{pj}) - \mathbf{c}(\mathbf{U}_\kappa^{pj})\mathbf{n}_e(\mathbf{x}_\kappa^{pj})\mathbf{U}_\kappa^{pj}\Big) + J_e(\mathbf{x}_\kappa^{0j})\Big(\mathbf{f}(\mathbf{U}_\kappa^{0j})\cdot\mathbf{n}_e(\mathbf{x}_\kappa^{0j}) - \mathbf{c}(\mathbf{U}_\kappa^{0j})\mathbf{n}_e(\mathbf{x}_\kappa^{0j})\mathbf{U}_\kappa^{0j}\Big) \\
&+ \sum_{i,k=0}^{p}\omega_i D_{ik}C(\mathbf{U}_\kappa^{ij},\mathbf{U}_\kappa^{kj},\mathbf{n}_{(i,k)j})\mathbf{U}_\kappa^{kj} + \omega_k D_{ki}C(\mathbf{U}_\kappa^{ij},\mathbf{U}_\kappa^{kj},\mathbf{n}_{(i,k)j})\mathbf{U}_\kappa^{ij}
\end{aligned}$$

$$
\begin{aligned}
&\underset{(37c)}{\overset{i\leftrightarrow k}{=}} J_e(\mathbf{x}_\kappa^{pj})\Big(\mathbf{f}(\mathbf{U}_\kappa^{pj})\cdot\mathbf{n}_e(\mathbf{x}_\kappa^{pj}) - \mathbf{c}(\mathbf{U}_\kappa^{pj})\mathbf{n}_e(\mathbf{x}_\kappa^{pj})\mathbf{U}_\kappa^{pj}\Big) + J_e(\mathbf{x}_\kappa^{0j})\Big(\mathbf{f}(\mathbf{U}_\kappa^{0j})\cdot\mathbf{n}_e(\mathbf{x}_\kappa^{0j}) - \mathbf{c}(\mathbf{U}_\kappa^{0j})\mathbf{n}_e(\mathbf{x}_\kappa^{0j})\mathbf{U}_\kappa^{0j}\Big)\\
&+\sum_{i,k=0}^{p}\omega_i D_{ik}\left(\mathbf{c}(\mathbf{U}_\kappa^{ij}) + \mathbf{c}(\mathbf{U}_\kappa^{kj})\right)\mathbf{n}_{(i,k)j}\mathbf{U}_\kappa^{kj}\\
&\underset{(37d)}{\overset{(23)}{=}} J_e(\mathbf{x}_\kappa^{pj})\mathbf{f}(\mathbf{U}_\kappa^{pj})\cdot\mathbf{n}_e(\mathbf{x}_\kappa^{pj}) + J_e(\mathbf{x}_\kappa^{0j})\mathbf{f}(\mathbf{U}_\kappa^{0j})\cdot\mathbf{n}_e(\mathbf{x}_\kappa^{0j}) + \sum_{i,k=0}^{p}\omega_i D_{ik}\mathbf{c}(\mathbf{U}_\kappa^{ij})\mathbf{n}_{(i,k)j}(\mathbf{U}_\kappa^{kj} - \mathbf{U}_\kappa^{ij}),
\end{aligned}
$$

where $i \leftrightarrow k$ indicates an inversion of indices i and k in some of the terms. Likewise, we have

$$
B_i = J_e(\mathbf{x}_\kappa^{ip})\mathbf{f}(\mathbf{U}_\kappa^{ip})\cdot\mathbf{n}_e(\mathbf{x}_\kappa^{ip}) + J_e(\mathbf{x}_\kappa^{i0})\mathbf{f}(\mathbf{U}_\kappa^{i0})\cdot\mathbf{n}_e(\mathbf{x}_\kappa^{i0}) + \sum_{j,k=0}^{p}\omega_j D_{jk}\mathbf{c}(\mathbf{U}_\kappa^{ij})\mathbf{n}_{i(j,k)}(\mathbf{U}_\kappa^{ik} - \mathbf{U}_\kappa^{ij}).
$$

From (41) we deduce

$$
\sum_{j=0}^{p}\omega_j A_j + \sum_{i=0}^{p}\omega_i B_i = \sum_{e\in\partial\kappa}\sum_{k=0}^{p}\omega_k J_e^k \mathbf{h}\Big(\mathbf{u}_h^-(\mathbf{x}_e^k,t)\Big)\mathbf{n}_e^k + \sum_{i,j,k=0}^{p}\omega_i\omega_j\left(D_{ik}\mathbf{c}(\mathbf{U}_\kappa^{ij})\mathbf{n}_{(i,k)j}\mathbf{U}_\kappa^{kj} + D_{jk}\mathbf{c}(\mathbf{U}_\kappa^{ij})\mathbf{n}_{i(j,k)}\mathbf{U}_\kappa^{ik}\right),
$$

and we get (38).

Entropy stability: Let us now consider EC fluxes in the volume integral in the semi-discrete DGSEM scheme (31). Left multiply (31) by $\boldsymbol{\vartheta}_\kappa^{ij} = \boldsymbol{\vartheta}(\mathbf{u}_\kappa^{ij})$ and sum up over $0 \leqslant i, j \leqslant p$ to get

$$
|\kappa|\frac{\mathrm{d}}{\mathrm{d}t}\langle\eta\rangle_\kappa(t) + \sum_{j=0}^{p}\omega_j C_j + \sum_{i=0}^{p}\omega_i E_i + \sum_{e\in\partial\kappa}\sum_{k=0}^{p}\omega_k J_e^k \boldsymbol{\vartheta}\Big(\mathbf{u}_h^-(\mathbf{x}_e^k,t)\Big)\cdot\mathbf{D}^-\Big(\mathbf{u}_h^-(\mathbf{x}_e^k,t),\mathbf{u}_h^+(\mathbf{x}_e^k,t),\mathbf{n}_e^k\Big) = 0,
$$

where

$$
C_j = \sum_{i,k=0}^{p}\omega_i D_{ik}\boldsymbol{\vartheta}_\kappa^{ij}\cdot\Big(\mathbf{D}_{ec}^-(\mathbf{U}_\kappa^{ij},\mathbf{U}_\kappa^{kj},\mathbf{n}_{(i,k)j}) - \mathbf{D}_{ec}^+(\mathbf{U}_\kappa^{kj},\mathbf{U}_\kappa^{ij},\mathbf{n}_{(i,k)j})\Big), \quad E_i = \sum_{j,k=0}^{p}\omega_j D_{jk}\boldsymbol{\vartheta}_\kappa^{ij}\cdot\Big(\mathbf{D}_{ec}^-(\mathbf{U}_\kappa^{ij},\mathbf{U}_\kappa^{ik},\mathbf{n}_{i(j,k)}) - \mathbf{D}_{ec}^+(\mathbf{U}_\kappa^{ik},\mathbf{U}_\kappa^{ij},\mathbf{n}_{i(j,k)})\Big).
$$

Using (35), we have

$$
\begin{aligned}
C_j &= \sum_{i,k=0}^{p}\omega_i D_{ik}\left(\boldsymbol{\vartheta}_\kappa^{ij}\cdot\mathbf{D}_{ec}^-(\mathbf{U}_\kappa^{ij},\mathbf{U}_\kappa^{kj},\mathbf{n}_{(i,k)j}) + \boldsymbol{\vartheta}_\kappa^{kj}\cdot\mathbf{D}_{ec}^-(\mathbf{U}_\kappa^{kj},\mathbf{U}_\kappa^{ij},\mathbf{n}_{(i,k)j}) - \Big(\mathbf{q}(\mathbf{U}_\kappa^{ij}) - \mathbf{q}(\mathbf{U}_\kappa^{kj})\Big)\cdot\mathbf{n}_{(i,k)j}\right)\\
&\underset{(34)}{\overset{(23)}{=}} J_e(\mathbf{x}_\kappa^{pj})\mathbf{q}(\mathbf{U}_\kappa^{pj})\cdot\mathbf{n}_e(\mathbf{x}_\kappa^{pj}) + J_e(\mathbf{x}_\kappa^{0j})\mathbf{q}(\mathbf{U}_\kappa^{0j})\cdot\mathbf{n}_e(\mathbf{x}_\kappa^{0j})\\
&+\sum_{i,k=0}^{p}\omega_i D_{ik}\boldsymbol{\vartheta}_\kappa^{ij}\cdot\mathbf{D}_{ec}^-(\mathbf{U}_\kappa^{ij},\mathbf{U}_\kappa^{kj},\mathbf{n}_{(i,k)j}) - \omega_k D_{ki}\boldsymbol{\vartheta}_\kappa^{kj}\cdot\mathbf{D}_{ec}^-(\mathbf{U}_\kappa^{kj},\mathbf{U}_\kappa^{ij},\mathbf{n}_{(i,k)j}) - \Big(\omega_i D_{ik}\mathbf{q}(\mathbf{U}_\kappa^{ij}) + \omega_k D_{ki}\mathbf{q}(\mathbf{U}_\kappa^{kj})\Big)\cdot\mathbf{n}_{(i,k)j}\\
&\underset{(22)}{\overset{i\leftrightarrow k}{=}} J_e(\mathbf{x}_\kappa^{pj})\mathbf{q}(\mathbf{U}_\kappa^{pj})\cdot\mathbf{n}_e(\mathbf{x}_\kappa^{pj}) + J_e(\mathbf{x}_\kappa^{0j})\mathbf{q}(\mathbf{U}_\kappa^{0j})\cdot\mathbf{n}_e(\mathbf{x}_\kappa^{0j}) - \sum_{i,k=0}^{p}\omega_i D_{ik}J_\kappa^{kj}\mathbf{q}(\mathbf{U}_\kappa^{ij})\nabla\xi(\mathbf{x}_\kappa^{kj}).
\end{aligned}
$$

Likewise

$$
E_i = J_e(\mathbf{x}_\kappa^{ip})\mathbf{q}(\mathbf{U}_\kappa^{ip})\cdot\mathbf{n}_e(\mathbf{x}_\kappa^{ip}) + J_e(\mathbf{x}_\kappa^{i0})\mathbf{q}(\mathbf{U}_\kappa^{i0})\cdot\mathbf{n}_e(\mathbf{x}_\kappa^{i0}) - \sum_{j,k=0}^{p}\omega_j D_{jk}J_\kappa^{ik}\mathbf{q}(\mathbf{U}_\kappa^{ij})\nabla\eta(\mathbf{x}_\kappa^{ik}),
$$

and again using the metric identities (24), we get

$$
|\kappa|\frac{\mathrm{d}}{\mathrm{d}t}\langle\eta\rangle_\kappa(t) + \sum_{e\in\partial\kappa}\sum_{k=0}^{p}\omega_k J_e^k\left(\boldsymbol{\vartheta}(\mathbf{x}_e^k)\cdot\mathbf{D}^-\Big(\mathbf{u}_h^-(\mathbf{x}_e^k,t),\mathbf{u}_h^+(\mathbf{x}_e^k,t),\mathbf{n}_e^k\Big) + \mathbf{q}\Big(\mathbf{u}_h^-(\mathbf{x}_e^k,t)\Big)\cdot\mathbf{n}_e^k\right) = 0.
$$

Then, using (40) we have

$$\boldsymbol{\vartheta}^- \cdot \mathbf{D}^-(\mathbf{u}^-, \mathbf{u}^+, \mathbf{n}) + \mathbf{q}^- \cdot \mathbf{n} = Q(\mathbf{u}^-, \mathbf{u}^+, \mathbf{n}) + \frac{1}{2}(\mathbf{q}^- - \mathbf{q}^+) \cdot \mathbf{n} + \frac{1}{2}\boldsymbol{\vartheta}^- \cdot \mathbf{D}^-(\mathbf{u}^-, \mathbf{u}^+, \mathbf{n}) + \frac{1}{2}\boldsymbol{\vartheta}^+ \cdot \mathbf{D}^+(\mathbf{u}^-, \mathbf{u}^+, \mathbf{n})$$

and since the sum of the three last terms are non-negative by (36), we obtain the desired entropy inequality (39). □

Remark 3.1. *Fluctuations with the following expressions fall into the category (37a):*

$$C^{\pm}(\mathbf{u}^-, \mathbf{u}^+, \mathbf{n}) = \frac{1}{2}\Big(\alpha \mathbf{c}(\mathbf{u}^{\pm}) + (1-\alpha)\mathbf{c}(\mathbf{u}^{\mp})\Big)\mathbf{n}, \quad 0 \leqslant \alpha \leqslant 1,$$

which belong to the Volpert path family of schemes [61] and correspond to the skew-symmetric splitting $\alpha \mathbf{c}\nabla\mathbf{u} + (1-\alpha)(\nabla \cdot (\mathbf{c}\mathbf{u}) - (\nabla \cdot \mathbf{c})\mathbf{u})$ *of the nonconservative product. Relations (37b) and (37d) indeed correspond to the consistency condition of the Volpert path family of schemes [61], while (37c) is only necessary to get (38) which will be useful to prove Theorem 6.1.*

In the next two sections, we describe the fluctuations we use in the DGSEM scheme (31) for the discretization of the SG-gamma model (1) and (2). In section 4, we first focus on designing CP and EC fluctuations that are applied in the volume integral. We then design in section 5 a HLLC approximate Riemann solver for (1a) that is applied at interfaces.

4. Numerical fluctuations for the volume integrals

In this section we focus on numerical fluctuations (30) for the scheme (31) that will be applied in the volume integrals. We will make use of the Leibniz identities, which we recall here: let $a^+, a^-, b^+, b^-, c^+, c^-$ in $\mathbb{R}$ and have finite values, then we have

$$[\![ab]\!] = \overline{a}[\![b]\!] + \overline{b}[\![a]\!], \quad [\![abc]\!] = \overline{a}\Big(\overline{b}[\![c]\!] + \overline{c}[\![b]\!]\Big) + \overline{bc}[\![a]\!], \tag{42}$$

where $\overline{a} = \dfrac{a^+ + a^-}{2}$ is the arithmetic mean and $[\![a]\!] = a^+ - a^-$ the jump.

4.1. Contact preserving numerical fluxes

Here, we focus on deriving conditions that will ensure that the numerical fluxes maintain uniform pressure and velocity profiles across an isolated material interface. To this purpose, we introduce CP fluctuations in (30), with index cp, where $\mathbf{h}_{cp}(\mathbf{u}^-, \mathbf{u}^+, \mathbf{n}) = (h^{\rho}_{cp}, \mathbf{h}^{\rho\mathbf{v}\top}_{cp}, h^{\rho E}_{cp}, 0, 0)^\top$ is the vector of numerical fluxes for the conservative equations of mass, momentum and energy, and $\mathbf{d}^{\pm}_{cp}(\mathbf{u}^-, \mathbf{u}^+, \mathbf{n}) = (0, 0, 0, d^{\pm}_{\Gamma}, d^{\pm}_{\Pi})^\top$ is the vector for the fluctuations for the nonconservative products in (1a).

For the sake of brevity, we here focus on volume fluctuations only, though the same relations may be derived for the interface fluctuations by following the same lines (see section 5.4.2). Instead of using the symmetrizer in (32), we assume that the numerical fluxes are symmetric: $\mathbf{h}_X(\mathbf{u}^-, \mathbf{u}^+, \mathbf{n}) = \mathbf{h}_{cp}(\mathbf{u}^+, \mathbf{u}^-, \mathbf{n})$ without loss of generality (they will be, see proposition 4.1). Let us represent the conserved and nonconserved quantities in (1a) using $A \in \{\rho, \rho\mathbf{v}, \rho E\}$ and $B \in \{\Gamma, \Pi\}$, respectively. The DGSEM scheme for (1a) now reads

$$\omega_i\omega_j J^{ij}_{\kappa}\frac{d}{dt}A^{ij}_{\kappa} + 2\omega_i\omega_j\sum_{k=0}^{p}\Big(D_{ik}\mathbf{h}^{A}_{cp}(\mathbf{U}^{ij}_{\kappa}, \mathbf{U}^{kj}_{\kappa}, \mathbf{n}_{(i,k)j}) + D_{jk}\mathbf{h}^{A}_{cp}(\mathbf{U}^{ij}_{\kappa}, \mathbf{U}^{ik}_{\kappa}, \mathbf{n}_{i(k,j)})\Big) + \sum_{e\in\partial\kappa}\sum_{k=0}^{p}\phi^{ij}_{\kappa}(\mathbf{x}^k_e)\omega_k J^k_e \mathbf{D}^-_A\Big(\mathbf{U}^{ij}_{\kappa}, \mathbf{u}^+_h(\mathbf{x}^k_e, t), \mathbf{n}^k_e\Big) \tag{43a}$$

$$\begin{aligned}\omega_i\omega_j J^{ij}_{\kappa}\frac{d}{dt}B^{ij}_{\kappa} &+ \omega_i\omega_j\sum_{k=0}^{p}\Big(D_{ik}\Big(\mathbf{d}^{B,-}_{cp}(\mathbf{U}^{ij}_{\kappa}, \mathbf{U}^{kj}_{\kappa}, \mathbf{n}_{(i,k)j}) - \mathbf{d}^{B,+}_{cp}(\mathbf{U}^{kj}_{\kappa}, \mathbf{U}^{ij}_{\kappa}, \mathbf{n}_{(i,k)j})\Big) + D_{jk}\Big(\mathbf{d}^{B,-}_{cp}(\mathbf{U}^{ij}_{\kappa}, \mathbf{U}^{ik}_{\kappa}, \mathbf{n}_{i(k,j)}) - \mathbf{d}^{B,+}_{cp}(\mathbf{U}^{ik}_{\kappa}, \mathbf{U}^{ij}_{\kappa}, \mathbf{n}_{i(k,j)})\Big)\Big)\\ &+ \sum_{e\in\partial\kappa}\sum_{k=0}^{p}\phi^{ij}_{\kappa}(\mathbf{x}^k_e)\omega_k J^k_e \mathbf{D}^-_B\Big(\mathbf{U}^{ij}_{\kappa}, \mathbf{u}^+_h(\mathbf{x}^k_e, t), \mathbf{n}^k_e\Big)\end{aligned} \tag{43b}$$

Now let us suppose that the initial condition consists of a material interface with uniform velocity, $\mathbf{v} = (u, v)^\top$, and pressure, p, and states ρ_L, Γ_L and π_L in Ω_L and ρ_R, Γ_R and π_R in Ω_R with $\overline{\Omega_L} \cup \overline{\Omega_R} = \overline{\Omega}$, then so do the DOFs. We now derive conditions for the numerical fluxes (30) to preserve the uniform states in time.

We, first, focus on the velocity state and impose the semi-discrete scheme (43) to satisfy a discrete counterpart to the differential relation $\rho \mathrm{d}\mathbf{v} = \mathrm{d}\rho\mathbf{v} - \mathbf{v}\mathrm{d}\rho = 0$. Ignoring the interface fluxes, $\omega_i\omega_j J^{ij}_\kappa \rho^{ij}_\kappa \mathrm{d}_t \mathbf{v}^{ij}_\kappa = 0$ requires

$$\omega_i\omega_j \sum_{k=0}^{p} \Big((\mathbf{h}^{\rho\mathbf{v}}_{cp}(\mathbf{U}^{ij}_\kappa, \mathbf{U}^{kj}_\kappa, \mathbf{n}_{(i,k)j}) - \mathbf{v} h^{\rho}_{cp}(\mathbf{U}^{ij}_\kappa, \mathbf{U}^{kj}_\kappa, \mathbf{n}_{(i,k)j}))D_{ik} + (\mathbf{h}^{\rho\mathbf{v}}_{cp}(\mathbf{U}^{ij}_\kappa, \mathbf{U}^{ik}_\kappa, \mathbf{n}_{i(k,j)}) - \mathbf{v} h^{\rho}_{cp}(\mathbf{U}^{ij}_\kappa, \mathbf{U}^{ik}_\kappa, \mathbf{n}_{i(k,j)}))D_{jk} \Big) = 0,$$

and a sufficient condition reads

$$\mathbf{h}^{\rho\mathbf{v}}_{cp}(\mathbf{u}^-, \mathbf{u}^+, \mathbf{n}) = \tilde{\mathbf{v}}(\mathbf{u}^-, \mathbf{u}^+) h^{\rho}_{cp}(\mathbf{u}^-, \mathbf{u}^+, \mathbf{n}) + \tilde{\mathrm{p}}(\mathbf{u}^-, \mathbf{u}^+, \mathbf{n}) \quad \forall \mathbf{u}^\pm \in \Omega_{\text{GM}}, \tag{44}$$

where $\tilde{\mathbf{v}}$ and $\tilde{\mathrm{p}}$ are any consistent discretizations of the velocity vector and pressure. Similarly, a semi-discrete equation for the pressure (5) can be obtained by using $\Gamma \mathrm{d}\mathrm{p} = \mathrm{d}\rho E - (\frac{1}{2}\mathbf{v}\cdot\mathbf{v})\mathrm{d}\rho - \mathrm{p}\mathrm{d}\Gamma - \mathrm{d}\Pi$ from (6), and again ignoring surface contributions in (43), $\omega_i\omega_j J^{ij}_\kappa \Gamma^{ij}_\kappa \mathrm{d}_t \mathrm{p}(\mathbf{U}^{ij}_\kappa) = 0$ requires

$$\begin{aligned}
\omega_i\omega_j \sum_{k=0}^{p} D_{ik} \Big(& 2h^{\rho E}_{cp}(\mathbf{U}^{ij}_\kappa, \mathbf{U}^{kj}_\kappa, \mathbf{n}_{(i,k)j}) - \mathbf{v}\cdot\mathbf{v} h^{\rho}_{cp}(\mathbf{U}^{ij}_\kappa, \mathbf{U}^{kj}_\kappa, \mathbf{n}_{(i,k)j}) - \mathrm{p}\left(d^-_\Gamma(\mathbf{U}^{ij}_\kappa, \mathbf{U}^{kj}_\kappa, \mathbf{n}_{(i,k)j}) - d^+_\Gamma(\mathbf{U}^{kj}_\kappa, \mathbf{U}^{ij}_\kappa, \mathbf{n}_{(i,k)j}) \right) \\
& - d^-_\Pi(\mathbf{U}^{ij}_\kappa, \mathbf{U}^{kj}_\kappa, \mathbf{n}_{(i,k)j}) + d^+_\Pi(\mathbf{U}^{kj}_\kappa, \mathbf{U}^{ij}_\kappa, \mathbf{n}_{(i,k)j}) \Big) \\
& + D_{jk} \Big(2h^{\rho E}_{cp}(\mathbf{U}^{ij}_\kappa, \mathbf{U}^{ik}_\kappa, \mathbf{n}_{i(k,j)}) - \mathbf{v}\cdot\mathbf{v} h^{\rho}_{cp}(\mathbf{U}^{ij}_\kappa, \mathbf{U}^{ik}_\kappa, \mathbf{n}_{i(j,k)}) - \mathrm{p}\left(d^-_\Gamma(\mathbf{U}^{ij}_\kappa, \mathbf{U}^{ik}_\kappa, \mathbf{n}_{i(k,j)}) - d^+_\Gamma(\mathbf{U}^{ik}_\kappa, \mathbf{U}^{ij}_\kappa, \mathbf{n}_{i(k,j)}) \right) \\
& - d^-_\Pi(\mathbf{U}^{ij}_\kappa, \mathbf{U}^{ik}_\kappa, \mathbf{n}_{i(k,j)}) + d^+_\Pi(\mathbf{U}^{ik}_\kappa, \mathbf{U}^{ij}_\kappa, \mathbf{n}_{i(k,j)}) \Big) = 0,
\end{aligned}$$

and subtracting the trivial quantity $2\omega_i\omega_j \sum_{k=0}^{p} \left(\mathbf{f}^{\rho E}(\mathbf{U}^{ij}_\kappa) - \frac{\mathbf{v}\cdot\mathbf{v}}{2}\mathbf{f}^{\rho}(\mathbf{U}^{ij}_\kappa) \right) \cdot (D_{ik}\mathbf{n}_{(i,k)j} + D_{jk}\mathbf{n}_{i(j,k)}) = 0$, from (41), a sufficient condition reads

$$\begin{aligned}
h^{\rho E}_{cp}(\mathbf{u}^-, \mathbf{u}^+, \mathbf{n}) - (\rho E^- + \mathrm{p})\mathbf{v}\cdot\mathbf{n} = \frac{\mathbf{v}\cdot\mathbf{v}}{2}\Big(& h^{\rho}_{cp}(\mathbf{u}^-, \mathbf{u}^+, \mathbf{n}) - \rho^- \mathbf{v}\cdot\mathbf{n} \Big) \\
& + \frac{\mathrm{p}}{2}\left(d^-_\Gamma(\mathbf{u}^-, \mathbf{u}^+, \mathbf{n}) - d^+_\Gamma(\mathbf{u}^+, \mathbf{u}^-, \mathbf{n}) \right) + \frac{1}{2}\Big(d^-_\Pi(\mathbf{u}^-, \mathbf{u}^+, \mathbf{n}) - d^+_\Pi(\mathbf{u}^+, \mathbf{u}^-, \mathbf{n}) \Big).
\end{aligned} \tag{45}$$

We can now propose CP fluxes for the volume integral.

Proposition 4.1. *Numerical fluxes of the form (30) where*

$$\mathbf{h}_{cp}(\mathbf{u}^-, \mathbf{u}^+, \mathbf{n}) = \begin{pmatrix} \overline{\rho}\,\overline{\mathbf{v}}\cdot\mathbf{n} \\ \overline{\rho}\,\overline{\mathbf{v}}\,\overline{\mathbf{v}}\cdot\mathbf{n} + \overline{\mathrm{p}}\mathbf{n} \\ (\overline{\rho E} + \overline{\mathrm{p}})\overline{\mathbf{v}}\cdot\mathbf{n} \\ 0 \\ 0 \end{pmatrix}, \quad \mathbf{d}^\pm_{cp}(\mathbf{u}^-, \mathbf{u}^+, \mathbf{n}) = \frac{1}{2}\mathbf{v}^\pm\cdot\mathbf{n} \begin{pmatrix} 0 \\ 0 \\ 0 \\ [\![\Gamma]\!] \\ [\![\Pi]\!] \end{pmatrix}, \tag{46}$$

preserve the uniform pressure and velocity fields across contact discontinuities and material interfaces for the SG-gamma model (1a) and (2), with the mixture EOS (5).

Proof. Checking that condition (44) holds for (46) is direct, wile using the mixture EOS (5), we get

$$\frac{\mathrm{p}}{2}\left(d^-_\Gamma(\mathbf{u}^-, \mathbf{u}^+, \mathbf{n}) - d^+_\Gamma(\mathbf{u}^+, \mathbf{u}^-, \mathbf{n}) \right) + \frac{1}{2}\Big(d^-_\Pi(\mathbf{u}^-, \mathbf{u}^+, \mathbf{n}) - d^+_\Pi(\mathbf{u}^+, \mathbf{u}^-, \mathbf{n}) \Big) = \frac{\mathbf{v}\cdot\mathbf{n}}{2}\Big(\mathrm{p}[\![\Gamma]\!] + [\![\Pi]\!] \Big) \overset{(42)}{=} \frac{\mathbf{v}\cdot\mathbf{n}}{2}\left([\![\rho E]\!] - \frac{\mathbf{v}\cdot\mathbf{v}}{2}[\![\rho]\!] \right), \tag{47}$$

so (45) holds as well. □

Remark 4.1. *The CP numerical fluxes (46) are similar to the one proposed in [37]. Here we have modified the contributions towards the energy equation to satisfy (45).*

4.2. Entropy conservative numerical fluxes

We, now, propose EC fluxes for the SG-gamma model that are applied to the modified volume integral in (31) and, according to Theorem 3.1, these numerical fluxes will contribute to the entropy stability of the numerical scheme.

Proposition 4.2. *Consider the entropy pair (11) with (12), then fluctuations of the form (30) with*

$$\mathbf{h}_{ec}(\mathbf{u}^-,\mathbf{u}^+,\mathbf{n}) = \begin{pmatrix} \hat{\rho}\overline{\mathbf{v}}\cdot\mathbf{n} \\ \mathbf{h}_{ec}^{\rho\mathbf{v}} \\ h_{ec}^{\rho E} \\ 0 \\ 0 \end{pmatrix}, \quad \mathbf{d}_{ec}^{\pm}(\mathbf{u}^-,\mathbf{u}^+,\mathbf{n}) = \frac{1}{2}\mathbf{v}^{\pm}\cdot\mathbf{n}\begin{pmatrix} 0 \\ 0 \\ 0 \\ [\![\Gamma]\!] \\ [\![\Pi]\!] \end{pmatrix}, \tag{48}$$

where

$$\mathbf{h}_{ec}^{\rho\mathbf{v}}(\mathbf{u}^-,\mathbf{u}^+,\mathbf{n}) = \hat{\rho}(\overline{\mathbf{v}}\cdot\mathbf{n})\overline{\mathbf{v}} + \left(\overline{\rho}\overline{(\gamma-1)}\overline{\left(\frac{\mathrm{C_v}}{\zeta}\right)} - \overline{\mathrm{p}_\infty}\right)\mathbf{n}, \quad h_{ec}^{\rho E}(\mathbf{u}^-,\mathbf{u}^+,\mathbf{n}) = \left(\widehat{\left(\frac{\mathrm{C_v}}{\zeta}\right)} + \frac{\mathbf{v}^-\cdot\mathbf{v}^+}{2}\right)\hat{\rho}\overline{\mathbf{v}}\cdot\mathbf{n} + \left(\overline{\rho}\overline{(\gamma-1)}\overline{\left(\frac{\mathrm{C_v}}{\zeta}\right)}\right)\overline{\mathbf{v}}\cdot\mathbf{n},$$

and $\frac{\mathrm{C_v}}{\zeta} = \frac{\Gamma}{\rho}(\mathrm{p} + \frac{\Pi}{\Gamma+1})$ *from (15), are EC in the sense (35) when excluding material interfaces, i.e.,* $[\![\Gamma]\!] \equiv [\![\Pi]\!] \equiv 0$.

Proof. As we consider pure phases, the system (1a) is conservative and (35) reduces to the Tadmor condition [55]

$$\mathbf{h}_{ec}(\mathbf{u}^-,\mathbf{u}^+,\mathbf{n})\cdot[\![\boldsymbol{\vartheta}]\!] - [\![\boldsymbol{\psi}(\mathbf{u})]\!]\cdot\mathbf{n} = 0 \quad \forall \mathbf{u}^{\pm}\in\Omega_{\mathrm{GM}},$$

where the entropy variables $\boldsymbol{\vartheta}$ are defined in (14), and $\boldsymbol{\psi} \equiv \mathbf{f}^\top\boldsymbol{\vartheta} - \mathbf{q}$ is the entropy potential and reads

$$\boldsymbol{\psi}(\mathbf{u}) \overset{(14)}{=} -\zeta(\rho E + \mathrm{p})\mathbf{v} + \zeta\mathbf{v}(\rho\mathbf{v}\cdot\mathbf{v} + \mathrm{p}) + \left(\gamma\mathrm{C_v} - s - \zeta\frac{\mathbf{v}\cdot\mathbf{v}}{2}\right)\rho\mathbf{v} + \rho s\mathbf{v} = (\gamma\mathrm{C_v} - \zeta e)\rho\mathbf{v} = \left((\gamma-1)\mathrm{C_v}\rho - \mathrm{p}_\infty\zeta\right)\mathbf{v},$$

so

$$[\![\boldsymbol{\psi}(\mathbf{u})]\!]\cdot\mathbf{n} \overset{(42)}{=} \left(\overline{(\gamma-1)\mathrm{C_v}}[\![\rho\mathbf{v}]\!] - \overline{\mathrm{p}_\infty}[\![\zeta\mathbf{v}]\!]\right)\cdot\mathbf{n}. \tag{49}$$

Using the definition of ζ in (15), the entropy of the mixture (12) may be reformulated as

$$s = \mathrm{C_v}\ln\left(\frac{\mathrm{p}+\mathrm{p}_\infty}{\rho^\gamma}\right) = -\mathrm{C_v}\ln\zeta - (\gamma-1)\mathrm{C_v}\ln\rho + \mathrm{C_v}\ln\left((\gamma-1)\mathrm{C_v}\right), \tag{50}$$

then we have

$$\begin{aligned}
\mathbf{h}_{ec}^\top(\mathbf{u}^-,\mathbf{u}^+,\mathbf{n})[\![\boldsymbol{\vartheta}(\mathbf{u})]\!] &= [\![\gamma\mathrm{C_v} - s - \zeta\frac{\mathbf{v}\cdot\mathbf{v}}{2}]\!]\hat{\rho}\overline{\mathbf{v}}\cdot\mathbf{n} + \left(\overline{\mathbf{v}}\cdot\overline{\mathbf{v}}\hat{\rho} + \frac{(\gamma-1)\mathrm{C_v}\overline{\rho}}{\overline{\zeta}} - \mathrm{p}_\infty\right)[\![\zeta\mathbf{v}]\!]\cdot\mathbf{n} - [\![\zeta]\!]\left(\left(\frac{\mathrm{C_v}}{\hat{\zeta}} + \frac{\mathbf{v}^-\cdot\mathbf{v}^+}{2}\right)\hat{\rho} + \frac{(\gamma-1)\mathrm{C_v}}{\overline{\zeta}}\overline{\rho}\right)\overline{\mathbf{v}}\cdot\mathbf{n} \\
&\overset{(50)}{\underset{(42)}{=}} \left(\frac{[\![\zeta]\!]}{\hat{\zeta}} + (\gamma-1)\frac{[\![\rho]\!]}{\hat{\rho}}\right)\mathrm{C_v}\hat{\rho}\overline{\mathbf{v}}\cdot\mathbf{n} + [\![\zeta\mathbf{v}]\!]\left(\overline{\mathbf{v}}\cdot\overline{\mathbf{v}}\hat{\rho} + \frac{(\gamma-1)\mathrm{C_v}\overline{\rho}}{\overline{\zeta}} - \mathrm{p}_\infty\right)\cdot\mathbf{n} \\
&\quad - [\![\zeta]\!]\left(\left(\frac{\mathrm{C_v}}{\hat{\zeta}} + \frac{\mathbf{v}^-\cdot\mathbf{v}^+}{2}\right)\hat{\rho} + \frac{(\gamma-1)\mathrm{C_v}}{\overline{\zeta}}\overline{\rho}\right)\overline{\mathbf{v}}\cdot\mathbf{n} \\
&= \left((\gamma-1)\mathrm{C_v}[\![\rho\mathbf{v}]\!] - \mathrm{p}_\infty[\![\zeta\mathbf{v}]\!]\right)\cdot\mathbf{n},
\end{aligned}$$

which cancels out with (49), so the proof is complete. □

5. An HLLC Riemann solver for the cell interfaces

We now look for two-point numerical fluctuations at interfaces and design an HLLC approximate Riemann solver for the SG-gamma model (1a) and analyze its properties. For the sake of generality, we assume that the entropy $\eta(\mathbf{u})$ in (9) is convex, which excludes material interfaces.

5.1. One-dimensional Riemann problem

We are interested in approximating solutions to the following Riemann problem in a given unit direction $\mathbf{n}$ in $\mathbb{R}^d$:

$$\partial_t \mathbf{u} + \partial_x \mathbf{f}(\mathbf{u}) \cdot \mathbf{n} + \mathbf{c}_\mathbf{n}(\mathbf{u}) \partial_x \mathbf{u} = 0, \tag{51a}$$

where $x = \mathbf{x} \cdot \mathbf{n}$ and $\mathbf{c}_\mathbf{n}(\mathbf{u}) = \mathbf{c}(\mathbf{u})\mathbf{n} = \sum_{i=1}^d n_i \mathbf{c}_i(\mathbf{u})$, together with initial data

$$\mathbf{u}_0(x) = \begin{cases} \mathbf{u}_L, & x < 0, \\ \mathbf{u}_R, & x > 0. \end{cases} \tag{51b}$$

By $\mathcal{W}(\frac{x}{t}, \mathbf{u}_L, \mathbf{u}_R, \mathbf{n})$ we denote the exact entropy weak solution to (51) for $t > 0$. Following [28], we integrate (51a) over the control volume $[-\frac{h}{2}, \frac{h}{2}] \times [0, \Delta t]$ with $h > 0$ and $\Delta t > 0$ the space and time steps, respectively. Using (51b), we obtain

$$\int_{-\frac{h}{2}}^{\frac{h}{2}} \mathcal{W}\left(\frac{x}{\Delta t}; \mathbf{u}_L, \mathbf{u}_R, \mathbf{n}\right) \mathrm{d}x - \frac{h}{2}(\mathbf{u}_L + \mathbf{u}_R) + \Delta t \left(\mathbf{f}(\mathbf{u}_R) - \mathbf{f}(\mathbf{u}_L)\right) \cdot \mathbf{n} + \int_0^{\Delta t} \int_{-\frac{h}{2}}^{\frac{h}{2}} \mathbf{c}_\mathbf{n}(\mathbf{u}) \partial_x \mathbf{u} \mathrm{d}x \mathrm{d}t = 0. \tag{52}$$

Note that both Γ and Π are continuous across shocks and discontinuous across the intermediate contact wave. Let us introduce the two last components $\mathbf{e}_\Gamma = (0, 0, 0, 1, 0)^\top$ and $\mathbf{e}_\Pi = (0, 0, 0, 0, 1)^\top$ of the canonical basis in $\mathbb{R}^{n_{eq}}$, and define $u := \mathbf{v} \cdot \mathbf{n}$. By (52) and (2) we have

$$\begin{aligned}
\int_0^{\Delta t} \int_{-\frac{h}{2}}^{\frac{h}{2}} \mathbf{c}_\mathbf{n}(\mathbf{u}) \partial_x \mathbf{u} \mathrm{d}x \mathrm{d}t &= \frac{h}{2}(\mathbf{u}_L + \mathbf{u}_R) - \Delta t \left(\mathbf{f}(\mathbf{u}_R) - \mathbf{f}(\mathbf{u}_L)\right) \cdot \mathbf{n} - \int_{-\frac{h}{2}}^{\frac{h}{2}} \mathcal{W}\left(\frac{x}{\Delta t}; \mathbf{u}_L, \mathbf{u}_R, \mathbf{n}\right) \mathrm{d}x \\
&= \frac{h}{2}(\Gamma_L + \Gamma_R)\mathbf{e}_\Gamma + \frac{h}{2}(\Pi_L + \Pi_R)\mathbf{e}_\Pi - \left(\frac{h}{2} - u^\star \Delta t\right)(\Gamma_R \mathbf{e}_\Gamma + \Pi_R \mathbf{e}_\Pi) - \left(u^\star \Delta t + \frac{h}{2}\right)(\Gamma_L \mathbf{e}_\Gamma + \Pi_L \mathbf{e}_\Pi) \\
&= \Delta t u^\star \Big((\Gamma_R - \Gamma_L)\mathbf{e}_\Gamma + (\Pi_R - \Pi_L)\mathbf{e}_\Pi\Big),
\end{aligned}$$

where u_L, $u^\star$, and u_R are the normal velocity components in the left state, the star region, and the right states, respectively. The integral form for (1a) thus reads

$$\frac{1}{\Delta t} \int_{-\frac{h}{2}}^{\frac{h}{2}} \mathcal{W}\left(\frac{x}{\Delta t}; \mathbf{u}_L, \mathbf{u}_R, \mathbf{n}\right) \mathrm{d}x - \frac{h}{2\Delta t}(\mathbf{u}_L + \mathbf{u}_R) + \Big(\mathbf{f}(\mathbf{u}_R) - \mathbf{f}(\mathbf{u}_L)\Big) \cdot \mathbf{n} + u^\star \Big((\Gamma_R - \Gamma_L)\mathbf{e}_\Gamma + (\Pi_R - \Pi_L)\mathbf{e}_\Pi\Big) = 0. \tag{53}$$

Likewise integrating (9) in the direction $\mathbf{n}$ over the control volume $[-\frac{h}{2}, \frac{h}{2}] \times [0, \Delta t]$ gives

$$\frac{1}{\Delta t} \int_{-\frac{h}{2}}^{\frac{h}{2}} \eta\left(\mathcal{W}\left(\frac{x}{\Delta t}; \mathbf{u}_L, \mathbf{u}_R, \mathbf{n}\right)\right) \mathrm{d}x \mathrm{d}t - \frac{h}{2\Delta t}\Big(\eta(\mathbf{u}_L) + \eta(\mathbf{u}_R)\Big) + \mathbf{q}(\mathbf{u}_R) \cdot \mathbf{n} - \mathbf{q}(\mathbf{u}_L) \cdot \mathbf{n} \leqslant 0. \tag{54}$$

5.2. Three-point schemes and the Godunov method

It will be convenient for the analysis of the HLLC solver to consider one-dimensional three-point numerical schemes in fluctuation form [43]

$$\mathbf{U}_j^{n+1} - \mathbf{U}_j^n + \frac{\Delta t}{h}\Big(\mathbf{D}^-(\mathbf{U}_j^n, \mathbf{U}_{j+1}^n, \mathbf{n}) + \mathbf{D}^+(\mathbf{U}_{j-1}^n, \mathbf{U}_j^n, \mathbf{n})\Big) = 0, \tag{55}$$

where $\mathbf{D}^\pm(\cdot, \cdot, \cdot)$ are assumed to be consistent (27). Here, $\mathbf{U}_j^n$ approximates the cell-averaged solution in the jth cell of size h at time $t^{(n)} = n\Delta t$. In the Godunov method, the fluctuations are defined by solving exact Riemann problems (51) centered at every interface $j + \frac{1}{2}$ of coordinate $x_{j+\frac{1}{2}}$, between cells j and $j+1$ (see Figure 2), with $\mathbf{U}_j^n$ and $\mathbf{U}_{j+1}^n$ as the left and right initial data, respectively. The solution at time t^{n+1} in the jth cell is defined as the cell-average of the exact solution at $t^{(n+1)} = t^{(n)} + \Delta t$:

$$\begin{aligned}
\mathbf{U}_j^{n+1} &= \frac{1}{h}\left(\int_{x_{j-\frac{1}{2}}}^{x_j} \mathcal{W}\left(\frac{x}{\Delta t}; \mathbf{U}_{j-1}^n, \mathbf{U}_j^n, \mathbf{n}\right) \mathrm{d}x + \int_{x_j}^{x_{j+\frac{1}{2}}} \mathcal{W}\left(\frac{x}{\Delta t}; \mathbf{U}_j^n, \mathbf{U}_{j+1}^n, \mathbf{n}\right) \mathrm{d}x\right), \\
&= \mathbf{U}_j^n - \frac{\Delta t}{h}\left(\frac{h}{2\Delta t}\mathbf{U}_j^n - \frac{1}{\Delta t}\int_{x_{j-\frac{1}{2}}}^{x_j} \mathcal{W}\left(\frac{x}{\Delta t}; \mathbf{U}_{j-1}^n, \mathbf{U}_j^n, \mathbf{n}\right) \mathrm{d}x + \frac{h}{2\Delta t}\mathbf{U}_j^n - \frac{1}{\Delta t}\int_{x_j}^{x_{j+\frac{1}{2}}} \mathcal{W}\left(\frac{x}{\Delta t}; \mathbf{U}_j^n, \mathbf{U}_{j+1}^n, \mathbf{n}\right) \mathrm{d}x\right),
\end{aligned} \tag{56}$$

with $x_j = x_{j-\frac{1}{2}} + \frac{h}{2} = x_{j+\frac{1}{2}} - \frac{h}{2}$ (see Figure 2), and takes the form (55) with the fluctuations defined as

$$\mathbf{D}^-(\mathbf{u}^-,\mathbf{u}^+,\mathbf{n}) = \frac{h}{2\Delta t}\mathbf{u}^- - \frac{1}{\Delta t}\int_{-\frac{h}{2}}^{0} \mathcal{W}\left(\frac{x}{\Delta t};\mathbf{u}^-,\mathbf{u}^+,\mathbf{n}\right)\mathrm{d}x \tag{57a}$$
$$= \mathbf{f}\Big(\mathcal{W}(0;\mathbf{u}^-,\mathbf{u}^+,\mathbf{n})\Big)\cdot\mathbf{n} - \mathbf{f}(\mathbf{u}^-)\cdot\mathbf{n} + \min(u^\star,0)\Big((\Gamma_R-\Gamma_L)\mathbf{e}_\Gamma + (\Pi_R-\Pi_L)\mathbf{e}_\Pi\Big),$$

$$\mathbf{D}^+(\mathbf{u}^-,\mathbf{u}^+,\mathbf{n}) := \frac{h}{2\Delta t}\mathbf{u}^+ - \frac{1}{\Delta t}\int_{0}^{\frac{h}{2}} \mathcal{W}\left(\frac{x}{\Delta t};\mathbf{u}^-,\mathbf{u}^+,\mathbf{n}\right)\mathrm{d}x \tag{57b}$$
$$= \mathbf{f}(\mathbf{u}^+)\cdot\mathbf{n} - \mathbf{f}\Big(\mathcal{W}(0;\mathbf{u}^-,\mathbf{u}^+,\mathbf{n})\Big)\cdot\mathbf{n} + \max(u^\star,0)\Big((\Gamma_R-\Gamma_L)\mathbf{e}_\Gamma + (\Pi_R-\Pi_L)\mathbf{e}_\Pi\Big).$$

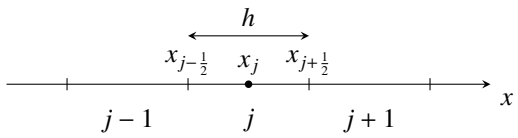

Figure 2: Notations for the mesh used for the three-point scheme (55).

Note that $\mathbf{D}^\pm(\cdot,\cdot,\cdot)$ in (57) satisfy the following path-conservation property [43]

$$\mathbf{D}^-(\mathbf{u}^-,\mathbf{u}^+,\mathbf{n}) + \mathbf{D}^+(\mathbf{u}^-,\mathbf{u}^+,\mathbf{n}) = \mathbf{f}(\mathbf{u}^+)\cdot\mathbf{n} - \mathbf{f}(\mathbf{u}^-)\cdot\mathbf{n} + u^\star(\Gamma_R-\Gamma_L)\mathbf{e}_\Gamma + u^\star(\Gamma_R-\Gamma_L)\mathbf{e}_\Pi, \tag{58}$$

for a path $\boldsymbol{\phi} : [0,1]\times\Omega_{\text{GM}}\times\Omega_{\text{GM}} \to \Omega_{\text{GM}}$ such that

$$u^\star(\Gamma_R-\Gamma_L) = \int_0^1 u\Big(\boldsymbol{\phi}(s;\mathbf{u}_L,\mathbf{u}_R)\Big)\partial_s\boldsymbol{\phi}(s;\mathbf{u}_L,\mathbf{u}_R)\cdot\mathbf{e}_\Gamma ds, \quad u^\star(\Pi_R-\Pi_L) = \int_0^1 u\Big(\boldsymbol{\phi}(s;\mathbf{u}_L,\mathbf{u}_R)\Big)\partial_s\boldsymbol{\phi}(s;\mathbf{u}_L,\mathbf{u}_R)\cdot\mathbf{e}_\Pi ds.$$

The interface Riemann problems are assumed to be noninteracting through the definition of a half CFL condition:

$$\frac{\Delta t}{h}\max_{j\in\mathbb{Z}} |\lambda|_{max}(\mathbf{U}_j^n,\mathbf{U}_{j+1}^n,\mathbf{n}) \leqslant \frac{1}{2}, \tag{59}$$

where $|\lambda|_{max}(\mathbf{u}_L,\mathbf{u}_R,\mathbf{n})$ is an upper bound of the absolute value of the signal speeds in the Riemann problem (51).

Finally, invoking a Jensen's inequality in (56) for any convex entropy function in (11), we obtain the following discrete entropy inequality [28] consistent with (9):

$$\eta(\mathbf{U}_j^{n+1}) \leqslant \eta(\mathbf{U}_j) - \frac{\Delta t}{h}\Big(Q(\mathbf{U}_j^n,\mathbf{U}_{j+1}^n,\mathbf{n}) - Q(\mathbf{U}_{j-1}^n,\mathbf{U}_j^n,\mathbf{n})\Big), \tag{60}$$

with the consistent entropy flux $Q(\mathbf{u}^-,\mathbf{u}^+,\mathbf{n}) = \mathbf{q}\left(\mathcal{W}(0;\mathbf{u}^-,\mathbf{u}^+,\mathbf{n})\right)\cdot\mathbf{n}$.

5.3. HLLC Riemann solver

The HLLC solver [60, 2] is a simple solver [8] with four uniform states separated by simple discontinuities, see Figure 3:

$$\mathcal{W}^{\text{HLLC}}\left(\frac{x}{t};\mathbf{u}_L,\mathbf{u}_R,\mathbf{n}\right) = \begin{cases} \mathbf{u}_L, & \frac{x}{t} < s_L, \\ \mathbf{u}_L^\star, & s_L < \frac{x}{t} < s^\star, \\ \mathbf{u}_R^\star, & s^\star < \frac{x}{t} < s_R, \\ \mathbf{u}_R, & s_R < \frac{x}{t}, \end{cases} \tag{61}$$

where the wave $s^\star$ approximates the speed of the intermediate contact wave. In contrast to [28], we here require an approximate consistency of the HLLC solver (61) with the integral form (53). Integrating (61) over $[-\frac{h}{2},\frac{h}{2}]$ at time Δt gives

$$\int_{-\frac{h}{2}}^{\frac{h}{2}} \mathcal{W}^{\text{HLLC}}\left(\frac{x}{\Delta t};\mathbf{u}_L,\mathbf{u}_R,\mathbf{n}\right)\mathrm{d}x = \left(\frac{h}{2} - s_R\Delta t\right)\mathbf{u}_R + \Delta t(s_R - s^\star)\mathbf{u}_R^\star + \Delta t(s^\star - s_L)\mathbf{u}_L^\star + \left(s_L\Delta t + \frac{h}{2}\right)\mathbf{u}_L, \tag{62}$$

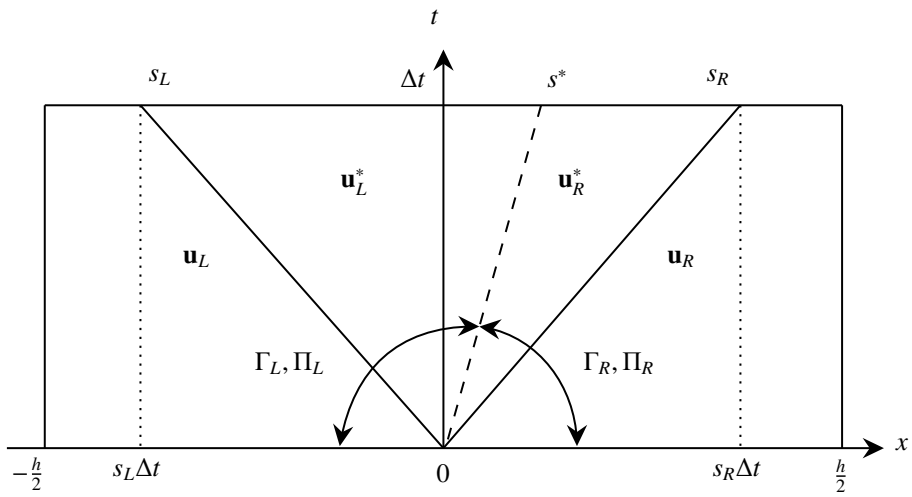

Figure 3: Wave pattern of the HLLC solver (61).

and using (53) with $\mathcal{W}^{\text{HLLC}}$ and $s^\star$ in place of $\mathcal{W}$ and $u^\star$, we obtain

$$s_R(\mathbf{u}_R^\star - \mathbf{u}_R) + s^\star(\mathbf{u}_L^\star - \mathbf{u}_R^\star) + s_L(\mathbf{u}_L - \mathbf{u}_L^\star) + \mathbf{f}(\mathbf{u}_R)\cdot\mathbf{n} - \mathbf{f}(\mathbf{u}_L)\cdot\mathbf{n} + s^\star\Big((\Gamma_R - \Gamma_L)\mathbf{e}_\Gamma + (\Pi_R - \Pi_L)\mathbf{e}_\Pi\Big) = 0. \tag{63}$$

The component on mass conservation in the above relation gives

$$\rho_R(s_R - u_R) + \rho_L(u_L - s_L) = \rho_R^\star(s_R - s^\star) + \rho_L^\star(s^\star - s_L),$$

which is satisfied by further requiring the half-consistency conditions [3] which give

$$Q_L = \rho_L(u_L - s_L) = \rho_L^\star(s^\star - s_L) > 0, \quad Q_R = \rho_R(s_R - u_R) = \rho_R^\star(s_R - s^\star) > 0, \tag{64}$$

and will be referred to as the mass fluxes [59]. Note that (64) will be shown to be important for the proof of entropy stability in section 5.4.1 are also usually invoked through the satisfaction of some jump relations across the s_L and s_R waves [60, 2] (see below).

From the approximate global consistency relation (63) we also deduce

$$\begin{aligned}
Q_R(u_R^\star - u_R) + Q_L(u_L^\star - u_L) &= \mathrm{p}_L - \mathrm{p}_R,\\
Q_R(\mathbf{v}_R^\perp - \mathbf{v}_R^{\star\perp}) + Q_L(\mathbf{v}_L^\perp - \mathbf{v}_L^{\star\perp}) &= 0,\\
Q_R(E_R^\star - E_R) + Q_L(E_L^\star - E_L) &= \mathrm{p}_L u_L - \mathrm{p}_R u_R,\\
s_R(\Gamma_R - \Gamma_R^\star) + s_L(\Gamma_L^\star - \Gamma_L) &= s^\star(\Gamma_R - \Gamma_R^\star) + s^\star(\Gamma_L^\star - \Gamma_L),\\
s_R(\Pi_R - \Pi_R^\star) + s_L(\Pi_L^\star - \Pi_L) &= s^\star(\Pi_R - \Pi_R^\star) + s^\star(\Pi_L^\star - \Pi_L),
\end{aligned}$$

where $\mathbf{v}^\perp = \mathbf{v} - u\mathbf{n}$ denotes the velocity component perpendicular to $\mathbf{n}$. The second and two latter conditions impose

$$\mathbf{v}_L^{\star\perp} = \mathbf{v}_L^\perp, \quad \mathbf{v}_R^{\star\perp} = \mathbf{v}_R^\perp, \quad \Gamma_L^\star = \Gamma_L, \quad \Gamma_R^\star = \Gamma_R, \quad \Pi_L^\star = \Pi_L, \quad \Pi_R^\star = \Pi_R, \tag{65}$$

meaning that $\mathbf{v}^\perp$, Γ, and Π are continuous across shocks and may be discontinuous across $s^\star$ in agreement with the fact that $\mathbf{v}^\perp$, Γ, and Π are associated to LD fields. The remaining unknowns can be computed by imposing the Rankine-Hugoniot relations across s_L and s_R

$$\mathbf{f}_L^\star - \mathbf{f}(\mathbf{u}_L)\cdot\mathbf{n} = s_L(\mathbf{u}_L^\star - \mathbf{u}_L), \quad \mathbf{f}_R^\star - \mathbf{f}(\mathbf{u}_R)\cdot\mathbf{n} = s_R(\mathbf{u}_R^\star - \mathbf{u}_R), \tag{66}$$

where $\mathbf{f}^\star_{X=L,R}$ means that we are considering $\mathrm{p}^\star_X$ as an unknown instead of evaluating the pressure via the EOS (5) and $\mathbf{u}^\star_X$. This leads to the following definition of the velocity in the star regions:

$$u^\star_L = u_L - \frac{\mathrm{p}^\star_L - \mathrm{p}_L}{Q_L}, \quad u^\star_R = u_R + \frac{\mathrm{p}^\star_R - \mathrm{p}_R}{Q_R}, \tag{67}$$

and to the following jump relation across the $s^\star$ wave:

$$\mathbf{f}^\star_R - \mathbf{f}^\star_L = s^\star\Big(\mathbf{u}^\star_R - \mathbf{u}^\star_L - (\Gamma_R - \Gamma_L)\mathbf{e}_\Gamma - (\Pi_R - \Pi_L)\mathbf{e}_\Pi\Big).$$

Further imposing continuity of the velocity and the pressure across the intermediate wave, $u^\star_L = u^\star_R = s^\star$ and $p^\star_L = p^\star_R = p^\star$, gives the expression for the pressure and velocity in the star region:

$$\mathrm{p}^\star = \frac{Q_L\mathrm{p}_R + Q_R\mathrm{p}_L + Q_RQ_L(u_L - u_R)}{Q_L + Q_R}, \quad s^\star = \frac{Q_Lu_L + Q_Ru_R + \mathrm{p}_L - \mathrm{p}_R}{Q_L + Q_R}. \tag{68}$$

The other states are then directly obtained:

$$\rho^\star_L = \frac{u_L - s_L}{s^\star - s_L}\rho_L, \quad e^\star_L = e_L + (s^\star - u_L)\left(\frac{s^\star - u_L}{2} - \frac{\mathrm{p}_L}{Q_L}\right), \quad E^\star_L = e^\star_L + \frac{1}{2}\mathbf{v}^\star_L\cdot\mathbf{v}^\star_L = E_L + (s^\star - u_L)\left(s^\star - \frac{\mathrm{p}_L}{Q_L}\right), \tag{69a}$$

$$\rho^\star_R = \frac{s_R - u_R}{s_R - s^\star}\rho_R, \quad e^\star_R = e_R + (s^\star - u_R)\left(\frac{s^\star - u_R}{2} + \frac{\mathrm{p}_R}{Q_R}\right), \quad E^\star_R = e^\star_R + \frac{1}{2}\mathbf{v}^\star_R\cdot\mathbf{v}^\star_R = E_R + (s^\star - u_R)\left(s^\star + \frac{\mathrm{p}_R}{Q_R}\right). \tag{69b}$$

As for the Godunov method in (57), we now define the fluctuations through

$$\mathbf{D}^-(\mathbf{u}_L,\mathbf{u}_R,\mathbf{n}) = \frac{h}{2\Delta t}\mathbf{u}_L - \frac{1}{\Delta t}\int_{-\frac{h}{2}}^{0}\mathcal{W}^{\mathrm{HLLC}}\left(\frac{x}{\Delta t};\mathbf{u}_L,\mathbf{u}_R,\mathbf{n}\right)dx, \tag{70a}$$

$$\mathbf{D}^+(\mathbf{u}_L,\mathbf{u}_R,\mathbf{n}) = \frac{h}{2\Delta t}\mathbf{u}_R - \frac{1}{\Delta t}\int_{0}^{\frac{h}{2}}\mathcal{W}^{\mathrm{HLLC}}\left(\frac{x}{\Delta t};\mathbf{u}_L,\mathbf{u}_R,\mathbf{n}\right)dx, \tag{70b}$$

and plugging (61) into (70) gives

$$\mathbf{D}^-(\mathbf{u}_L,\mathbf{u}_R,\mathbf{n}) = \begin{cases} 0, & 0 < s_L, \\ s_L(\mathbf{u}^\star_L - \mathbf{u}_L), & s_L < 0 < s^\star, \\ \mathbf{f}^\star_R - \mathbf{f}(\mathbf{u}_L)\cdot\mathbf{n} + s^\star(\Gamma_R - \Gamma_L)\mathbf{e}_\Gamma + s^\star(\Pi_R - \Pi_L)\mathbf{e}_\Pi, & s^\star < 0 < s_R, \\ \mathbf{f}(\mathbf{u}_R)\cdot\mathbf{n} - \mathbf{f}(\mathbf{u}_L)\cdot\mathbf{n} + s^\star(\Gamma_R - \Gamma_L)\mathbf{e}_\Gamma + s^\star(\Pi_R - \Pi_L)\mathbf{e}_\Pi, & s_R < 0, \end{cases} \tag{71a}$$

$$\mathbf{D}^+(\mathbf{u}_L,\mathbf{u}_R,\mathbf{n}) = \begin{cases} \mathbf{f}(\mathbf{u}_R)\cdot\mathbf{n} - \mathbf{f}(\mathbf{u}_L)\cdot\mathbf{n} + s^\star(\Gamma_R - \Gamma_L)\mathbf{e}_\Gamma + s^\star(\Pi_R - \Pi_L)\mathbf{e}_\Pi, & 0 < s_L, \\ \mathbf{f}(\mathbf{u}_R)\cdot\mathbf{n} - \mathbf{f}^\star_R + s^\star(\Gamma_R - \Gamma_L)\mathbf{e}_\Gamma + s^\star(\Pi_R - \Pi_L)\mathbf{e}_\Pi, & s_L < 0 < s^\star, \\ s_R(\mathbf{u}_R - \mathbf{u}^\star_R), & s^\star < 0 < s_R, \\ 0, & s_R < 0. \end{cases} \tag{71b}$$

Note that by construction the numerical fluxes (71) satisfy the relation

$$\mathbf{D}^-(\mathbf{u}_L,\mathbf{u}_R,\mathbf{n}) + \mathbf{D}^+(\mathbf{u}_L,\mathbf{u}_R,\mathbf{n}) = \mathbf{f}(\mathbf{u}_R)\cdot\mathbf{n} - \mathbf{f}(\mathbf{u}_L)\cdot\mathbf{n} + s^\star(\Gamma_R - \Gamma_L)\mathbf{e}_\Gamma + s^*(\Pi_R - \Pi_L)\mathbf{e}_\Pi$$

similar to the path-conservation property (58) [43]. Note that for (58) to hold, one needs $s^\star = u^\star$ which would require a root-finding algorithm to evaluate $u^\star$. We here follow another strategy where we approximate $u^\star$ by $s^\star$ in (68), this is justified by the fact that the nonconservative product is here associated to a LD field.

Finally, we define the updated cell-averaged solution as

$$\mathbf{U}^{(n+1)}_j = \frac{1}{h}\int_{x_{j-\frac{1}{2}}}^{x_j}\mathcal{W}^{\mathrm{HLLC}}\left(\frac{x}{\Delta t};\mathbf{U}^n_{j-1},\mathbf{U}^n_j,\mathbf{n}\right)dx + \frac{1}{h}\int_{x_j}^{x_{j+\frac{1}{2}}}\mathcal{W}^{\mathrm{HLLC}}\left(\frac{x}{\Delta t};\mathbf{U}^n_j,\mathbf{U}^n_{j+1},\mathbf{n}\right)dx, \tag{72}$$

so the HLLC solver may be recast into the three-point scheme form (55) with (71).

5.4. Properties of the HLLC solver

In this section, we analyse the properties of the numerical scheme (55) using fluxes (71), where the time step $\Delta t > 0$ is assumed to satisfy the CFL condition

$$\frac{\Delta t}{h} \max_{j\in\mathbb{Z}} \left(\left| s_R(\mathbf{U}_j^n, \mathbf{U}_{j+1}^n, \mathbf{n}) \right|, \left| s_L(\mathbf{U}_j^n, \mathbf{U}_{j+1}^n, \mathbf{n}) \right| \right) \leqslant \frac{1}{2}, \tag{73}$$

where the wave speeds s_L and s_R are defined in section 5.4.4.

5.4.1. Discrete entropy inequality

We are here interested in the nonlinear stability of the scheme (55) and follow [3] to use the local entropy minimum principles and first prove in Theorem 5.1 the entropy inequality in integral form (60) for the HLLC solution (61). We then prove in Lemma 5.1 that the local entropy minimum principles hold for the intermediate states.

Theorem 5.1. *Suppose that condition (73) on the time step holds and that the intermediate states in the HLLC solver (61), satisfy* $\mathbf{u}_L^\star, \mathbf{u}_R^\star \in \Omega_{\text{GM}}$ *together with the following local minimum entropy principles*

$$s(\mathbf{u}_L^\star) \geqslant s(\mathbf{u}_L), \quad s(\mathbf{u}_R^\star) \geqslant s(\mathbf{u}_R), \tag{74}$$

for the specific entropy (12). Then, the three-point scheme (55) satisfies an entropy inequality (60) with the consistent numerical flux

$$Q(\mathbf{U}_{j-1}^n, \mathbf{U}_j^n, \mathbf{n}) = \mathbf{q}(\mathbf{U}_j^n) \cdot \mathbf{n} + \frac{1}{\Delta t} \int_{x_{j-\frac{1}{2}}}^{x_j} \eta\left(\boldsymbol{\mathcal{W}}^{\text{HLLC}}\left(\frac{x}{\Delta t}; \mathbf{U}_{j-1}^n, \mathbf{U}_j^n, \mathbf{n} \right) \right) \mathrm{d}x - \frac{h}{2\Delta t} \eta\left(\mathbf{U}_j^n \right). \tag{75}$$

Proof. We first prove the entropy inequality in integral form (54) using (62), therefore, we have

$$\begin{aligned}
\int_{-\frac{h}{2}}^{\frac{h}{2}} \eta\left(\boldsymbol{\mathcal{W}}^{\text{HLLC}}\left(\frac{x}{\Delta t}; \mathbf{u}_L, \mathbf{u}_R, \mathbf{n} \right) \right) \mathrm{d}x &= \left(s_L \Delta t + \frac{h}{2} \right) \eta(\mathbf{u}_L) + (s^\star - s_L)\Delta t \eta(\mathbf{u}_L^\star) + (s_R - s^\star)\Delta t \eta(\mathbf{u}_R^\star) + \left(\frac{h}{2} - s_R \Delta t \right) \eta(\mathbf{u}_R), \\
&\overset{(11)}{=} \frac{h}{2}\Big(\eta(\mathbf{u}_L) + \eta(\mathbf{u}_R) \Big) - \Delta t \Big(s_L \rho_L s(\mathbf{u}_L) + (s^\star - s_L)\rho_L^\star s(\mathbf{u}_L^\star) \Big) - \Delta t \Big((s_R - s^\star)\rho_R^\star s(\mathbf{u}_R^\star) - s_R \rho_R s(\mathbf{u}_R) \Big), \\
&\overset{(74)}{\leqslant} \frac{h}{2}\Big(\eta(\mathbf{u}_L) + \eta(\mathbf{u}_R) \Big) - \Delta t s(\mathbf{u}_L) \Big(s_L \rho_L + (s^\star - s_L)\rho_L^\star \Big) - \Delta t \Big((s_R - s^\star)\rho_R^\star - s_R \rho_R \Big) s(\mathbf{u}_R), \\
&= \frac{h}{2}\Big(\eta(\mathbf{u}_L) + \eta(\mathbf{u}_R) \Big) - \Delta t \Big(\rho_R \mathbf{v}_R s(\mathbf{u}_R) - \rho_L \mathbf{v}_L s(\mathbf{u}_L) \Big) \cdot \mathbf{n},
\end{aligned}$$

where we have used the half-consistency conditions (64). As a consequence, setting $\mathbf{u}_L = \mathbf{U}_j^n$ and $\mathbf{u}_R = \mathbf{U}_{j+1}^n$, the numerical flux (75) satisfies

$$Q(\mathbf{U}_j^n, \mathbf{U}_{j+1}^n, \mathbf{n}) \leqslant \mathbf{q}(\mathbf{U}_j^n) \cdot \mathbf{n} - \frac{1}{h} \int_{x_j}^{x_{j+\frac{1}{2}}} \eta\left(\boldsymbol{\mathcal{W}}^{\text{HLLC}}\left(\frac{x}{\Delta t}; \mathbf{U}_j^n, \mathbf{U}_{j+1}^n, \mathbf{n} \right) \right) \mathrm{d}x + \frac{h}{2\Delta t} \eta(\mathbf{U}_j^n), \tag{76}$$

and using (72) we have the following relation through Jensen's inequality for the convex entropy function (11)

$$\begin{aligned}
\eta(\mathbf{U}_j^{n+1}) &\leqslant \frac{1}{h} \int_{x_{j-\frac{1}{2}}}^{x_j} \eta\left(\boldsymbol{\mathcal{W}}^{\text{HLLC}}\left(\frac{x}{\Delta t}; \mathbf{U}_{j-1}^n, \mathbf{U}_j^n, \mathbf{n} \right) \right) \mathrm{d}x + \frac{1}{h} \int_{x_j}^{x_{j+\frac{1}{2}}} \eta\left(\boldsymbol{\mathcal{W}}^{\text{HLLC}}\left(\frac{x}{\Delta t}; \mathbf{U}_j^n, \mathbf{U}_{j+1}^n, \mathbf{n} \right) \right) \mathrm{d}x, \\
&\underset{(76)}{\overset{(75)}{\leqslant}} \frac{\Delta t}{h} \left(Q(\mathbf{U}_{j-1}^n, \mathbf{U}_j^n, \mathbf{n}) - \mathbf{q}(\mathbf{U}_j^n) \cdot \mathbf{n} + \frac{h}{2\Delta t} \eta(\mathbf{U}_j^n)) \right) + \frac{\Delta t}{h} \left(-Q(\mathbf{U}_j^n, \mathbf{U}_{j+1}^n, \mathbf{n}) + \mathbf{q}(\mathbf{U}_j^n) \cdot \mathbf{n} + \frac{h}{2\Delta t} \eta(\mathbf{U}_j^n) \right), \\
&= \eta(\mathbf{U}_j^n) - \frac{\Delta t}{h} \Big(Q(\mathbf{U}_j^n, \mathbf{U}_{j+1}^n, \mathbf{n}) - Q(\mathbf{U}_{j-1}^n, \mathbf{U}_j^n, \mathbf{n}) \Big).
\end{aligned}$$

□

Lemma 5.1. *There exist wave speed estimates s_L and s_R large enough that: (i) bound the minimum and maximum wave speeds in the exact entropy weak solution of the Riemann problem (51), (ii) satisfy the interlacing condition $s_L < s^\star < s_R$, (iii) ensure that the local minimum entropy principles (74) hold.*

Proof. The first result (i) is obvious under the assumption that the wave speeds are finite in the exact Riemann solution. Then, (ii) and (iii) are consequences of [3, Prop. 3.2] and we now show that the required assumptions on the half domains separated by $\frac{x}{t} = s^\star$ hold, see [3, after Prop. 3.2]. This is justified here because the EOS (5) does not change accross the extreme waves s_L and s_R, hence $\frac{x}{t} = s^\star$ therefore separates domains with one unique equivalent "pure phase" and its associated physical entropy (12) which is strictly convex and satisfies the Gibbs principle (13). The required conditions across the extreme waves are: first, the half-consistency relations hold through (64); then, the following quantities must be invariant across the s_L and s_R waves [3, § 4.2]:

$$\mathrm{p}_X^\star + \frac{Q_X^2}{\rho_X^\star} = \mathrm{p}_X + \frac{Q_X^2}{\rho_X}, \quad e_X^\star - \frac{(\mathrm{p}_X^\star)^2}{2Q_X^2} = e_X - \frac{\mathrm{p}_X^2}{2Q_X^2}, \quad X = L, R.$$

The first relation is a direct consequence of (67), with $u_L^\star = u_R^\star = s^\star$:

$$\mathrm{p}_L^\star = \mathrm{p}_L + Q_L(u_L - s^\star), \quad \mathrm{p}_R^\star = \mathrm{p}_R + Q_R(s^\star - u_R),$$

and (64). For the second relation, we inject the above relations in the expression of $e_{X=L,R}^\star$ in (69) to get

$$e_X^\star - \mathrm{p}_X = \frac{\mathrm{p}_X - \mathrm{p}_X^\star}{Q_X}\left(\frac{\mathrm{p}_X - \mathrm{p}_X^\star}{2Q_X} - \frac{\mathrm{p}_X -}{Q_X}\right) = -\frac{(\mathrm{p}_X^\star)^2 - \mathrm{p}_X^2}{2Q_X}, \quad X = L, R,$$

which concludes the proof. □

We finally link the discrete entropy inequality (54) to the entropy stable character of the numerical fluctuations [9], so that the HLLC fluxes can be used at the interfaces in the DGSEM scheme to prove the semi-discrete entropy inequality established in Theorem 3.1.

Corollary 5.1. *Let a three-point scheme of the form (55) to discretize (1a). Then, the entropy inequality (60) implies the entropy stability of the numerical fluxes in the sense of (36).*

Proof. The proof relies on similar arguments as the ones used in [5, Lemma 2.8] in the conservative setting. Let $\mathbf{U}_{j-1}^n = \mathbf{U}_j^n = \mathbf{u}^-$ and $\mathbf{U}_{j+1}^n = \mathbf{u}^+$, then from (55), we obtain $\mathbf{U}_j^{n+1} = \mathbf{u}^- - \frac{\Delta t}{h}\mathbf{D}^-(\mathbf{u}^-, \mathbf{u}^+, \mathbf{n})$ and (60) gives

$$\eta\left(\mathbf{u}^- - \frac{\Delta t}{h}\mathbf{D}^-(\mathbf{u}^-, \mathbf{u}^+, \mathbf{n})\right) \leqslant \eta(\mathbf{u}^-) - \frac{\Delta t}{h}\left(Q(\mathbf{u}^-, \mathbf{u}^+, \mathbf{n}) - \mathbf{q}(\mathbf{u}^-)\cdot\mathbf{n}\right).$$

Likewise, using $\mathbf{U}_{j-1}^n = \mathbf{u}^-$ and $\mathbf{U}_j^n = \mathbf{U}_{j+1}^n = \mathbf{u}^+$, we get $\mathbf{U}_j^{n+1} = \mathbf{u}^+ - \mathbf{D}^+(\mathbf{u}^-, \mathbf{u}^+, \mathbf{n})$ and

$$\eta\left(\mathbf{u}^+ - \frac{\Delta t}{h}\mathbf{D}^+(\mathbf{u}^-, \mathbf{u}^+, \mathbf{n})\right) \leqslant \eta(\mathbf{u}^+) - \frac{\Delta t}{h}\left(\mathbf{q}(\mathbf{u}^+)\cdot\mathbf{n} - Q(\mathbf{u}^-, \mathbf{u}^+, \mathbf{n})\right).$$

Summing both equations and letting $\Delta t \to 0^+$ with fixed h, we have up to $O(\Delta t)$:

$$\eta(\mathbf{u}^-) - \frac{\Delta t}{h}\boldsymbol{\vartheta}(\mathbf{u}^-)\cdot\mathbf{D}^-(\mathbf{u}^-, \mathbf{u}^+, \mathbf{n}) + \eta(\mathbf{u}^+) - \frac{\Delta t}{h}\boldsymbol{\vartheta}(\mathbf{u}^+)\cdot\mathbf{D}^+(\mathbf{u}^-, \mathbf{u}^+, \mathbf{n}) \leqslant \eta(\mathbf{u}^-) + \eta(\mathbf{u}^+) - \frac{\Delta t}{h}\left(\mathbf{q}(\mathbf{u}^+) - \mathbf{q}(\mathbf{u}^-)\right)\cdot\mathbf{n},$$

and simplifying terms gives (36). □

Finally, as an immediate consequence of the local minimum entropy principles (74) and the definition of the updated solution (72), the HLLC solver also satisfies a discrete minimum principle on the specific physical entropy $s(\mathbf{u})$:

$$s(\mathbf{U}_j^{n+1}) \geqslant \min\left(s(\mathbf{U}_{j-1}^n), s(\mathbf{U}_j^n), s(\mathbf{U}_{j+1}^n)\right). \tag{77}$$

5.4.2. Preservation of material interfaces and pure phases

We, first, prove that the three-point scheme (55), with numerical fluxes (71), preserves material interfaces [1] by following the same analysis as in section 4.1. Let us assume that the left and right states satisfy $\mathbf{v}_L = \mathbf{v}_R = \mathbf{v}$ and $\mathrm{p}_L = \mathrm{p}_R = \mathrm{p}$, then (68) gives $\mathrm{p}^\star = \mathrm{p}$ and $s^\star = u$, respectively. As a result, the discrete requirements $\mathrm{d}\mathbf{v}\rho = \mathbf{v}\mathrm{d}\rho$ and $\mathrm{d}\rho E = (\frac{1}{2}\mathbf{v}\cdot\mathbf{v})\mathrm{d}\rho + \mathrm{p}\mathrm{d}\Gamma + \mathrm{d}\Pi$ applied to the three-point scheme (55) impose

$$D_{\rho u}^\pm = uD_\rho^\pm, \quad D_{\rho E}^\pm = \frac{\mathbf{v}\cdot\mathbf{v}}{2}D_\rho^\pm + \mathrm{p}D_\Gamma^\pm + D_\Pi^\pm, \tag{78}$$

and are obviously satisfied. Now assume that $\Gamma_L = \Gamma_R$ and $\Pi_L = \Pi_R$, then $D_\Gamma^\pm = 0$ and $D_\Pi^\pm = 0$ and the fluxes reduce to the conservative HLLC solver for the Euler equations so pure phases are preserved.

5.4.3. *Positivity of the solution*

Since the updated solution (72) is the cell-average of the superposition of approximate Riemann solutions from the HLLC solver (61), and assuming that the left and right states are positive, it is sufficient to prove positivity of the intermediate states in the Riemann solution [20]. Note that the intermediate states should be evaluated from the intermediate fluxes [2], $\mathbf{f}^\star_{X=L,R}$ in (66) since we are imposing the pressure via (68), and not evaluating it from the EOS (5), see section 5.3.

The proof for positivity of density in the star region can be directly stated following its definition in (69) since $s_L < u_L$, $u_R < s_R$ from the wave estimates in section 5.4.4, and the interlacing property $s_L < s^\star < s_R$ in Lemma 5.1. According to (7) hyperbolicity of (1a) and positivity of the solution in the star region require satisfying $\rho^\star_X e^\star_X > \mathrm{p}_{\infty_X}$, $X = L, R$, which gives for the left intermediate state:

$$
\begin{aligned}
\rho^\star_L\left(E^\star_L - \frac{(s^\star)^2}{2}\right) > \mathrm{p}_{\infty_L} &\overset{(69)}{\underset{(64)}{\Leftrightarrow}} \rho^\star_L\left(E_L + s^\star(s^\star - u_L) - (s^\star - u_L)\frac{\mathrm{p}_L}{\rho_L(s_L - u_L)} - \frac{(s^\star)^2}{2}\right) > \mathrm{p}_{\infty_L} \\
&\Leftrightarrow \rho^\star_L\left(e_L + \frac{(u_L - s^\star)^2}{2} - (s^\star - u_L)\frac{\mathrm{p}_L}{\rho_L(u_L - s_L)}\right) > \mathrm{p}_{\infty_L} \\
&\overset{(5)}{\underset{(64)}{\Leftrightarrow}} \left(\frac{u_L - s_L}{s^\star - s_L}\right)\left(\frac{\mathrm{p}_L + \gamma_L \mathrm{p}_{\infty_L}}{\gamma_L - 1}\right) + \left(\frac{u_L - s_L}{s^\star - s_L}\right)\frac{\rho_L(u_L - s^\star)^2}{2} - \left(\frac{s^\star - u_L}{s^\star - s_L}\right)\mathrm{p}_L - \mathrm{p}_{\infty_L} > 0 \\
&\overset{s^\star > s_L}{\Leftrightarrow} (u_L - s_L)\left(\frac{\mathrm{p}_L + \gamma_L \mathrm{p}_{\infty_L}}{\gamma_L - 1}\right) + (u_L - s_L)\frac{\rho_L}{2}\sigma^2 + \sigma \mathrm{p}_L - (s^\star - s_L)\mathrm{p}_{\infty_L} > 0 \\
&\Leftrightarrow (u_L - s_L)\frac{\rho_L}{2}\sigma^2 + (\mathrm{p}_L + \mathrm{p}_{\infty_L})\sigma + (u_L - s_L)\left(\frac{\mathrm{p}_L + \mathrm{p}_{\infty_L}}{\gamma_L - 1}\right) > 0,
\end{aligned}
$$

where $\sigma = u_L - s^\star$. The sign for this inequality holds for all $\sigma \in \mathbb{R}$ if the discriminant $\mathcal{D}$ of the above quadratic equation is negative:

$$
\mathcal{D} = (\mathrm{p}_L + \mathrm{p}_{\infty_L})^2 - 2\rho_L(u_L - s_L)^2\left(\frac{\mathrm{p}_L + \mathrm{p}_{\infty_L}}{\gamma_L - 1}\right)
$$

Using $\gamma_L(\mathrm{p}_L + \mathrm{p}_{\infty_L}) = \rho_L c_L^2$, $\mathcal{D} < 0$ implies $s_L < u_L - \sqrt{(\gamma_L - 1)/2\gamma_L}\, c_L$ which is satisfied by the wave speed estimates in section 5.4.4 since $\frac{\gamma_L - 1}{2\gamma_L} < 1$. A similar result holds for the right intermediate state. Note that the above relations are the same as in [2] with $\mathrm{p}_X + \mathrm{p}_{\infty_X}$ instead of p_X.

Finally, let prove positivity of Γ and Π through a discrete maximum principle. The discrete equation for $X \in \{\Gamma, \Pi\}$ in (55) with fluctuations (71) reads

$$
\begin{aligned}
X^{n+1}_j &= X^n_j - \frac{\Delta t}{h}\left(\min(s^*_{j+\frac{1}{2}}, 0)\left(X^n_{j+1} - X^n_j\right) + \max(s^*_{j-\frac{1}{2}}, 0)\left(X^n_{j-1} - X^n_j\right)\right) \\
&= \left(1 - \frac{\Delta t}{h}\left(\max(s^*_{j-\frac{1}{2}}, 0) - \min(s^*_{j+\frac{1}{2}}, 0)\right)\right)X^n_j - \frac{\Delta t}{h}\min(s^*_{j+\frac{1}{2}}, 0)X^n_{j+1} + \frac{\Delta t}{h}\max(s^*_{j-\frac{1}{2}}, 0)X^n_{j-1}
\end{aligned} \tag{79}
$$

which shows that X^{n+1}_j is a convex combination of the $X^n_{i=j\pm1,j}$ under the CFL condition (73).

5.4.4. *Wave speed estimates*

The fan of waves of the HLLC solver must contain the fan of waves of the exact Riemann problem (51). This is in particular required to ensure the local entropy minimum principles (74), see [3, Prop. 3.2]. Direct wave speed estimates have been proposed that do not require to solve the exact Riemann problem [57, 5]. Note that the usual estimate $S_R = -S_L = \max(|u_L| + c_L, |u_R| + c_R)$ may be wrong due to the Lax entropy condition across a shock. On the other hand, the time steps can be affected by overestimating wave speed estimates through (73). We propose the following wave speeds estimates

$$
s_L = u_L - \tilde{c}_L, \quad s_R = u_R + \tilde{c}_R, \tag{80}
$$

where $u_X = \mathbf{v}_X \cdot \mathbf{n}$, $X = L, R$, and

$$
\text{if } \mathrm{p}_R \geqslant \mathrm{p}_L : \begin{cases} \tilde{c}_L = c_L + \frac{\gamma+1}{2}\max\left(\frac{\mathrm{p}_R - \mathrm{p}_L}{\rho_R c_R} + u_L - u_R, 0\right), \\ \tilde{c}_R = c_R + \frac{\gamma+1}{2}\max\left(\frac{\mathrm{p}_L - \mathrm{p}_R}{\rho_L \tilde{c}_L} + u_L - u_R, 0\right), \end{cases} \quad \text{else} : \begin{cases} \tilde{c}_R = c_R + \frac{\gamma+1}{2}\max\left(\frac{\mathrm{p}_L - \mathrm{p}_R}{\rho_L c_L} + u_L - u_R, 0\right), \\ \tilde{c}_L = c_L + \frac{\gamma+1}{2}\max\left(\frac{\mathrm{p}_R - \mathrm{p}_L}{\rho_R \tilde{c}_R} + u_L - u_R, 0\right), \end{cases} \tag{81}
$$

and $\gamma = \max(\gamma_L, \gamma_R)$, $c_X = \sqrt{\gamma(\mathrm{p}_X + \mathrm{p}_{\infty_X})/\rho_X}$ for $X = L, R$. These estimates will bound the wave speeds in the exact Riemann solution in the case of pure phases [5]. Then, the above definition of γ will allow to bound the signal speeds in the case of polytropic gases, $\mathrm{p}_{\infty_L} = \mathrm{p}_{\infty_R} = 0$ [41]. Though, it is difficult to guarantee such properties in the general case when $\Gamma_L \neq \Gamma_R$ and $\Pi_L \neq \Pi_r$, these estimates proved to be robust in the present numerical experiments.

6. Properties of the DGSEM scheme

We recall here the main properties of the DGSEM scheme proposed in this work for the discretization of the SG-gamma model (1) with a stiffened gas EOS (5).

6.1. Semi-discrete scheme

The semi-discrete scheme (31) with the EC fluxes (48) in the volume integral and the HLLC flux (71) at interfaces satisfy the semi-discrete entropy inequality, see Theorem 3.1. In contrast, the scheme with the CP fluxes (46) in the volume integral, along with the HLLC solver at the interfaces, preserves uniform pressure and velocity profiles across material interfaces.

6.2. Fully discrete scheme

We restrict ourselves to the use of a one-step first-order explicit time discretization for both CP and EC numerical fluctuations in the volume integral. High-order time integration will be done by using a strong-stability preserving explicit Runge-Kutta method from [52] that is a convex combination of forward Euler steps and thus keeps the properties of the first-order in time scheme under some condition on the time step. The fully discrete DGSEM scheme reads

$$\omega_i \omega_j J_\kappa^{ij} \frac{\mathbf{U}_\kappa^{ij,n+1} - \mathbf{U}_\kappa^{ij,n}}{\Delta t^{(n)}} + \mathbf{R}_\kappa^{ij}(\mathbf{u}_h^{(n)}) = 0 \quad \forall \kappa \in \Omega_h,\ 0 \leqslant i, j \leqslant p,\ n \geqslant 0, \tag{82}$$

where $\Delta t^{(n)} = t^{(n+1)} - t^{(n)}$ is the time step, $\mathbf{U}_\kappa^{ij,n} = \mathbf{U}_\kappa^{ij}(t^{(n)})$, $\mathbf{u}_h^{(n)} = \mathbf{u}_h(\cdot, t^{(n)})$, and the vector of space residuals $\mathbf{R}_\kappa^{ij}(\cdot)$ is defined from (31). The following theorem summarizes the properties of the above scheme with fluctuations (30) and (26). These properties are independent of the EC or CP character of the volume fluctuations and therefore hold for both EC and CP fluxes for the SG-gamma model (2), though the minimum entropy principle holds when excluding material interfaces. Likewise, any other interface flux that satisfy properties (i) to (iv) below can be used in place of the HLLC solver.

The derivation of the CFL condition will rely on the work in [6, Lemma 3.4] that proves that there exist pseudo-equilibrium states $\mathbf{u}_\kappa^{\star,n}$ in Ω_{GM} and finite wave speed estimates $\lambda_\kappa^{\star,n} > 0$ such that

$$\sum_{e \in \partial\kappa} \sum_{k=0}^{p} \omega_k J_e^k \mathbf{h}^{\text{Rus}}\Big(\mathbf{u}_\kappa^{\star,n}, \mathbf{u}_h^-(\mathbf{x}_e^k, t^{(n)}), \mathbf{n}_e^k\Big) = 0, \quad \lambda_\kappa^{\star,n} \geqslant \max_{0 \leqslant k \leqslant p,\ e \in \partial\kappa} \Big(|\lambda|_{max}\Big(\mathbf{u}_\kappa^{\star,n}, \mathbf{u}_h^-(\mathbf{x}_e^k, t^{(n)}), \mathbf{n}_e^k\Big)\Big), \tag{83}$$

where $\mathbf{h}^{\text{Rus}}(\mathbf{u}^-, \mathbf{u}^+, \mathbf{n}) = \frac{1}{2}\Big(\mathbf{f}(\mathbf{u}^-) + \mathbf{f}(\mathbf{u}^+)\Big) \cdot \mathbf{n} - \frac{\lambda_\kappa^{\star,n}}{2}(\mathbf{u}^+ - \mathbf{u}^-)$ is the Rusanov flux and $\lambda_\kappa^{\star,n}$ bounds the fans of waves in the exact Riemann problems (51) with $\mathbf{n} = \mathbf{n}_e^k$ and left and right states $\mathbf{u}_\kappa^{\star,n}$ and $\mathbf{u}_h^-(\mathbf{x}_e^k, t^{(n)})$, see (84). Note that other conditions adapted to unstructured meshes may be used [49].

Theorem 6.1. *Let us consider the DGSEM scheme (82) with consistent fluctuations (30) of the form (37) in the volume integrals and consistent interface fluctuations (26) such that the associated three-point scheme (55): (i) is robust: $\mathbf{U}_{j\in\mathbb{Z}}^{n\geqslant 0} \in \Omega_{\text{GM}}$; (ii) satisfies a discrete entropy inequality (60) with consistent numerical flux; (iii) satisfies a discrete minimum principle (77) on the specific physical entropy $s(\mathbf{u})$; (iv) satisfies discrete maximum principles (79) on Γ and Π. Then, the updated cell-averaged solution $\langle \mathbf{u}_h^{(n+1)} \rangle_\kappa$ is a convex combination of DOFs at time $t^{(n)}$ and updates of three-point schemes under the following conditions on the time step:*

$$\Delta t^{(n)} \max_{e \in \mathcal{E}_h} \max_{0 \leqslant k \leqslant p} \frac{\omega_k J_e^k}{\tilde{\omega}_k \min J_{\kappa^\pm}(\mathbf{x}_e^k))} \max\Big(\big|s_{L_{j+\frac{1}{2}}}^n\big|, \big|s_{R_{j-\frac{1}{2}}}^n\big|, \lambda_{\kappa^-}^{\star,n}, \lambda_{\kappa^+}^{\star,n}\Big) \leqslant \frac{1}{p(p+1)}, \tag{84a}$$

$$\Delta t^{(n)} \max_{\kappa \in \Omega_h} \max_{0 \leqslant i,j \leqslant p} \sum_{k=0}^{p} \frac{\omega_k}{\tilde{\omega}_{ij} J_\kappa^{ij}} \Big(\omega_j D_{ki} \mathbf{v}_\kappa^{kj,n} \cdot \mathbf{n}_{(i,k)j} + \omega_i D_{kj} \mathbf{v}_\kappa^{ik,n} \cdot \mathbf{n}_{i(j,k)}\Big) \leqslant 1, \tag{84b}$$

where $\lambda_\kappa^{\star,n}$ is defined in (83), $\tilde{\omega}_{ij} = \omega_i\omega_j$ when $0 < i, j < p$, $\tilde{\omega}_{ij} = \frac{\omega_i\omega_j}{2}$ else, and $\tilde{\omega}_k = \omega_k$ when $0 < k < p$, $\tilde{\omega}_0 = \tilde{\omega}_p = \frac{\omega_0}{2} = \frac{1}{p(p+1)}$. Assuming that the DOFs $\mathbf{U}_\kappa^{ij,n}$ are in Ω_{GM} for all $\kappa \in \Omega_h$ and $0 \leqslant i, j \leqslant p$, the DGSEM scheme (82) guarantees positivity of the cell-averaged solution:

$$\langle \mathbf{u}_h^{n+1} \rangle_\kappa \in \Omega_{\text{GM}} \quad \forall \kappa \in \Omega_h,$$

together with a minimum principle on the specific entropy when excluding material interfaces

$$s(\langle \mathbf{u}_h^{(n+1)} \rangle_\kappa) \geqslant \min\Big\{ s(\mathbf{U}_\kappa^{ij,n}) : \ 0 \leqslant i, j \leqslant p \Big\} \cup \Big\{ s\Big(\mathbf{u}_h^+(\mathbf{x}_e^k, t^{(n)})\Big) : \ e \in \partial\kappa, 0 \leqslant k \leqslant p \Big\},$$

and maximum principles on the EOS parameters Y in $\{\Gamma, \Pi\}$:

$$\min \mathcal{S}_\kappa(Y_h^{(n)}) \leqslant \langle Y_h^{(n+1)} \rangle_\kappa \leqslant \max \mathcal{S}_\kappa(Y_h^{(n)}), \quad \mathcal{S}_\kappa(Y_h^{(n)}) = \{Y_\kappa^{ij,n} : 0 \leqslant i, j \leqslant p\} \cup \Big\{ Y_h^+(\mathbf{x}_e^k, t^{(n)}) : e \in \partial\kappa, 0 \leqslant k \leqslant p \Big\} \quad \forall \kappa \in \Omega_h.$$

Proof. From (38) and (82), the cell-averaged discrete scheme for the $d+2$ first components of (1a), Y in $\{\rho, \rho\mathbf{v}, \rho E\}$, reads

$$\langle Y_h^{(n+1)} \rangle_\kappa = \langle Y_h^{(n)} \rangle_\kappa - \frac{\Delta t^{(n)}}{|\kappa|} \sum_{e \in \partial\kappa} \sum_{k=0}^{p} \omega_k J_e^k \mathbf{h}_Y^{\text{HLLC}}\Big(\mathbf{u}_h^-(\mathbf{x}_e^k, t^{(n)}), \mathbf{u}_h^+(\mathbf{x}_e^k, t^{(n)}), \mathbf{n}_e^k\Big),$$

where $\mathbf{h}_Y^{\text{HLLC}}(\mathbf{u}^-, \mathbf{u}^+, \mathbf{n}) = \mathbf{D}_Y^-(\mathbf{u}^-, \mathbf{u}^+, \mathbf{n}) + \mathbf{f}_Y(\mathbf{u}^-) \cdot \mathbf{n}$ is the numerical flux in conservation form associated to the HLLC fluctuations (71). Following [6, Sec. 4.2], we add $\frac{\Delta t^{(n)}}{|\kappa|}$ times the flux balance in (83) to the above relation and decompose $\langle Y_h^{(n)} \rangle_\kappa$ in (20) to get

$$\begin{aligned}\langle Y_h^{(n+1)} \rangle_\kappa = &\sum_{i,j=1}^{p-1} \omega_i\omega_j \frac{J_\kappa^{ij}}{|\kappa|} Y_\kappa^{ij,n} + \sum_{e \in \partial\kappa} \sum_{k=0}^{p} \omega_0 \tilde{\omega}_k \frac{J_\kappa(\mathbf{x}_e^k)}{|\kappa|} \Bigg(\mathbf{u}_h^-(\mathbf{x}_e^k, t^{(n)}) \\ &- \frac{\Delta t^{(n)} \omega_k J_e^k}{\omega_0 \tilde{\omega}_k J_\kappa(\mathbf{x}_e^k)} \Big(\mathbf{h}_Y^{\text{HLLC}}\Big(\mathbf{u}_h^-(\mathbf{x}_e^k, t^{(n)}), \mathbf{u}_h^+(\mathbf{x}_e^k, t^{(n)}), \mathbf{n}_e^k\Big) - \mathbf{h}_Y^{Rus}\Big(\mathbf{u}_\kappa^{\star,n}, \mathbf{u}_h^-(\mathbf{x}_e^k, t^{(n)}), \mathbf{n}_e^k\Big) \Big) \Bigg).\end{aligned}$$

As a consequence, the first $d+2$ components of $\langle \mathbf{u}_h^{(n+1)} \rangle_\kappa$ are convex combination of quantities in Ω_{GM} under (84a) which confirms positivity of $\langle \rho_h^{(n+1)} \rangle_\kappa$ and $\rho e(\langle \mathbf{u}_h^{(n+1)} \rangle_\kappa)$ by concavity of $\rho e(\mathbf{u}) = \rho E - \frac{\rho\mathbf{v}\cdot\rho\mathbf{v}}{2\rho}$. Excluding material interfaces, we also get the minimum entropy principle.

Likewise, the two last components Y in $\{\Gamma, \Pi\}$ satisfy

$$\langle Y_h^{(n+1)} \rangle_\kappa = \langle Y_h^{(n)} \rangle_\kappa - \frac{\Delta t^{(n)}}{|\kappa|} \Bigg(\sum_{i,j,k=0}^{p} \omega_i\omega_j \Big(D_{ik} \mathbf{v}_\kappa^{ij,n} \cdot \mathbf{n}_{(i,k)j} Y_\kappa^{kj,n} + D_{jk} \mathbf{v}_\kappa^{ij,n} \cdot \mathbf{n}_{i(j,k)} Y_\kappa^{ik,n} \Big) + \sum_{e \in \partial\kappa} \sum_{k=0}^{p} \omega_k J_e^k \mathbf{D}_Y^-\Big(\mathbf{u}_h^-(\mathbf{x}_e^k, t^{(n)}), \mathbf{u}_h^+(\mathbf{x}_e^k, t^{(n)}), \mathbf{n}_e^k\Big) \Bigg).$$

Inverting indices i and k, then j and k in the volume integral, then using consistency of the interface fluctuations (27) to add the trivial quantity

$$-\frac{\Delta t^{(n)}}{|\kappa|} \sum_{e \in \partial\kappa} \sum_{k=0}^{p} \omega_k J_e^k \mathbf{D}_Y^+\Big(\mathbf{u}_h^-(\mathbf{x}_e^k, t^{(n)}), \mathbf{u}_h^-(\mathbf{x}_e^k, t^{(n)}), \mathbf{n}_e^k\Big) = 0,$$

and finally using the convex decomposition $\langle Y_h^{(n)} \rangle_\kappa = \sum_{i,j=0}^{p} \tilde{\omega}_{ij} \frac{J_\kappa^{ij}}{|\kappa|} Y_\kappa^{ij,n} + \sum_{e \in \partial\kappa} \sum_{k=0}^{p} \tilde{\omega}_0 \tilde{\omega}_k \frac{J_\kappa(\mathbf{x}_e^k)}{|\kappa|} Y_h^-(\mathbf{x}_e^k, t^{(n)})$ from (20) we get

$$\begin{aligned}\langle Y_h^{(n+1)} \rangle_\kappa = &\sum_{i,j=0}^{p} \tilde{\omega}_{ij} \frac{J_\kappa^{ij}}{|\kappa|} \Bigg(1 - \frac{\Delta t^{(n)}}{J_\kappa^{ij}} \sum_{k=0}^{p} \frac{\omega_k\omega_j}{\tilde{\omega}_{ij}} D_{ki} \mathbf{v}_\kappa^{kj,n} \cdot \mathbf{n}_{(i,k)j} + \frac{\omega_i\omega_k}{\tilde{\omega}_{ij}} D_{kj} \mathbf{v}_\kappa^{ik,n} \cdot \mathbf{n}_{i(j,k)} \Bigg) Y_\kappa^{ij,n} \\ &+ \sum_{e \in \partial\kappa} \sum_{k=0}^{p} \tilde{\omega}_0 \tilde{\omega}_k \frac{J_\kappa(\mathbf{x}_e^k)}{|\kappa|} \Bigg(Y_h^+(\mathbf{x}_e^k, t^{(n)}) - \frac{\Delta t^{(n)} \omega_k J_e^k}{\tilde{\omega}_0 \tilde{\omega}_k J_\kappa(\mathbf{x}_e^k)} \Big(\mathbf{D}_Y^-\Big(\mathbf{u}_h^-(\mathbf{x}_e^k, t^{(n)}), \mathbf{u}_h^+(\mathbf{x}_e^k, t^{(n)}), \mathbf{n}_e^k\Big) + \mathbf{D}_Y^+\Big(\mathbf{u}_h^-(\mathbf{x}_e^k, t^{(n)}), \mathbf{u}_h^-(\mathbf{x}_e^k, t^{(n)}), \mathbf{n}_e^k\Big) \Big) \Bigg),\end{aligned}$$

and invoking the metric identities in (41), $\langle Y_h^{(n+1)} \rangle_\kappa$ is indeed a convex combination of the DOFs associated to $Y_h^{(n)}$ and updates of three-point scheme (55) under (84). Positivity and the minimum and maximum principles follow directly. □

7. A posteriori limiters

Properties of the discrete DGSEM scheme in Theorem 6.1 hold for the cell-averaged solution and a posteriori limiters are applied at the end of each Runge-Kutta stage to extend these properties to all DOFs within elements. Here we describe these limiters for (82) that are similar to the ones proposed in [66, 65, 14, 62]. The basic principle consists in limiting DOFs at time $t^{(n+1)}$ through a linear scaling around the cell-average (20):

$$\tilde{\mathbf{U}}_\kappa^{i,j,n+1} = \theta_\kappa\Big(\mathbf{U}_\kappa^{i,j,n+1} - \langle \mathbf{u}_h^{(n+1)}\rangle_\kappa\Big) + \langle \mathbf{u}_h^{(n+1)}\rangle_\kappa \quad \forall 0 \leqslant i,j \leqslant p, \quad \kappa \in \Omega_h,$$

where $0 \leqslant \theta_\kappa \leqslant 1$ is the limiter coefficient. We here apply successive limiters $(\theta_\kappa^\rho, \theta_\kappa^{\rho e}, \theta_\kappa^\Gamma, \theta_\kappa^\Pi)$ on:

- mixture density:

$$\tilde{\rho}_\kappa^{i,j,n+1} = \theta_\kappa^\rho\Big(\rho_\kappa^{i,j,n+1} - \langle \rho_h^{(n+1)}\rangle_\kappa\Big) + \langle \rho_h^{(n+1)}\rangle_\kappa, \quad \theta_\kappa^\rho = \min\left(\frac{\langle \rho_h^{(n+1)}\rangle_\kappa - \epsilon}{\langle \rho_h^{(n+1)}\rangle_\kappa - \rho_\kappa^{\min}}, 1\right), \quad \rho_\kappa^{\min} = \min_{0\leqslant i,j\leqslant p} \rho_\kappa^{i,j,n+1}; \tag{85}$$

- EOS parameters Γ and Π:

$$\tilde{Y}_\kappa^{i,j,n+1} = \theta_\kappa^Y\left(Y_\kappa^{i,j,n+1} - \langle Y_h^{(n+1)}\rangle_\kappa\right) + \langle Y_h^{(n+1)}\rangle_\kappa, \quad \theta_\kappa^Y = \min\left(\frac{\langle Y_h^{(n+1)}\rangle_\kappa - m_Y}{\langle Y_h^{(n+1)}\rangle_\kappa - Y_\kappa^{\min}}, \frac{M_Y - \langle Y_h^{(n+1)}\rangle_\kappa}{Y_\kappa^{\max} - \langle Y_h^{(n+1)}\rangle_\kappa}, 1\right), \quad Y \in \{\Gamma, \Pi\}, \tag{86}$$

  where $Y_\kappa^{\min} = \min_{0\leqslant i,j\leqslant p} Y_\kappa^{i,j,n+1}$, $Y_\kappa^{\max} = \max_{0\leqslant i,j\leqslant p} Y_\kappa^{i,j,n+1}$, and

$$m_\Gamma = \min_{1\leqslant i\leqslant n_s} \frac{1}{\gamma_i - 1}, \quad M_\Gamma = \max_{1\leqslant i\leqslant n_s} \frac{1}{\gamma_i - 1}, \quad m_\Pi = \min_{1\leqslant i\leqslant n_s} \frac{\gamma_i \mathrm{p}_{\infty_i}}{\gamma_i - 1}, \quad M_\Pi = \max_{1\leqslant i\leqslant n_s} \frac{\gamma_i \mathrm{p}_{\infty_i}}{\gamma_i - 1};$$

- mixture total internal energy:

$$\tilde{Y}_\kappa^{i,j,n+1} = \theta_\kappa^{\rho e}\Big(Y_\kappa^{i,j,n+1} - \langle Y_h^{(n+1)}\rangle_\kappa\Big) + \langle Y_h^{(n+1)}\rangle_\kappa, \quad Y \in \{\rho, \rho\mathbf{v}, \rho E\}, \tag{87}$$

  where $\rho e(\mathbf{u}) = \rho E - \frac{\rho\mathbf{v}.\rho\mathbf{v}}{2\rho}$ and

$$\theta_\kappa^{\rho e} = \min\left(\min_{0\leqslant i,j\leqslant p}\left(\frac{\rho e(\langle \mathbf{u}_h\rangle_\kappa^{n+1}) - \tilde{\mathrm{p}}_{\infty_\kappa}^{i,j,n+1} - \epsilon}{\rho e(\langle \mathbf{u}_h\rangle_\kappa^{n+1}) - \rho e_\kappa^{i,j,n+1}}\right), 1\right). \tag{88}$$

Note that in (85) and (88), $0 < \epsilon \ll 1$ is a small parameter, which we set as $\epsilon = 10^{-8}$ in our numerical tests. The limiters (85) and (87) thus guarantee that $\tilde{\rho}_\kappa^{0\leqslant ij\leqslant p,n+1} > 0$ and $\tilde{\rho e}_\kappa^{0\leqslant ij\leqslant p,n+1} > \tilde{\mathrm{p}}_{\infty_\kappa}^{0\leqslant ij\leqslant p,n+1}$, respectively. Recalling (6), we have $m_Y \leqslant Y \leqslant M_Y$, with Y in $\{\Gamma, \Pi\}$, formally which may be viewed as relaxed maximum principles. The limiters in (86) thus impose similar maximum principles:

$$m_\Gamma \leq \tilde{\Gamma}_j^{0\leqslant k\leqslant p,n+1} \leqslant M_\Gamma, \quad m_\Pi \leqslant \tilde{\Pi}_j^{0\leqslant k\leqslant p,n+1} \leqslant M_\Pi.$$

8. Numerical experiments

We now perform numerical tests on the DGSEM scheme for the SG-gamma model (1)-(2) where the space discretization is defined in (31) and where the three-stage third-order strong stability-preserving Runge-Kutta scheme by Shu and Osher [52] is used for the time discretization. The time step is evaluated from the CFL condition (84a) and the limiter, introduced in section 7, is applied at the end of each stage. We consider numerical tests from [13, 15, 14, 35, 16]. The scheme was implemented in the CFD code *Aghora* developed at ONERA [50]. We recall that here we have proposed two DGSEM schemes for the SG-gamma model that differ in the fluctuations (32) in the volume integral: a CP scheme with (46); a semi-discrete entropy stable scheme with EC fluxes (48). We will compare the performances of both schemes in this section. All numerical tests are performed at fourth-order accuracy, $p = 3$, in space unless stated otherwise.

8.1. Advection of a density wave

We begin by validating the high-order accuracy of the scheme (31) by advecting a density wave in a uniform flow in the domain $\Omega = [0,1]^2$, discretized with unstructured meshes with fourth-order curved elements (see Figure 4(a)), with periodic conditions and initial condition $\mathbf{u}_0(\mathbf{x})$:

$$\alpha_{1_0}(\mathbf{x}) = \frac{1}{2} + \frac{1}{4}\sin 4\pi(x+y), \quad \rho_0(\mathbf{x}) = 1 + \frac{1}{2}\sin 2\pi(x+y), \quad u_0(\mathbf{x}) = v_0(\mathbf{x}) = 1, \quad \mathrm{p}_0(\mathbf{x}) = 1,$$

along with the EOS parameters $\mathrm{C_{v1}} = \mathrm{C_{v2}} = 1$, $\gamma_1 = 1.4$, $\mathrm{p}_{\infty_1} = 0$, $\gamma_2 = 3$, $\mathrm{p}_{\infty_2} = 2$. In this case, the density and EOS parameters are purely convected in uniform velocity and pressure fields. Norms on the mixture density error, $e_h = \rho_h - \rho$, under h- and p-refinements are displayed in Table 1 with either CP fluxes, or EC fluxes in the volume integral. We observe that as the mesh is refined the expected $p+1$ order of convergence is recovered by both schemes, but lower error levels are obtained with the CP flux.

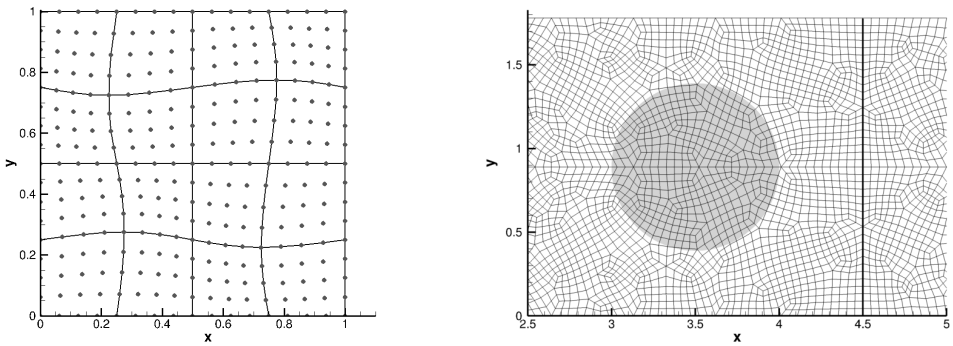

(a) (b)

Figure 4: Examples of meshes used for the numerical tests: (a) square mesh $h = 1/4$ with 16 fourth-order curved quadrangles with representation of the nodes; (b) example of unstructured mesh in the range $2.5 \leqslant x \leqslant 5$ with 1580 elements and initial positions of the shock and bubble (see section 8.3).

8.2. Riemann problems

We first consider the advection of an isolated material discontinuity to assess the contact preservation property of the present scheme. The computational domain for this test is chosen to be $\Omega_h = [-0.5, 0.5]$ with 100 elements. The Riemann initial data are

$$(\alpha_1, \rho, u, \mathrm{p}) = \begin{cases} (0.375, 2, 1, 1), & x < 0, \\ (0.146342, 1, 1, 1), & x > 0, \end{cases}$$

with $\mathrm{C_{v1}} = 1$, $\mathrm{C_{v2}} = 2$, $\gamma_1 = 1.4$, $\gamma_2 = 1.5$, $\mathrm{p}_{\infty_1} = \mathrm{p}_{\infty_2} = 0$. Results at time $t = 0.2$ are displayed in Figure 5. As expected, computations with CP fluxes preserve uniform profiles of pressure and velocity across the material interface, while spurious oscillations occur when using EC fluxes. In both cases, the interface is well captured with low amplitude oscillations in the ρ and Γ profiles.

We now consider a gas-gas shock-interface interaction problem which was originally proposed in [40]. Here a shock wave in helium gas travels at Mach 8.96 and interacts with an helium-air interface. The computational domain $\Omega_h = [-1, 1]$ with 100 elements and the initial condition is as follows:

$$(\alpha_1, \rho, u, \mathrm{p}) = \begin{cases} (0, 0.386, 26.59, 100), & x < -0.8, \\ (0, 0.1, -0.5, 1), & -0.8 < x < -0.2, \\ (1, 1.0, -0.5, 1), & x > -0.2, \end{cases}$$

with $\mathrm{C_{v1}} = 1$, $\mathrm{C_{v2}} = 2.5$, $\gamma_1 = 1.4$, $\gamma_2 = 5/3$, $\mathrm{p}_{\infty_1} = \mathrm{p}_{\infty_2} = 0$. The results are displayed in Figure 6, where the solution shows two shocks, one traveling left and the other traveling right, with a right traveling material interface in between. As a result, the shocks and interface are well captured, while spurious oscillations of small amplitude occur in the pressure and velocity fields.

	p	h	$\|e_h\|_{L^1(\Omega_h)}$	O_1	$\|e_h\|_{L^2(\Omega_h)}$	O_2	$\|e_h\|_{L^\infty(\Omega_h)}$	O_∞
CP	1	1/8	3.76E-01	–	4.16E-01	–	6.25E-01	–
		1/16	1.82E-01	1.05	2.04E-01	1.03	3.69E-01	0.76
		1/32	5.47E-02	1.73	6.11E-02	1.74	1.08E-01	1.77
		1/64	1.43E-02	1.93	1.59E-02	1.94	2.56E-02	2.08
	2	1/8	1.17E-02	–	1.41E-02	–	3.32E-02	–
		1/16	1.06E-03	3.46	1.23E-03	3.52	3.64E-03	3.19
		1/32	9.64E-05	3.45	1.17E-04	3.40	4.82E-04	2.90
		1/64	1.01E-05	3.25	1.30E-05	3.16	6.50E-05	2.90
	3	1/8	3.51E-04	–	4.68E-04	–	3.18E-03	–
		1/16	1.73E-05	4.35	2.65E-05	4.14	1.98E-04	4.01
		1/32	1.05E-06	4.04	1.66E-06	4.00	1.20E-05	4.04
		1/64	6.73E-08	3.96	1.05E-07	3.98	7.54E-07	3.99
EC	1	1/8	3.72E-01	–	4.11E-01	–	6.24E-01	–
		1/16	1.78E-01	1.06	2.05E-01	1.01	4.29E-01	0.54
		1/32	5.62E-02	1.66	7.14E-02	1.52	2.12E-01	1.02
		1/64	1.52E-02	1.89	1.99E-02	1.84	6.81E-02	1.64
	2	1/8	2.78E-02	–	3.48E-02	–	9.99E-02	–
		1/16	3.95E-03	2.81	5.23E-03	2.73	1.76E-02	2.50
		1/32	3.56E-04	3.47	4.55E-04	3.52	1.56E-03	3.50
		1/64	2.91E-05	3.61	3.77E-05	3.59	1.41E-04	3.46
	3	1/8	4.58E-03	–	5.78E-03	–	1.62E-02	–
		1/16	2.35E-04	4.28	3.10E-04	4.22	1.10E-03	3.88
		1/32	8.53E-06	4.78	1.21E-05	4.68	6.62E-05	4.06
		1/64	2.91E-07	4.87	4.63E-07	4.71	4.01E-06	4.05

Table 1: Advection of a density wave: results using either CP (top) numerical fluxes (46), or EC (bottom) numerical fluxes (48) in the volume integral. Norms of the error on density under p- and h-refinements and associated orders of convergence at time $t = 2$.

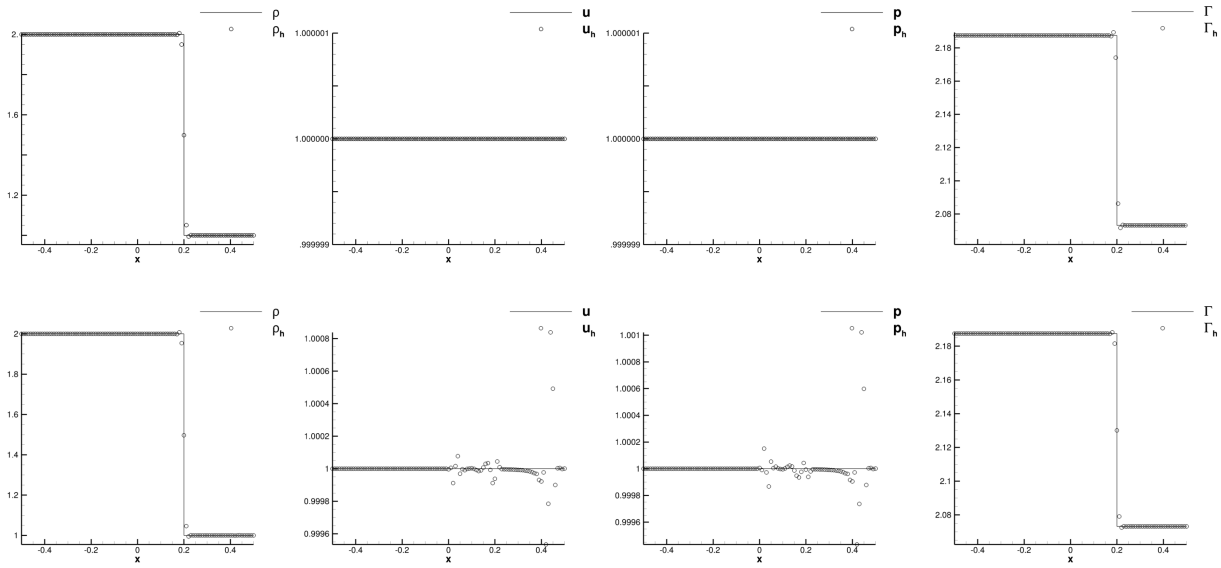

Figure 5: Advection of an isolated material interface: fourth-order accurate simulations obtained on a mesh with 100 elements, and using either CP (top), or EC (bottom) fluxes in the volume integral. Approximate results (symbols) are shown at $t = 0.2$ and are compared to the exact solution (lines).

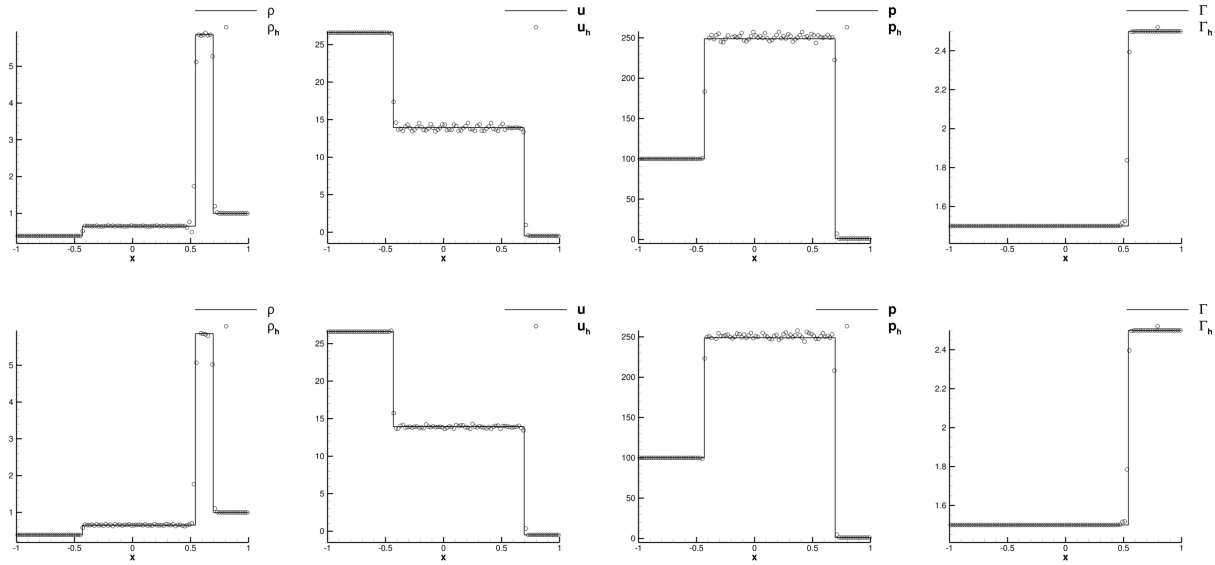

Figure 6: Shock-material interface interaction: fourth-order accurate, $p = 3$, simulations obtained on a mesh with 100 elements, and using either CP (top), or EC (bottom) fluxes in the volume integral. Approximate results (symbols) are shown at $t = 0.07$ and are compared to the exact solution (lines).

The last test case concerns a gas-water shock-interface interaction problem and simulates an underwater explosion, where the initial condition consists of a material interface separating highly compressed air to the left and water at atmospheric pressure to the right. The computational domain is $\Omega_h = [-5, 5]$ with 100 elements, and the initial data are given as

$$(\alpha_1, \rho, u, \mathrm{p}) = \begin{cases} (1, 1.241, 0, 2.753), & x < 0, \\ (0, 0.991, 0, 3.059 \times 10^{-4}), & x > 0, \end{cases}$$

with $\mathrm{C_{v1}} = 1.2$, $\mathrm{C_{v2}} = 0.073037$, $\gamma_1 = 1.4$, $\gamma_2 = 5.5$, $\mathrm{p}_{\infty_1} = 0$, and $\mathrm{p}_{\infty_2} = 1.505$. The results, in Figure 7, show a right traveling shock, a right traveling contact wave, a right advected material interface and a left rarefaction wave. We observe small oscillations on the velocity and pressure profiles even though the shock is of large amplitude, and the shock and material interface are well captured.

8.3. Shock wave-helium bubble interaction

We now consider the interaction of a shock with a helium bubble, which was experimentally investigated in [27] and used to assess numerical schemes for multiphase and multicomponent flows [14, 26, 32, 35, 36, 49, 44]. The test involves a stationary helium bubble ($\gamma_1 = 1.648$ and $\mathrm{C_{v1}} = 6.0598$) which is surrounded by air ($\gamma_2 = 1.4$ and $\mathrm{C_{v2}} = 1.7857$) and interacts with a left moving Mach 1.22 shock. The computational domain $\Omega_h = [0.0, 6.5] \times [0, 1.78]$ is discretized with an unstructured mesh with 433016 elements (see Figure 4(b)). The helium bubble of unit diameter is centered at $x = 3.5$ and $y = 0.89$ and the left traveling shock is located at $x = 4$. Periodic boundary conditions are imposed on the top and bottom boundaries, while non-reflective conditions are applied at the left and right boundaries. The initial data are made nondimensional with the initial bubble diameter, density, temperature and sound speed of air in the pre-shock region.

We first test the ability of both schemes to preserve material interfaces and consider the advection of the bubble only on a mesh with 64×64 fourth-order curved elements (see Figure 4(a)). We thus remove the shock wave, impose a uniform velocity field $\mathbf{v}_0(\mathbf{x}) = (1, 0)^\top$ and reduce the size of the bubble which is now initially centered at $(0.5, 0.5)$. Figure 8 shows the bubble at time $t = 76.19\mu s$ corresponding to a transport of the bubble over a unit distance. The scheme with the CP fluxes captures the interface sharply and preserves the uniform velocity and pressure profiles across the interface, while spurious oscillations are observed with the EC flux.

We now consider the shock-bubble interaction. Figure 9 shows the deformation of the bubble at several physical times as the left traveling shock passes through it and represents contours of void fraction of the helium bubble, α_1, and mixture pressure,

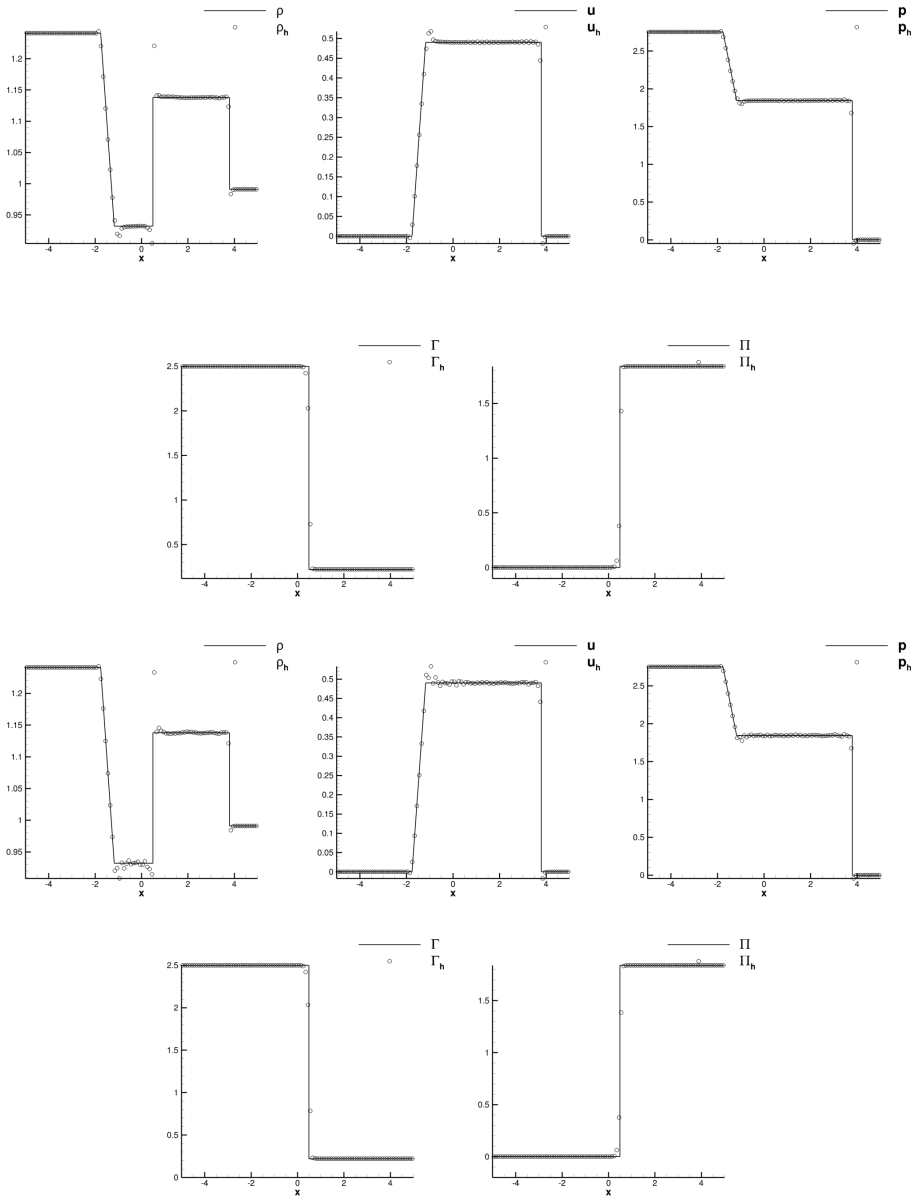

Figure 7: Gas-water shock-interface interaction problem: fourth-order accurate, $p = 3$, simulations obtained on a mesh with 100 elements, and using either CP (top), or EC (bottom) fluxes in the volume integral. Approximate results (symbols) are shown at $t = 1$ and are compared to the exact solution (lines).

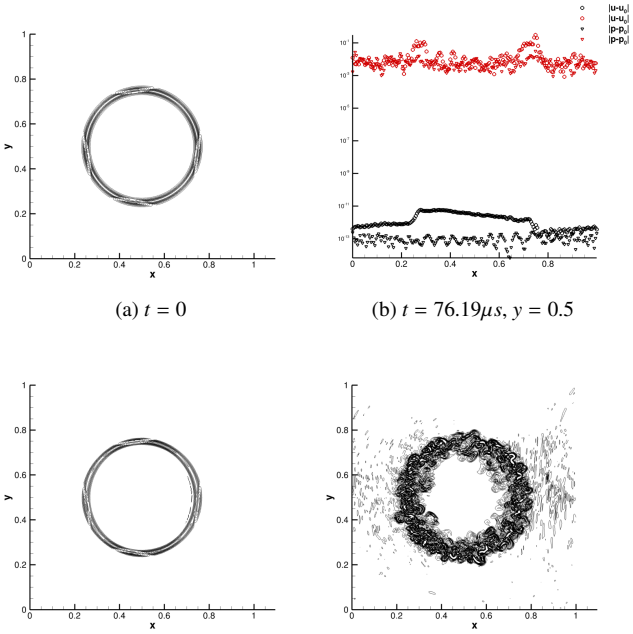

(a) $t = 0$ (b) $t = 76.19\mu s$, $y = 0.5$

(c) $t = 76.19\mu s$, CP (d) $t = 76.19\mu s$, EC

Figure 8: Advection of a helium bubble in air: (a) initial condition, and results obtained with fourth-order accuracy ($p = 3$) in space with either CP fluxes, or EC fluxes: (b) absolute error levels (logarithmic scale) on the pressure and velocity distributions along $y = 0.5$ obtained with either CP (black symbols), or EC (red symbols) fluctuations; (c,d) numerical Schlieren $\phi = \exp(|\nabla\rho|/|\nabla\rho|_{\max})$.

p, together with numerical Schlieren. We observe that the scheme with CP fluxes allows a better and sharper resolution of the bubble interface for all physical times and is able to accurately capture the shock and bubble dynamics. The bubble interface develops vortices after interacting with shock due to a Kelvin-Helmholtz instability. Once again, results with the EC fluxes show some spurious oscillations at the material interface before and after the interaction in contrast to CP fluxes, while both CP and EC schemes show good resolutions of the shock.

8.4. Strong shock wave-hydrogen bubble interaction

We finally consider an interaction problem of a strong $M = 2$ shock in air with a hydrogen bubble that has been numerically investigated in [4, 54]. Compared to section 8.3, these conditions result in faster shock and bubble dynamics. The computational domain for this test is $\Omega_h = [0, 22.5] \times [0, 7.5]$ and is discretized with an unstructured mesh with 154622 elements. The hydrogen bubble ($\gamma_1 = 1.41$ and $C_{v1} = 7.424$) is initially centered at $x = 4$ and $y = 0$, and the right traveling shock located at $x = 7$ in air ($\gamma_2 = 1.353$ and $C_{v2} = 0.523$). The initial data is made nondimensional with the pre-shock density, velocity and temperature of the air and a length scale of 1mm. We impose symmetry conditions at the top and bottom boundaries, along with supersonic inflow condition at the left boundary and nonreflecting conditions at the right boundary.

Figure 10 shows the deformation of the bubble as the shock passes through it, where we plot contours of the void fraction of the hydrogen bubble, α_1, mixture pressure pressure, p, and the numerical Schlieren. Here, we once again observe that the numerical scheme is able to resolve the bubble interface well along with the shock. The oscillations at the interface are due to the Kelvin-Helmholtz instability and they were also observed in [4]. Using CP fluxes maintains sharp resolution of the interface while also proving to well capture shocks.

9. Concluding remarks

In this work, we propose a high-order, robust and entropy stable discretization of the nonconservative multicomponent SG-gamma model [53]. The space discretization of this system relies on the DGSEM framework [47, 14] based on the modification of

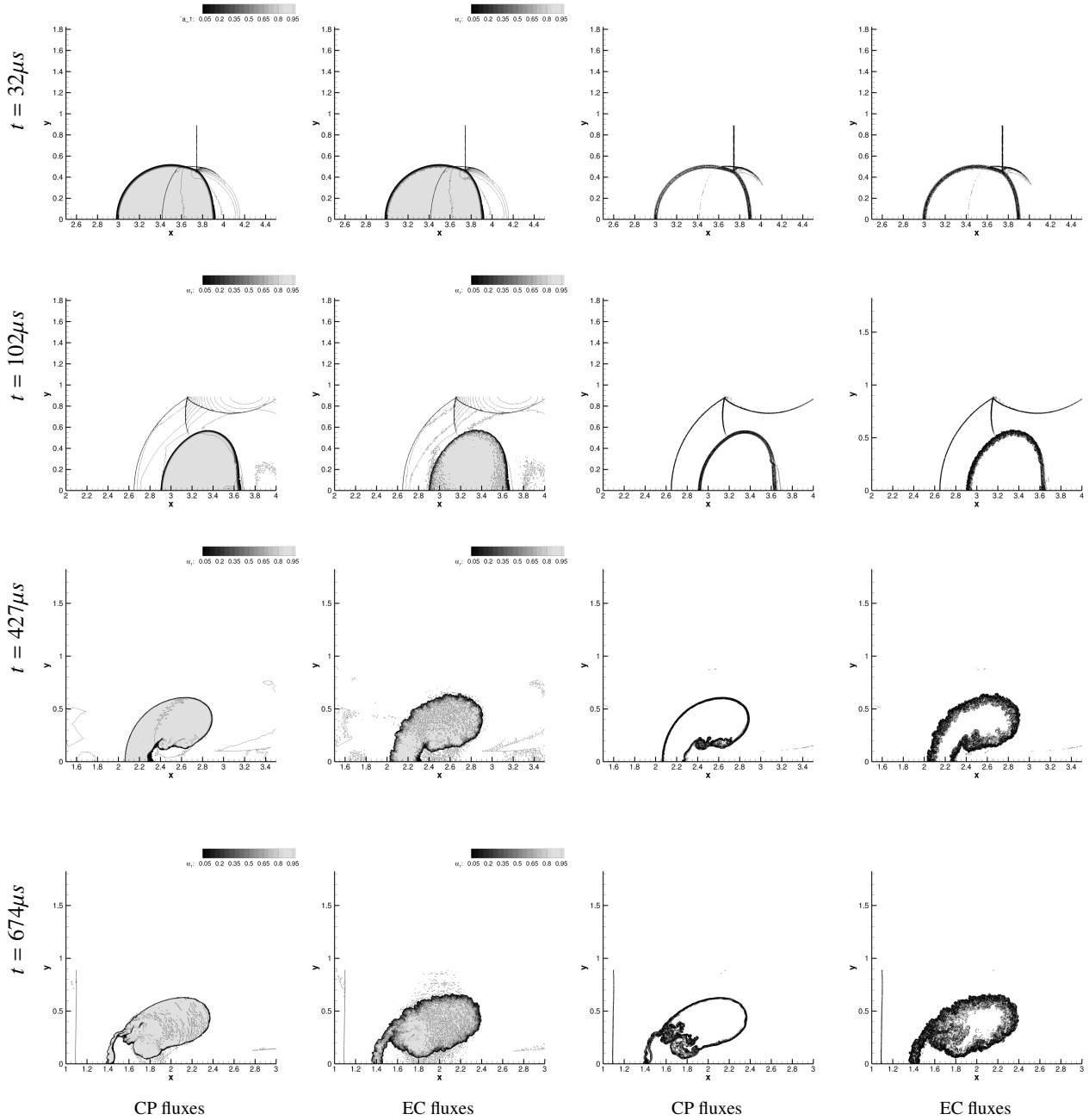

Figure 9: Interaction of a $M = 1.22$ shock in air with a helium bubble: fourth order accurate in space, $p = 3$, numerical simulations obtained at different times using either CP, or EC fluxes in the volume integral, on an unstructured mesh with 433016 elements. For each snapshot the left image shows the helium void fraction contours (color levels) and the pressure contours (lines), while the right image shows the numerical Schlieren of the density $\phi = \exp|\nabla\rho|/|\nabla\rho_{\max}|$.

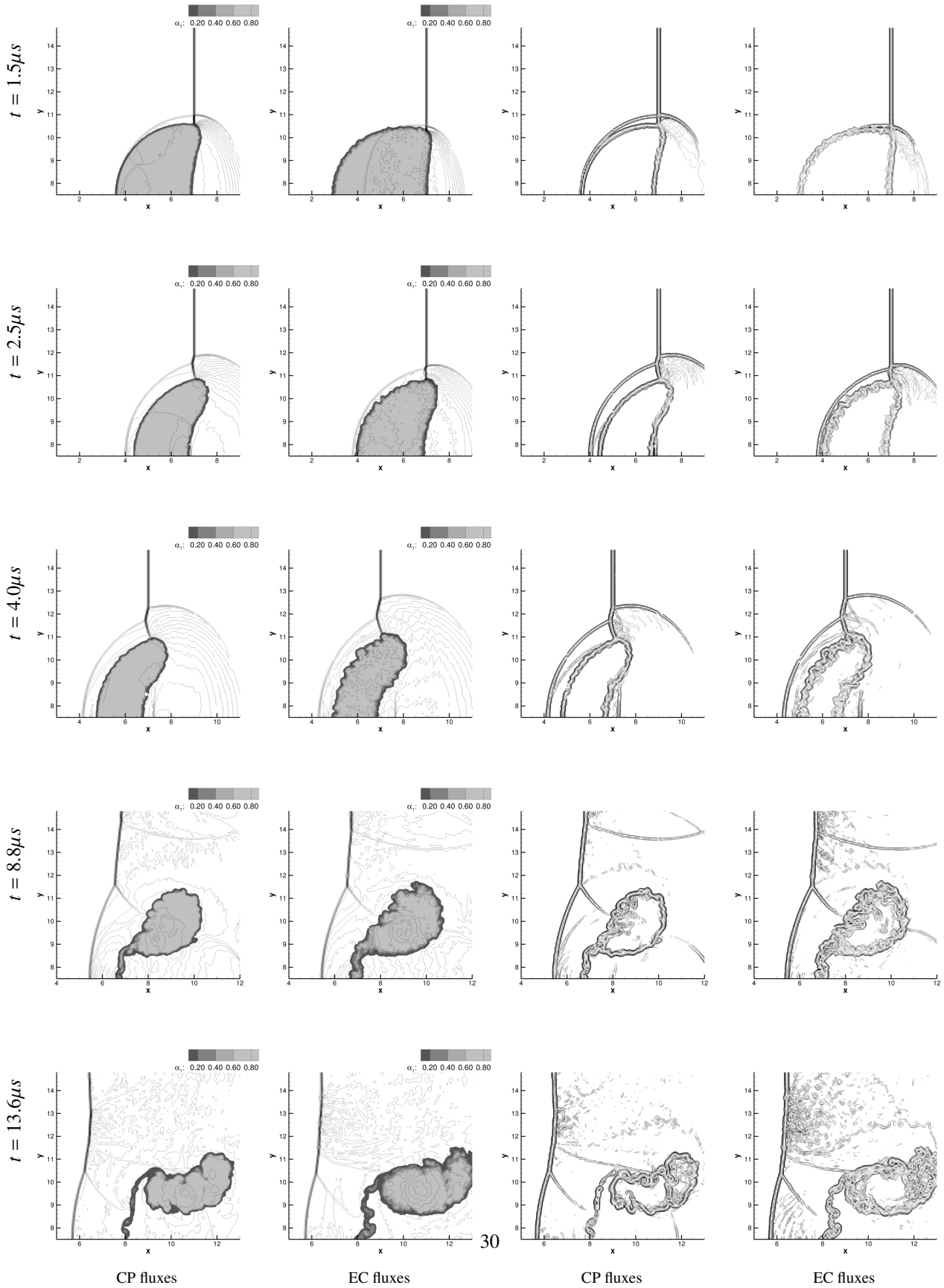

Figure 10: Interaction of a $M = 2$ shock in air with a Hydrogen bubble: fourth-order accurate in space, $p = 3$, numerical solutions obtained at different times using either CP, or EC numerical fluxes in the volume integral, on an unstructured mesh with 154622 elements. For each snapshot the left image shows the helium void fraction contours (color levels) and the pressure contours (lines), while the right image shows the numerical Schlieren of the density $\phi = \exp|\nabla\rho|/|\nabla\rho_{\max}|$.

the integral over discretization elements where we replace the physical fluxes and nonconservative products by two-point numerical fluctuations. We first extend this framework to multidimensional unstructured grids with curved elements and derive conditions under which the semi-discrete scheme is high-order accurate, free-stream preserving and entropy stable. We then design a robust, entropy stable, material interface preserving, and maximum principles preserving HLLC solver for the SG-gamma model that does not require a root-finding algorithm to evaluate the nonconservative product. The HLLC solver is then used as interface fluctuations in the DGSEM scheme, while we consider either EC, or CP fluctuations in the integrals over discretization elements. The DGSEM scheme is shown to either satisfy a semi-discrete entropy inequality with EC fluctuations (when excluding material interfaces), or to preserve material interfaces with CP fluctuations.

We then analyze the fully discrete DGSEM scheme with a forward Euler time discretization. We derive conditions on the time step to guaranty that the cell-averaged solution remains in the set of states and satisfies minimum principles on entropy and maximum principles on EOS parameters with either EC, or CP fluctuations. We use a posteriori scaling limiters [65, 66] to extend these properties to all DOFs within elements, while a strong-stability preserving Runge-Kutta scheme [52] is used for the high-order time integration and keeps properties of the first-order in time scheme.

High-order accurate numerical simulations of flows in one and two space dimensions with discontinuous solutions and complex wave interactions confirm robustness, stability and accuracy of the present scheme with either EC, or CP fluctuations, and the scheme with CP fluxes present better resolution capabilities.

References

[1] R. Abgrall, *How to prevent pressure oscillations in multicomponent flow calculations: a quasi conservative approach*, J. Comput. Phys., 125 (1996), pp. 150–160.

[2] P. Batten, N. Clarke, C. Lambert, and D. M. Causon, *On the choice of wavespeeds for the HLLC Riemann solver*, J. Sci. Comput., 18 (1997), pp. 1553–1570.

[3] C. Berthon, B. Dubroca, and A. Sangam, *A local entropy minimum principle for deriving entropy preserving schemes*, SIAM J. Numer. Anal., 50 (2012), pp. 468–491.

[4] G. Billet, V. Giovangigli, and G. De Gassowski, *Impact of volume viscosity on a shock–hydrogen-bubble interaction*, Combust. Theory Model., 12 (2008), pp. 221–248.

[5] F. Bouchut, *Nonlinear stability of finite Volume Methods for hyperbolic conservation laws: And Well-Balanced schemes for sources*, Springer Science & Business Media, 2004.

[6] V. Carlier and F. Renac, *Invariant domain preserving high-order spectral discontinuous approximations of hyperbolic systems*, arXiv:2203.05452 [math.NA], (2022).

[7] M. H. Carpenter, T. C. Fisher, E. J. Nielsen, and S. H. Frankel, *Entropy stable spectral collocation schemes for the Navier–Stokes equations: Discontinuous interfaces*, SIAM J. Sci. Comput., 36 (2014), pp. B835–B867.

[8] M. J. Castro, T. M. de Luna, and C. Parés, *Well-balanced schemes and path-conservative numerical methods*, in Handbook of Numer. Anal., vol. 18, Elsevier, 2017, pp. 131–175.

[9] M. J. Castro, U. S. Fjordholm, S. Mishra, and C. Parés, *Entropy conservative and entropy stable schemes for nonconservative hyperbolic systems*, SIAM J. Numer. Anal., 51 (2013), pp. 1371–1391.

[10] M. J. Castro, J. Gallardo, and C. Parés, *High order finite volume schemes based on reconstruction of states for solving hyperbolic systems with nonconservative products. applications to shallow-water systems*, Math. Comput., 75 (2006), pp. 1103–1134.

[11] Castro Díaz, Manuel Jesús, Fernández-Nieto, Enrique Domingo, Morales de Luna, Tomás, Narbona-Reina, Gladys, and Parés, Carlos, *A hllc scheme for nonconservative hyperbolic problems. application to turbidity currents with sediment transport*, ESAIM: M2AN, 47 (2013), pp. 1–32.

[12] T. Chen and C.-W. Shu, *Entropy stable high order discontinuous Galerkin methods with suitable quadrature rules for hyperbolic conservation laws*, J. Comput. Phys., 345 (2017), pp. 427–461.

[13] J. Cheng, F. Zhang, and T. Liu, *A discontinuous Galerkin method for the simulation of compressible gas-gas and gas-water two-medium flows*, J. Computat. Phys., 403 (2020), p. 109059.

[14] F. Coquel, C. Marmignon, P. Rai, and F. Renac, *An entropy stable high-order discontinuous Galerkin spectral element method for the Baer-Nunziato two-phase flow model*, J. Comput. Phys., 431 (2021), p. 110135.

[15] V. Coralic and T. Colonius, *Finite-volume WENO scheme for viscous compressible multicomponent flows*, J. Computat. Phys., 274 (2014), pp. 95–121.

[16] M. T. H. de Frahan, S. Varadan, and E. Johnsen, *A new limiting procedure for discontinuous Galerkin methods applied to compressible multiphase flows with shocks and interfaces*, J. Comput. Phys., 280 (2015), pp. 489–509.

[17] D. Derigs, A. R. Winters, G. J. Gassner, and S. Walch, *A novel averaging technique for discrete entropy-stable dissipation operators for ideal MHD*, J. Comput. Phys., 330 (2017), pp. 624–632.

[18] B. Despres, *Entropy inequality for high order discontinuous Galerkin approximation of Euler equations*, in Hyperbolic Problems: Theory, Numerics, Applications, M. Fey and R. Jeltsch, eds., Basel, 1999, Birkhäuser Basel, pp. 225–231.

[19] M. Dumbser and D. S. Balsara, *A new efficient formulation of the hllem riemann solver for general conservative and non-conservative hyperbolic systems*, J. Comput. Phys., 304 (2016), pp. 275–319.

[20] B. Einfeldt, C.-D. Munz, P. L. Roe, and B. Sjögreen, *On godunov-type methods near low densities*, J. Comput. Phys., 92 (1991), pp. 273–295.

[21] T. C. Fisher and M. H. Carpenter, *High-order entropy stable finite difference schemes for nonlinear conservation laws: Finite domains*, J. Comput. Phys., 252 (2013), pp. 518–557.

[22] U. S. Fjordholm, S. Mishra, and E. Tadmor, *Arbitrarily high-order accurate entropy stable essentially nonoscillatory schemes for systems of conservation laws*, SIAM J. Numer. Anal., 50 (2012), pp. 544–573.
[23] E. Franquet and V. Perrier, *Runge–Kutta discontinuous Galerkin method for the approximation of Baer and Nunziato type multiphase models*, J. Comput. Phys., 231 (2012), pp. 4096–4141.
[24] G. J. Gassner, *A skew-symmetric discontinuous Galerkin spectral element discretization and its relation to SBP-SAT finite difference methods*, SIAM J. Sci. Comput., 35 (2013), pp. A1233–A1253.
[25] G. J. Gassner, A. R. Winters, and D. A. Kopriva, *Split form nodal discontinuous Galerkin schemes with summation-by-parts property for the compressible Euler equations*, J. Comput. Phys., 327 (2016), pp. 39–66.
[26] J. Giordano and Y. Burtschell, *Richtmyer-Meshkov instability induced by shock-bubble interaction: Numerical and analytical studies with experimental validation*, Phys. Fluids, 18 (2006), p. 036102.
[27] J. F. Haas and B. Sturtevant, *Interaction of weak shock waves with cylindrical and spherical gas inhomogeneities*, J. Fluid Mech., 181 (1987), pp. 41–76.
[28] A. Harten, P. D. Lax, and B. V. Leer, *On upstream differencing and Godunov-type schemes for hyperbolic conservation laws*, SIAM review, 25 (1983), pp. 35–61.
[29] Helluy, Philippe and Seguin, Nicolas, *Relaxation models of phase transition flows*, ESAIM: M2AN, 40 (2006), pp. 331–352.
[30] A. Hiltebrand and S. Mishra, *Entropy stable shock capturing space–time discontinuous Galerkin schemes for systems of conservation laws*, Numer. Math., 126 (2014), pp. 103–151.
[31] A. Hiltebrand, S. Mishra, and C. Parés, *Entropy-stable space–time DG schemes for non-conservative hyperbolic systems*, ESAIM: M2AN, 52 (2018), pp. 995–1022.
[32] X. Y. Hu, B. Khoo, N. A. Adams, and F. L. Huang, *A conservative interface method for compressible flows*, J. Comput. Phys., 219 (2006), pp. 553–578.
[33] F. Ismail and P. L. Roe, *Affordable, entropy-consistent Euler flux functions ii: Entropy production at shocks*, J. Comput. Phys., 228 (2009), pp. 5410–5436.
[34] G. S. Jiang and C.-W. Shu, *On a cell entropy inequality for discontinuous Galerkin methods*, Math. Comput., 62 (1994), pp. 531–538.
[35] E. Johnsen and T. Colonius, *Implementation of WENO schemes in compressible multicomponent flow problems*, J. Comput. Phys., 219 (2006), pp. 715–732.
[36] S. Kawai and H. Terashima, *A high-resolution scheme for compressible multicomponent flows with shock waves*, Int. J. Numer. Methods. Fluids, 66 (2011), pp. 1207–1225.
[37] C. A. Kennedy and A. Gruber, *Reduced aliasing formulations of the convective terms within the navier–stokes equations for a compressible fluid*, J. Comput. Phys., 227 (2008), pp. 1676–1700.
[38] D. A. Kopriva, *Metric identities and the discontinuous spectral element method on curvilinear meshes.*, J. Sci. Comput., 26 (2006), pp. 302–327.
[39] D. A. Kopriva and G. Gassner, *On the quadrature and weak form choices in collocation type discontinuous Galerkin spectral element methods*, J. Sci. Comput., 44 (2010), pp. 136–155.
[40] T. G. Liu, B. C. Khoo, and K. S. Yeo, *Ghost fluid method for strong shock impacting on material interface*, J. Comput. Phys., 190 (2003), pp. 651–681.
[41] C. Marmignon, F. Naddei, and F. Renac, *Energy relaxation approximation for the compressible multicomponent flows in thermal nonequilibrium*, arXiv:2103.03731 [math.NA], (2021).
[42] R. Menikoff and B. J. Plohr, *The riemann problem for fluid flow of real materials*, Rev. Mod. Phys., 61 (1989), pp. 75–130.
[43] C. Parés, *Numerical methods for nonconservative hyperbolic systems: a theoretical framework.*, SIAM J. Numer. Anal., 44 (2006), pp. 300–321.
[44] J. J. Quirk and S. Karni, *On the dynamics of a shock–bubble interaction*, J. Fluid Mech., 318 (1996), pp. 129–163.
[45] H. Ranocha, *Comparison of some entropy conservative numerical fluxes for the Euler equations*, J. Sci. Comput., 76 (2018), pp. 216–242.
[46] F. Renac, *A robust high-order discontinuous Galerkin method with large time steps for the compressible Euler equations*, Commun. Math. Sci., 15 (2017), pp. 813–837.
[47] ———, *Entropy stable DGSEM for nonlinear hyperbolic systems in nonconservative form with application to two-phase flows*, J. Comput. Phys., 382 (2019), pp. 1–26.
[48] ———, *Entropy stable, positive DGSEM with sharp resolution of material interfaces for a* 4×4 *two-phase flow system: a legacy from three-point schemes*, arXiv preprint arXiv:2001.05710, (2019).
[49] ———, *Entropy stable, robust and high-order DGSEM for the compressible multicomponent Euler equations*, J. Comput. Phys., (2021), p. 110584.
[50] F. Renac, M. de la Llave Plata, E. Martin, J. B. Chapelier, and V. Couaillier, *Aghora: A High-Order DG Solver for Turbulent Flow Simulations*, Springer International Publishing, Cham, 2015, pp. 315–335.
[51] R. Saurel and C. Pantano, *Diffuse-interface capturing methods for compressible two-phase flows*, Annu. Rev. Fluid Mech., 50 (2018), pp. 105–130.
[52] C.-W. Shu and S. Osher, *Efficient implementation of essentially non-oscillatory shock-capturing schemes*, J. Comput. Phys., 77 (1988), pp. 439–471.
[53] K.-M. Shyue, *An efficient shock-capturing algorithm for compressible multicomponent problems*, J. Comput. Phys., 142 (1998), pp. 208–242.
[54] B. Sjögreen and H. C. Yee, *Grid convergence of high order methods for multiscale complex unsteady viscous compressible flows*, J. Comput. Phys., 185 (2003), pp. 1–26.
[55] E. Tadmor, *The numerical viscosity of entropy stable schemes for systems of conservation laws. I*, Math. Comput., 49 (1987), pp. 91–103.
[56] S. A. Tokareva and E. F. Toro, *HLLC-type Riemann solver for the Baer–Nunziato equations of compressible two-phase flow*, J. Comput. Phys., 229 (2010), pp. 3573–3604.
[57] E. Toro, L. Müller, and A. Siviglia, *Bounds for wave speeds in the Riemann problem: Direct theoretical estimates*, Comput. Fluids, 209 (2020), p. 104640.

[58] E. F. Toro, *Riemann-problem-based techniques for computing reactive two-phased flows*, in Numer. Combustion, Springer, 1989, pp. 472–481.

[59] ———, *Riemann solvers and numerical methods for fluid dynamics: a practical introduction*, Springer Science & Business Media, 2013.

[60] E. F. Toro, M. Spruce, and W. Speares, *Restoration of the contact surface in the hll-riemann solver*, Shock waves, 4 (1994), pp. 25–34.

[61] A. Volpert, *The spaces BV and quasilinear equations*, Math. USSR Sbornik, 115 (1967), pp. 255–302.

[62] C. Wang, X. Zhang, C.-W. Shu, and J. Ning, *Robust high order discontinuous Galerkin schemes for two-dimensional gaseous detonations*, J. Comput. Phys., 231 (2012), pp. 653–665.

[63] M. Waruszewski, J. E. Kozdon, L. C. Wilcox, T. H. Gibson, and F. X. Giraldo, *Entropy stable discontinuous galerkin methods for balance laws in non-conservative form: Applications to euler with gravity*, 2021.

[64] N. Wintermeyer, A. R. Winters, G. J. Gassner, and D. A. Kopriva, *An entropy stable nodal discontinuous Galerkin method for the two dimensional shallow water equations on unstructured curvilinear meshes with discontinuous bathymetry*, J. Comput. Phys., 340 (2017), pp. 200–242.

[65] X. Zhang and C. Shu, *On positivity-preserving high order discontinuous Galerkin schemes for compressible Euler equations on rectangular meshes*, J. Comput. Phys., 229 (2010), pp. 8918–8934.

[66] X. Zhang and C.-W. Shu, *On maximum-principle-satisfying high order schemes for scalar conservation laws*, J. Comput. Phys., 229 (2010), pp. 3091–3120.